NTNU – Trondheim
Norwegian University of
Science and Technology

Transient Dynamic Response of Ship Hull

Meitong Liu

Marine Technology
Submission date: June 2015
Supervisor: Bernt Johan Leira, IMT

Norwegian University of Science and Technology
Department of Marine Technology

NTNU – Trondheim
Norwegian University of
Science and Technology

Transient Dynamic Response of Ship Hull

Meitong Liu

June 2015

MASTER THESIS

Department of Maine Technology

Faculty of Engineer Science and Technology

Norwegian University of Science and Technology

Supervisor: Professor Bernt J. Leira

NTNU
Norwegian University of Science and Technology
Department of Marine Technology

Master Thesis, Spring 2015

for

Master student Meitong Liu

Transient Dynamic Response of Ship Hull

Transient Dynamisk Respons av Skipsskrog

The subject of interaction between the fluid and a flexible structure has been gaining prominence in research and applications in the last few decades. The study of global and local dynamic elastic behavior of marine vessels and structures forms the basis for the field of marine hydroelasticity. In addition to consideration of the global flexural strength, localized hydroelastic analysis is frequently necessary in order to ensure sufficient strength in areas like the bow, wetdeck, stern and bow flare. Slamming or impact is a common phenomenon, in particular for severe seas. The vessel hull typically emerges once every few wave encounters, followed by a slamming event.

The following subjects are to be examined in this thesis:

1. Different types of external loads which act on the ship hull are to be described. This comprises ordinary loads due to waves and transient loads e.g. due to slamming. Corresponding load models and methods for response analysis are to be summarized briefly with focus on transient loads. Relevant computer programs for dynamic response analysis are to be considered.

2. The methods which are applied by the computer program Abaqus for analysis of free-vibration mode shapes as well as dynamic response for a given load time-history are to be described.

3. A numerical model of a specific ship hull is to be established in Abaqus based on information which is available from a benchmark study. A beam and/or a shell model can be relevant. Dry and wet natural modes and frequencies for the basic mode shapes are to be computed.

4. For some given time histories of the load impulse that acts on the fore part of the hull, dynamic response analyses are to be performed. Sensitivity studies with respect to important parameters can be carried out to the extent that time allows.

The work-scope may prove to be larger than initially anticipated. Subject to approval from the supervisor, topics may be deleted from the list above or reduced in extent.

In the thesis the candidate shall present his personal contribution to the resolution of problems within the scope of the thesis work. Theories and conclusions should be based on mathematical derivations and/or logic reasoning identifying the various steps in the deduction. The candidate should utilise the existing possibilities for obtaining relevant literature.

The thesis should be organised in a rational manner to give a clear exposition of results, assessments, and conclusions. The text should be brief and to the point, with a clear language. Telegraphic language should be avoided.

The thesis shall contain the following elements: A text defining the scope, preface, list of contents, summary, main body of thesis, conclusions with recommendations for further work, list of symbols and acronyms, references and (optional) appendices. All figures, tables and equations shall be numerated.

The original contribution of the candidate and material taken from other sources shall be clearly defined. Work from other sources shall be properly referenced using an acknowledged referencing system.

The thesis shall be submitted in 3 copies:

- Signed by the candidate
- The text defining the scope included
- In bound volume(s)
- Drawings and/or computer prints which cannot be bound should be organised in a separate folder.

Supervisor: Professor Bernt J. Leira

Deadline: June 10th, 2015

Trondheim, January 14th, 2015

Bernt J. Leira

Abstract

Slamming often occurs in severe sea states particular for high speed vessels, which can cause damage to ship hulls or even equipment on ships. Analysis of transient dynamic response of ship hulls is useful in establishing criterion related to slamming loads and predicting seakeeping behavior of the ship. Thus this thesis is mainly focused on dynamic response of the ship due to slamming loads.

Experimental study of the floating structure dynamics can be very expensive. Hence, numerical methods are considered to be very useful for dynamic analysis of the ship. The ship to be analyzed in this work is owned by Wagenborg which is a multi-purpose cargo/container ship. The bench mark committee has provided all the information about the ship and corresponding sea condition. Three-dimensional finite element model is established in Sesam Genie. Hydrodynamic coefficients are computed in Sesam HydroD. The model made in Genie is imported in ABAQUS for dynamic analysis. The material properties, sections, mesh size and load cases are defined in ABAQUS.

The introductory part of this thesis gives an overview of slamming phenomenon and reviews of previous literature. The second part of the thesis introduces different types of external loads which act on the ship hull and the response induced by these loads. Slamming load theories are described especially. The third part elaborates dynamic response analysis theories and corresponding analysis methods. The analysis methods used in ANAQUS are also specified in this section. The forth part of the thesis presents details of the finite element modelling of the ship using software Sesam and ABAQUS. Different ship models are established for comparison. The final part presents the results of eigenvalue analysis and dynamic response analysis. Parametric studies are performed in this section. The conclusions are made in the final part.

Preface

This master thesis has been written during the spring semester of 2015 at the Department of Marine Technology, the Norwegian University of Science and Technology. It has been completed to satisfy the final requirement for completing the degree of Master of Science. Some preliminary work was carried out in the project during the autumn of 2014.

I would like to express my gratitude towards my supervisor Professor Bernt J. Leira for his guidance and for providing me the necessary information of the ship model. I would also like to thank Ekaterina Kim, Postdoctoral Fellow at the Department of Marine Technology, for her help in modelling in ABAQUS.

Finally, I would like to thank all my friends here in Trondheim for their accompanying and help during the two years in Norway. Special thanks to my parents for their supporting on my studies and life.

Meitong Liu

Trondheim, June 10th, 2015

Table of Contents

List of Figures

List of Tables

Nomenclature

Subscripts

$j, k = 1,...,6$ jth or kth degree of freedom for a rigid body

Roman Letters

$a(t)$ Ship-fixed x-coordinate of upstream deck-water intersection

A_{jk} Added mass coefficients

A_n Fourier coefficients

$b(t)$ Ship-fixed x-coordinate of downstream deck-water intersection

B_{jk} Damping coefficients

B_{gen} Damping matrix for the three-body system

$c(t)$ Half length of the wetted deck area

E Young's modulus

F_j jth mode excitation force or moment

Fn Froude number

t Time variable

T Incident wave period

Te Encounter wave period

Tn Natural period

C_{kj} Restoring coefficient

ρ Density of water

g acceleration due to gravity

A_{wp} water plane area

B maximum wedge breadth

ϕ velocity potential

λ	wavelength
A	submerged cross sectional area
d	sectional draft
a_{33}	2D infinite frequency added mass in heave
U	ship speed
w	elastic deflection of beam
EI	bending stiffness
h(x)	time-independent wetdeck height above calm water
s	motion at any point on the body
β	dead rise angle
Pa	atmospheric pressure

Terminology

Amidships (or midships): In the middle portion of ship, along the line of the keel.

Bow: The front of a vessel.

Cargo Ship: Any sort of ship or vessel that carries cargo, goods, and materials from one port to another, including general cargo ships (designed to carry break bulk cargo), bulk carriers, container ships, multipurpose vessels, and tankers. Tankers, however, although technically cargo ships, are routinely thought of as constituting a completely separate category

Dead rise: The design angle between the keel (q.v.) and horizontal.

Flare: A curvature of the topsides outward towards the gunwale.

Head sea: A sea where waves are directly opposing the motion of the ship.

Hull Girder: The primary hull structure such as the shell plating and continuous strength decks contributing to flexural rigidity of the hull and the static and dynamic behavior of which can be described by a free-free non-uniform beam approximation.

Length Between perpendiculars: The length of a vessel along the waterline from the forward surface of the stem, or main bow perpendicular member, to the after surface of the sternpost, or main stern perpendicular member. Believed to give a reasonable idea of the vessel's carrying capacity, as it excludes the small, often unusable volume contained in her overhanging ends

1 Introduction

1.1 General

The subject of flexible fluid structure interaction has been gaining prominence in diverse research for several decades. There are several detrimental effects caused by impact-induced vibrations, such as global whipping, high localized slamming pressures, transient local high-frequency vibrations, cavitation and ventilation. Thus, transient dynamic response analysis of ships and floating offshore structures is a concern in terms of safety and habitability.

Slamming is a common phenomenon which vessel hull always encounters especially in severe seas. It works on ships and other floating structures as an impulsive impact load when the structure impact with waves. The floating structure starts to vibrate after slamming occurs and such transient vibration is called whipping. In general, the response of the floating structure to non-impulsive wave loads is quasi-static response, which is in low frequency range. Such vibration induced by non-impulsive loads is called springing. However, the response of the structure caused by slamming impact is in high frequency range.

Experiments were performed on water with impact against wetdecks and hull structures before, especially for high-speed vessels. Aarsnes and Hoff (1998) and Faltinsen (1999) executed full scale experiments of the 30m long Ulstein test catamaran and demonstrated that this minimum height was not sufficient to avoid slamming [2]. The full scale measurements on the Ulstein test vessel demonstrated that even for a small vessel there existed the effect of wetdeck slamming induced transient vertical accelerations with a period corresponding to the global two-node bending [2]. It can be shown that the whipping response clearly causes a significant increase in stress after slamming impacts. The slamming induced whipping also increases the loading of the ship structure. It does not only increase the global loads, but also the loads at local beam and shell structures. Thus the ship may experience a structure failure since the actual loading of the structure exceeds the design load. An example of the accident due to slamming is shown in the report on the

structural failure of MSC Napoli English Channel [26]. Another example shows that the oceanographic research vessel USN Hayes of length 220ft (67.0m) experienced local deformations of the shell plating due to wetdeck slamming [1].

Slamming occurs when the relative vertical motions between the ship and the water is large. Take the oceanographic research vessel USN Hayes of length 220ft for instance, when the ship design was altered by introducing foils between the side hulls in the forward part of the ship, the relative vertical motions was reduced by 30% [1]. It was found to have a better seakeeping behavior.

Slamming is more easily to occur for ships with horizontal member placed near the mean water level, like catamaran. The horizontal member will be alternatively in water and air as waves pass it. If the axis of the horizontal member is parallel to the wave crest, it will experience sudden impact or slamming loads as the wave comes up underneath it. [27]

Slamming also occurs in case of high vessel speed. The ship with higher speed is subjected to larger loads. There is a basic criterion related to slamming loads that the shipmaster should reduce the speed if slamming occurs as frequently as three out of 100 waves passing the ship.

In reality, the position that the water hits on the wetdeck has a great influence. Figure 1.1 shows how the impact position depends on the wave period in regular head sea waves for a given catamaran and Froude number, as well as the minimum wave amplitude to excite slamming corresponding to each wave length [4].

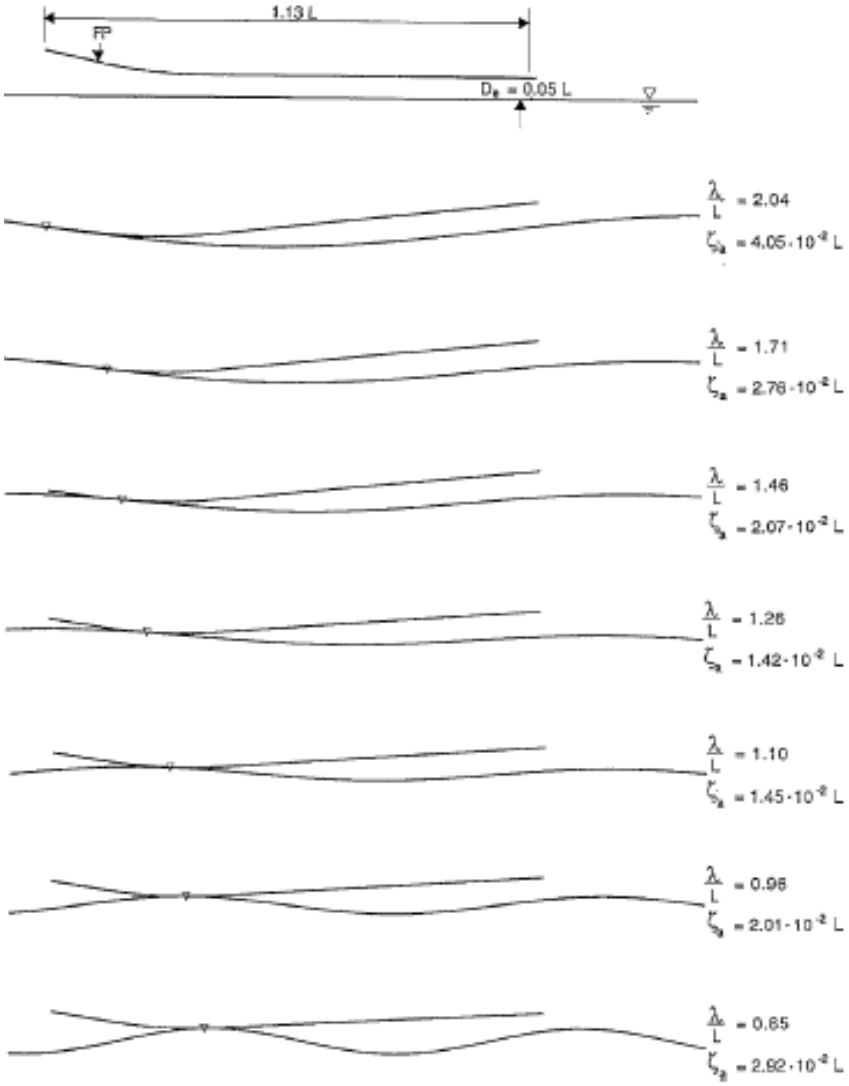

Figure 1. 1 Position of slamming on the wetdeck of a catamaran in regular head sea waves as a function of wavelength λ. The figure shows a longitudinal cross section at the centerplane of the catamaran. The bow ramp is seen in the fore part. Fn = 0.5, ζa = ζslam = lowest incident wave amplitude when slamming occurs, L= LPP = length between perpendiculars [6].

In figure 1.1, it can be seen that impact occurs much closer to the bow for longer wave length. For short wave length, when the impact does not occur at the end of the forward deck, the water surface is initially tangential to the wetdeck surface at the impact position [4].

In fact, slamming is rarely taken into account in the design of ships even though it contributes significantly to the loading of the ship. It is rarely included when performing seakeeping computations. The reason is that it is difficult to do the exact loading or response calculation related to slamming. The corresponding software to analyze the response due to slamming has not yet been developed for the reason of the complexity and unpredictable nature of slamming. While, the Classification Societies rules provides some

empirical ‘dynamic loading’ factors. Experimental results show that it is better to define the magnitude of the slamming loads as 2-3 times of the wave induced drag loads [28].

In order to understand the behavior of ships under slamming phenomenon, study of dynamic response of the structure subjected to transient impact loads can be very useful. Several methods are available for studying transient dynamic response of ships. Experimental techniques are useful but also normally expensive and restricted in real ship model. Hence, numerical method such as finite element analysis performed by ABAQUS is used in this thesis. The closed-form solution for the dynamic equations of motion is solved in time domain.

1.2 Literature review

Slamming on ships is categorized as bottom, bow-flare, bow-stem and wet-deck slamming [25]. Wet-deck slamming often occurs on high-speed catamarans and SES. Bow-stem slamming and green-water impact on deck structures are important for Floating Production Storage and Offloading (FPSO) units, as shown in figure 1.2 [29].

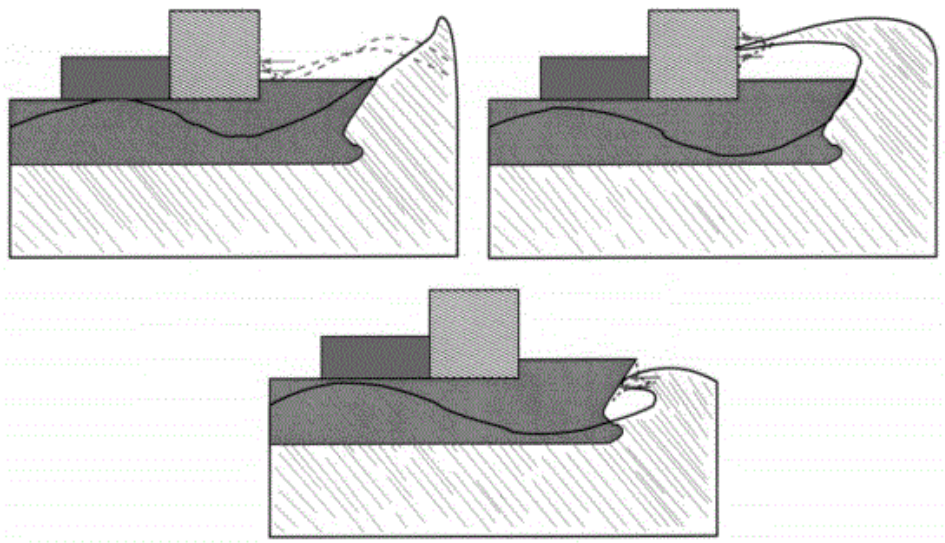

Figure 1. 2 Green-water slamming on deck and bow-stem slamming [29]

Von Karman (1929) and Wagner (1932) developed asymptotic theories that are most frequently used in slamming studies. They dealt with flat impact problems with a two dimensional wedge, assuming linearized free surface and body boundary condition. The slamming period is divided into the water entry and exit phase. The difference between the two theory is that whether the water surface elevation is accounted or not. [3]

Verhagen (1967) and Haugen (1999) studied details of air cushions. Kv˚alsvold (1994), Faltinsen (1997) and Haugen (1999) studied the effect of hydro-elasticity on local slamming induced stresses. They tried originally to use a Boundary Element Method to calculate the slamming loads. However very large numerical errors were introduced, and then they decided to use more analytically based methods.

Guedes Soares, C. (1989) presented a method for predicting the slamming load, using strip theory to determine the relative motion between the ship and waves, and the rate of change in the momentum of the fluid to calculate the impact force. He used a two-dimensional Timoshenko beam finite elements with a consistent mass formulation to determine mode shapes and natural frequencies. The response was obtained using a Newmark integration scheme.

Morris (1991) performed quasi-dynamic analysis using a three-dimensional finite element model and loading patterns provided by Lloyd's. He studied the concentrated stresses in both local and global response.

Zhao Rui and Faltinsen (1994) studied the slamming load on hull cross-sections using a boundary element method and got an asymptotic solution for wetdeck slamming. Limitation on the wedge deadrise angle was presented. The results showed the importance of wave slope to slamming loads.

Ulstein (1995) showed the importance of local hydro-elasticity effects caused by slamming and the influence of the horizontal velocity of the flow at the point where wave impact happens. He considered impact loads on the stern seal bag of a Surface Effect Ship (SES) at high forward speed.

Ojeda et al (2004) created a three dimensional finite element model of a catamaran using ANSYS 6.0. The quasi-static slamming load conditions provide by DNV HSLC rules were used and hollow landing and crest landing were studied.

2 Theory

2.1 Linear wave-induced motions and loads

Knowledge about wave induced loads and motions of ships is important in design and operation. The rigid-body motions in linear seakeeping consist of three translations and three rotations. Motions of floating structures can be divided into wave-frequency motion, high-frequency motion, slow-drift motion and mean drift motion. The wave-frequency motion is linearly excited by frequencies within the wave-frequency range. However, the other three types of motion are excited by non-linear effects.

Linear theory is applicable to calculate the wave-frequency motions and loads on ships. Ship response in irregular waves can be obtained by adding together responses in regular waves of different amplitudes, wave lengths and propagation directions [3].

The motion of any point on the body can be written as

$$\mathbf{s} = \eta_1 \boldsymbol{i} + \eta_2 \boldsymbol{j} + \eta_3 \boldsymbol{k} + \boldsymbol{\omega} \times \boldsymbol{r} \tag{1}$$

where

$$\boldsymbol{\omega} = \eta_4 \boldsymbol{i} + \eta_5 \boldsymbol{j} + \eta_6 \boldsymbol{k} \tag{2}$$

$$\mathbf{r} = \mathrm{x} \boldsymbol{i} + \boldsymbol{y} \boldsymbol{j} + \boldsymbol{z} \boldsymbol{k} \tag{3}$$

where

and ***i, j, k*** are unit vectors along the x-, y- and z- axis, respectively.

This means

$$\mathbf{s} = (\eta_1 + z\eta_5 - y\eta_6)\boldsymbol{i} + (\eta_2 - z\eta_4 + x\eta_6)\boldsymbol{j} + (\eta_3 + y\eta_4 - x\eta_5)\boldsymbol{k} \tag{4}$$

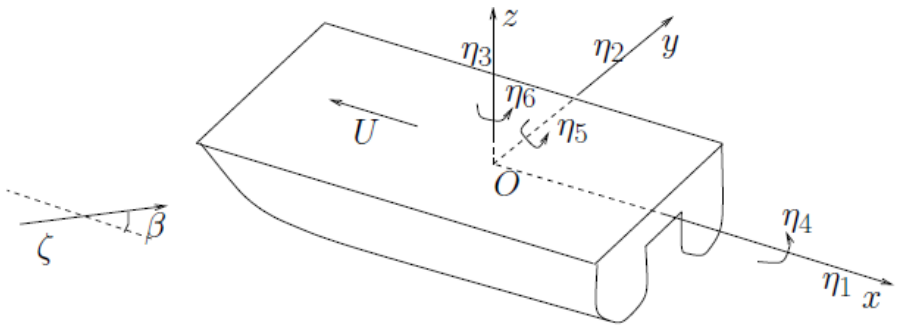

Figure 2. 1 Global coordinate and degree-of-freedom system of the catamaran [2].

Linear equation in six degrees of freedom using body axes in general form is given by

$$\sum_{k=1}^{6} \Delta_{jk}\ddot{\eta}_k(t) = F_j(t) \qquad j=1,\ldots,6 \tag{5}$$

where

Δ_{jk} = Generalized inertia matrix component for the ship,

$F_j(t)$ = Total forces and moments acting on the body.

The above equation can also be written in Euler's equation of motion (with only fluid forces and gravitational forces acting on the ship):

$$\sum_{k=1}^{6} \Delta_{jk}\ddot{\eta}_k(t) = F_j(t) = F_{Gj} + F_{Hj} \qquad j=1,\ldots,6 \tag{6}$$

where

F_{Gj} is the gravitational force component, which is normally canceled by the buoyancy.

F_{Hj} is the fluid force component acting on the ship, involving both hydrodynamic and hydrostatic forces. The force can be obtained by integrating the fluid pressure within the underwater part of the hull. The equation is given by:

$$F_{Hj} = \iint_S p n_j dS \qquad j=1,\ldots,6 \tag{7}$$

where

p is the fluid pressure calculated by Bernoulli's equation, including both hydrostatic and dynamic part.

S is the wetted surface of the body.

The hydrodynamic problem in regular waves is normally dealt with as two sub-problems. When the structure is restrained from oscillating and there are incident regular waves, the

hydrodynamic loads are called excitation loads and are composed of so-called Froude-Kriloff and diffraction forces and moments. When the structure is forced to oscillate with the wave excitation frequency in any rigid-body motion mode, in case of no incident waves, the hydrodynamic loads are identified as added mass, damping and restoring terms [3]. The total hydrodynamic load is obtained by adding the results from two sub-problems together.

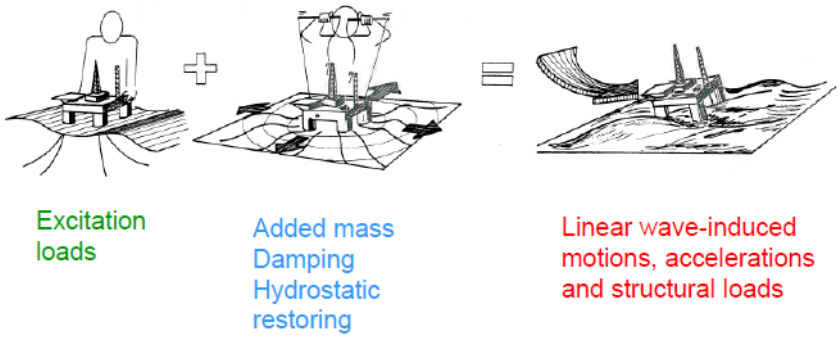

Figure 2. 2 Superposition of wave excitation, added mass, damping and restoring loads [22].

2.1.1 Added mass and damping forces

In case of no incident waves, the forced motion of the ship generates outgoing waves. The forced motion results in oscillating fluid pressures on the body surface. Integration of this pressure over the wetted surface of the body gives resulting forces and moments on the structure, namely the added mass and damping forces. We can formally write the hydrodynamic added mass and damping loads due to harmonic motion mode η_j as [3]:

$$\mathrm{F_k} = -A_{kj}\frac{d^2\eta_j}{dt^2} - B_{kj}\frac{d\eta_j}{dt} \tag{8}$$

where A_{kj} and B_{kj} are defined as added mass and damping coefficients. In total, there are 36 added mass coefficients and 36 damping coefficients. In case of no current and no forward speed, $A_{kj} = A_{jk}$, $B_{kj} = B_{jk}$.

Added mass and damping loads are frequency dominated. They are dependable on the motion mode, body shape, as well as the choice of axis. Current and forward speed have significant influence on added mass and damping coefficients. The important effect for a ship at forward speed comes from the frequency of an encounter wave.

In case of no forward speed, strip theory can be used to calculate two dimensional added mass and damping coefficients. The 3D problem can be approximated as the sum of 2D problems.

In this thesis, due to the short time scale of slamming process, it is assumed that hydrodynamic added mass can be determined based on the limit value when the oscillating frequency approaches infinity. Further it is assumed that the added mass in the vertical direction that is proportional to heave acceleration dominates.

Thus, strip theory is applied here. Added mass results based on Lewis form technique are shown in Figure 2.3:

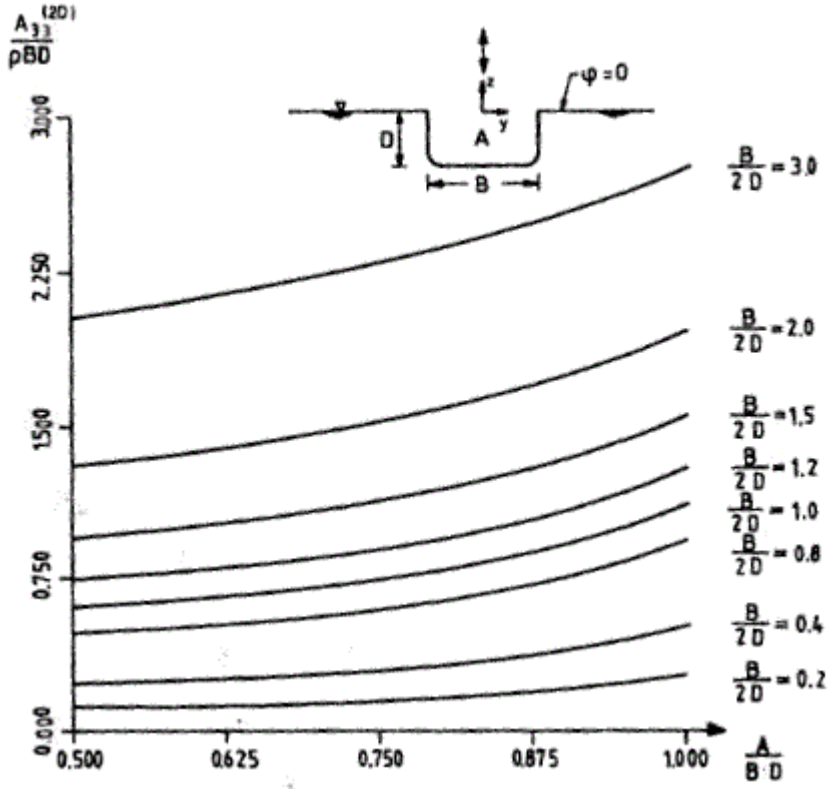

Figure 2. 3 Two-dimensional added mass in heave A_{33}^{2D} for Lewis form sections for infinite oscillation frequency [3]

The results from Figure 2.3 is restricted to the body that has symmetry geometry with respect to *y* axis. Here, *A* represents the submerged cross-sectional area, *B* is the beam, *D* is the draught. A_{33}^{2D} here is the two-dimensional added mass coefficient of the mid-ship section. The three-dimensional added mass coefficient is obtained by integrating along the ship length. This is time consuming. Hence, the ratio $\frac{A_{33}^{2D}}{\rho BD}$ is assumed to be the ratio of added mass to actual mass per unit length of each section, which is considered constant

over the whole ship approximately. Hydrodynamic added mass is then obtained by multiplying this ratio by the displacement of the ship.

2.1.2 Hydrostatic Stiffness

The hydrostatic stiffness of a ship is a result of the buoyancy. When a body is freely floating, restoring forces will follow from hydrostatic and mass considerations. The force and moment components can be written as [3]

$$F_k = -C_{kj}\eta_j \tag{9}$$

where C_{kj} is the hydrostatic stiffness coefficient. The only non-zero coefficients for a body with the x-z plane as a symmetry plan for the submerged volume are [3]:

$$C_{33} = \rho g A_{wp} \tag{10}$$

$$C_{53} = C_{35} = -\rho g \iint_{A_{wp}} x ds \tag{11}$$

$$C_{44} = \rho g V \overline{GM_T} \tag{12}$$

$$C_{55} = \rho g V \overline{GM_L} \tag{13}$$

where, A_{wp} is total waterplane area, $\overline{GM_T}$ is transverse metacentric height, $\overline{GM_L}$ is longitudinal metacentric height.

Slamming can cause transient heave, pitch and global vertical elastic vibrations. In thesis, it is assumed that the hydrostatic stiffness in heave direction C_{33} dominates.

2.2 Second-order non-linear problems

The linear solutions are calculated related to the mean position of the free-surface and the submerged hull surface. In the second-order theory, the calculation should be related to the instantaneous position of the body in order to get more accurate nonlinear velocities and fluid pressures. The most common way to solve non-linear wave-structure problems in ship and offshore hydrodynamics is to use perturbation analysis with the wave amplitude

as a small parameter [3]. All the terms linear to the wave amplitude or square to the wave amplitude will be considered.

The solution of the second-order problem results in mean forces, and forces due to sum-frequency and difference-frequency effects. The mean drift loads are due to the structure ability to generate waves in assumption of potential flow theory. They can be calculated by Maruo's formula. The slowly-varying motions are resonance oscillations excited at frequencies lower than incident wave frequencies and are usually caused by the wave-current-wind environment. The linear wave-radiation damping is small near the slow-drift resonance, however, viscous damping and wave-drift damping matter. Slow-drift loads can be calculated by using Newmans approximation. The 2^{nd} order sum-frequency effects result in springing, while, the 3^{rd} and 4^{th} order sum-frequency effects result in ringing.

2.3 Slamming

2.3.1 Physical effects caused by slamming

Slamming is a problem for both the local structural integrity and the global elastic behavior. It is also of concern for fatigue, operations and comfort.

Here, we introduce the definition of dead-rise angle β, which is the angle between the body and the water at the impact position.

Different physical effects occur during slamming. Compressibility of water in initial acoustic phase gives large possible (acoustic) pressure. In case of small dead-rise angle, air-cushion may be entrapped between water and structure. Due to the air compressibility, the air-cushion oscillates and interacts with the water flow, which is also influenced by compressibility of the water. Air bubbles will be formed when the air-cushion collapses. When the dead-rise angle is small, the large hydrodynamic loads induced by slamming can trigger local dynamic hydro-elastic effects. That is to say these large loads may excite structural vibrations which affect the surrounding fluid flow. The hydro-elasticity may lead to cavitation and ventilation.

All these physical effects have different time scales. Slamming problem is hydro-dynamically studied from a structural point of view, and the time scale when maximum

stresses occur is of concern. This time scale is regarded as the highest wet natural period of the structure. The time scale of the formation and collapse of an air cushion is normally much smaller than the time scale for maximum stresses occur and is less important. Thus, the effect on maximum local stresses is small.

For different vessel types, slamming causes different global effects. These effects can cause transient heave, pitch and global vertical elastic vibrations. For ships longer than 50m, it is more easily to have global longitudinal vertical bending deformations than small ships. Whipping occurs in head sea waves, in terms of two-node longitudinal vertical bending, which has a natural period of around 1s. However, the typical duration of local hydro-elastic slamming is of the order of 10^{-2}s. Thus, in the following analysis in this thesis, the ship of 134m can be regarded as locally rigid. [4]

2.3.2 Wagner's method

Wagner's method can be applied to estimate slamming in many cases.

The whole slamming process has two important transient phases: water-entry and water-exit phase of a body. The beginning of the water entry phase is highly localized in space and time. Consequently, impact loads caused by water entry will influence both the local structural safety and the global response of the body. Compared with water-entry phenomenon, water-exit of a body is less studied and known. It is usually studied in case of a partially or fully immersed body existing the water. [23]

The occurrence and involved features of water-entry and water-exit depend on the body geometry, operational conditions (ballast, loaded; fixed, moored, with forward speed; etc.) and the sea state. This implies that the local body shape where the impact happens, as well as the relative velocity between the body and wave will have a great influence on the severity of the water-entry phase. [23]

Assuming that impact occurs between a 2D wedge and a flat free surface. The entry velocity V is constant at time $t=0$. Wagner's model assumes a small dead-rise angle and accounts for the uprise of the water when determining the wetted length if the body. The problem can be shown in the figures below:

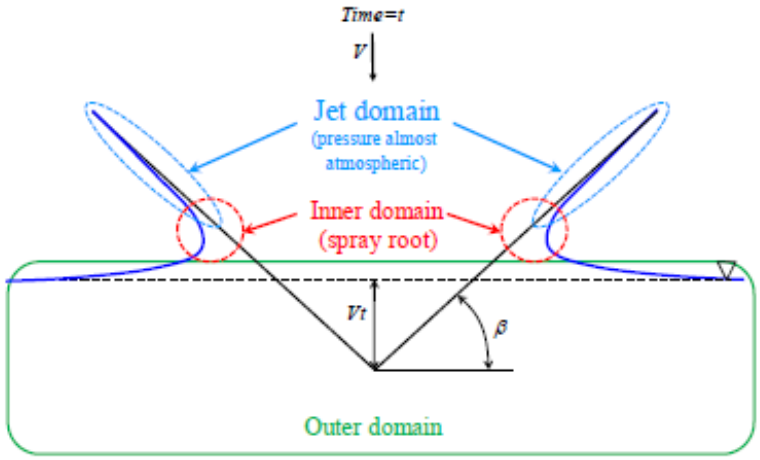

Figure 2. 4 Water entry of a wedge with constant velocity V. Definition of inner and jet flow domains [22].

In Figure 2.4, *Vt* is the instantaneous draught at time *t*. When the wedge entering into the water, the water raises up along the body and forms a jet, which is in fact a layer of water with high speed. Because of the surface tension, the jet becomes spray at the intersection of the body and free surface. The pressure in the jet domain area is almost constant and equal to atmospheric pressure. However, there is large spatial variation of the pressure at the spray root, i.e. inner domain. Thus we are more interested in the inner and outer domain, which provide the pressure distribution induced by slamming. [22]

In addition, hydro-elasticity is neglected here, the hydrodynamic loads are estimated. Thus, a quasi-static approach is used to estimate the stresses and deformations.

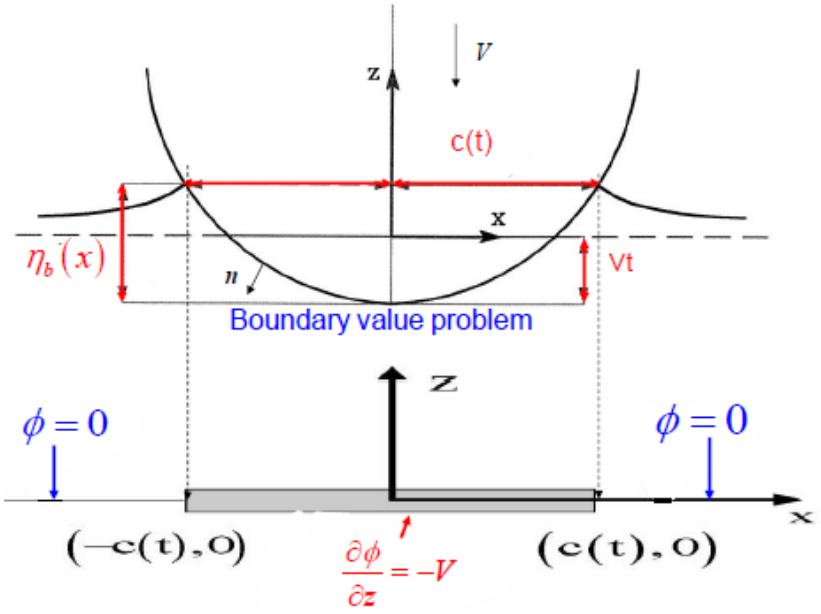

Figure 2. 5 Definition of parameters and boundary-value problem in analysis [22].

Figure 2.5 shows a circular cylinder, but the procedure given in the following is valid for other geometries with small dead-rise angle. There is no flow transferred to the straight line between $x=-c(t)$ and $x=c(t)$. The end points $x = \pm c$ are the spray roots, correspond to the instantaneous intersections between the outer flow free surface and the body surface. The boundary value problem is illustrated assuming dynamic free surface condition $\phi=0$ on $z=0$. This condition is the same as the high-frequency boundary value problem. [4]

In an earth-fixed coordinate system with positive z-axis upward (as illustrated in Figure 2.5), Euler equation states that [4]

$$\frac{\partial \boldsymbol{u}}{\partial t} + \boldsymbol{u} \cdot \nabla \boldsymbol{u} = -\frac{\nabla p}{\rho} - g\boldsymbol{k} \tag{14}$$

where, $\boldsymbol{u}$ is the fluid velocity, p is the pressure, and $\boldsymbol{k}$ is the unit vector along the z-axis. Since that fluid accelerations dominate, $\mathbf{u}\cdot\nabla\mathbf{u}$ and $g\mathbf{k}$ are small relative to $\partial\mathbf{u}/\partial t$, thus we can get the approximation

$$\rho\frac{\partial \boldsymbol{u}}{\partial t} = -\nabla p \tag{15}$$

Substituting $\mathbf{u} = \nabla\varphi$ gives that

$$\nabla\left(\rho\frac{\partial \varphi}{\partial t} + p\right) = 0 \tag{16}$$

This means that $\rho\partial\varphi/\partial t + p$ is a constant. If we assume no surface tension and atmospheric pressure p_a on the free surface, this gives

$$p - p_a = -\rho\frac{\partial \varphi}{\partial t} \tag{17}$$

Because $p=p_a$ on the free surface, we get that $\partial\phi/\partial t = 0$ on the free surface. If we now follow fluid particles on the free surface, they start at initial time with $\phi = 0$. Because $\partial\phi/\partial t = 0$, $\phi = 0$ remains for all time as a condition on the free surface. However, the free surface moves because $\partial\phi/\partial n \neq 0$. The final step is to assume small deviations between ϕ on $z = 0$ and the free surface and transfer this condition to $z = 0$, again by Taylor expansion. [4]

To solve the boundary-value problem shown in figure 3.2, introduce the complex variables $Z=x+iz$. The complex velocity potential can be expressed as [5]

$$\phi = \varphi + i\psi = iVZ - iV(Z^2 - c^2)^{1/2} \tag{18}$$

where ϕ is the velocity potential ψ and is the stream function. The complex velocity is

$$\frac{d\phi}{dZ} = u - iw = iV - iV\frac{Z}{(Z^2 - c^2)^{1/2}} \tag{19}$$

We introduce $Z - c = r_1 e^{i\theta_1}$ and $Z + c = r_2 e^{i\theta_2}$, where θ_1 and θ_2 vary from –π to π. This means

$$(Z^2 - c^2)^{1/2} = \sqrt{r_1 r_2}\, e^{i\frac{1}{2}(\theta_1 + \theta_2)} \tag{20}$$

We can write $\theta_1 = -\pi$ and $\theta_2 = 0$ when $|x| < c$ and $z = 0-$. This gives

$$(Z^2 - c^2)^{1/2} = -i(c^2 - x^2)^{1/2}, \qquad |x| < c \text{ and } z = 0^- \tag{21}$$

Here $z = 0-$ corresponds to the underside of the body. When $x>c$ and $z=0$, both θ_1 and θ_2 are zero, that is,

$$(Z^2 - c^2)^{1/2} = (x^2 - c^2)^{1/2}, \qquad x > c \text{ and } z = 0 \tag{22}$$

Eq. (18) gives, then, $\phi = 0$ for $|x| > c$ on $z = 0$. Further, Eq. (19) gives

$$\frac{d\phi}{dZ} = u - iw = iV + V\frac{x}{(c^2 - x^2)^{1/2}} \qquad |x| < c \text{ and } z = 0^- \tag{23}$$

Because $w = \partial\phi/\partial z$, we see from eq. (23) that the body boundary condition is satisfied. Further, eq. (19) gives that the fluid velocity goes asymptotically to zero when $|Z| \to \infty$. Eq. (18) gives

$$\phi = \varphi + i\psi = iVx - V(c^2 - x^2)^{1/2}, \qquad |x| < c \text{ and } z = 0^- \tag{24}$$

Then we can write the velocity potential on the body is

$$\varphi = -V(c^2 - x^2)^{1/2}, \qquad |x| < c(t) \tag{25}$$

The pressure equation can be written as

$$p - p_a = \rho V \frac{c}{(c^2 - x^2)^{1/2}} \frac{dc}{dt} + \rho \frac{dV}{dt} (c^2 - x^2)^{1/2} \tag{26}$$

The first term is denoted as the slamming pressure. It is associated with the rate of change of the wetted surface which is approximately *2dc/dt*. The second term is called the added mass pressure. We note that the slamming pressure is infinite at $x = \pm c$. This is unphysical. A detailed analysis near the spray roots (inner domain solution) is needed to find the correct pressure near $x = \pm c$. If *V* is constant, this gives a maximum pressure of $p - p_a = 0.5\rho(dc/dt)^2$. However, Eq. (26) is integrable, the singularity appearing in the outer domain solution is not serious. [4]

The two-dimensional vertical force acting on the impacting body can be expressed as

$$F_3 = \int_{-c}^{c} p dx = \rho V c \frac{dc}{dt} \int_{-c}^{c} \frac{dx}{\sqrt{c^2 - x^2}} + \rho \frac{dV}{dt} \int_{-c}^{c} (c^2 - x^2)^{1/2} dx$$

$$= \rho \pi V c \frac{dc}{dt} + \rho \frac{\pi}{2} c^2 \frac{dV}{dt} \tag{27}$$

The term $\rho \frac{\pi}{2} c^2$ is the two-dimensional added mass in heave a_{33} for the plate shown in Figure 2.5. However, this added mass is half the heave-added mass of a plate in infinite fluid. Because when we find the resulting hydrodynamic force on the plate in infinite fluid, we have to integrate pressure on both sides of the plate. In our problem, we have only to integrate pressures on the lower side. [4]

The force in Eq. (27) can also be expressed as

$$F_3 = \frac{d}{dt}(a_{33} V) = a_{33} \frac{dV}{dt} + V \frac{a_{33}}{dt} \tag{28}$$

Where $V da_{33}/dt$ is the slamming force. This is a common way to express the slamming force in connection with the Von Karman method. The Eq. (28) can also be applied to 3D model by using the 3D added mass in heave A_{33} instead of the 2D added mass in heave a_{33}.

From Eq. (28), we see that the variation in time of the added mass in heave affects the vertical force. The faster the increase of the wetted surface is, the larger the vertical force is. This means that slamming is important for blunt body.

Thus, the evolution of the wetted surface is important in calculation of the loads. Now, we use Wagner's method to find *c(t)*.[22]

We can still use Eq. (19), (21), (22) to express the vertical velocity $w = \partial\phi/\partial z$ on the free surface. This gives

$$\frac{\partial \varphi}{\partial z} = \frac{V|x|}{\sqrt{x^2 - c^2(t)}} - V \qquad on\ z = 0, |x| > c(t) \tag{29}$$

As we can see from Eq. (29) that this expression for vertical velocity can only be applied to surface where $|x| > c(t)$. Because for the surface where $|x| < c(t)$, $\partial\varphi/\partial z = -V$.

Now, we focus on the surface where $|x| > c(t)$, the elevation of the body intersection with the free surface relative to the bottom of the body is $\eta_b(x)$ can be expressed as

$$\eta_b(x) = \int_0^t \frac{V|x|}{\sqrt{x^2 - c^2(t)}} dt \tag{30}$$

Here, $t=0$ corresponds to initial impact. Introducing $\mu(c) = Vdt/dc$, $\eta_b(x)$ can be expressed as

$$\eta_b(x) = \int_0^x \frac{x\mu(c)}{\sqrt{x^2 - c^2}} dc \tag{31}$$

Assuming that c is small for small t, we get the approximate expression of the first order

$$\mu(c) \approx A_0 + A_1 c \tag{32}$$

With unknown coefficients A_0 and A_1. Introducing this in Eq. (31), the integral can be found analytically

$$\eta_b(x) = A_0 \frac{\pi}{2} x + A_1 x^2 \tag{33}$$

If $\eta_b(x)$ can be found from the body geometry, A_0 and A_1 can be obtained from Eq. (33). Thus we can calculate $\mu(c)$.

For instance the symmetric impact on a 2D wedge with deadrise angle β

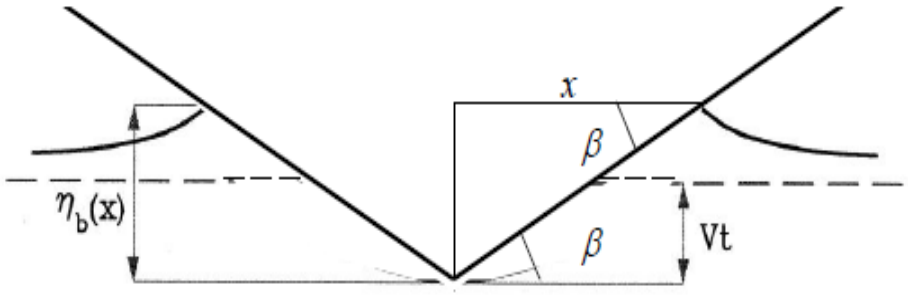

Figure 2. 6 Wedge with deadrise angle β [22].

As we can see from the figure 2.6 that $\eta_b = xtan\beta$, using this expression in Eq. (33), we can get

$$x\,tan\beta = A_0\frac{\pi}{2}x + A_1x^2 \Rightarrow A_0 = \frac{2}{\pi}tan\beta, A_0 = 0 \tag{34}$$

$$Vdt/dc = \mu(c) = 2tan\beta/\pi \xrightarrow[\text{for constant } V]{} c = \pi Vt/(2tan\beta) \tag{35}$$

Note that we can get the conclusion that the wetted surface increases more quickly as β reduces, i.e. for blunter impacts.

If we examine another simplified geometry: 2D circular cylinder as shown in Figure 2.7.

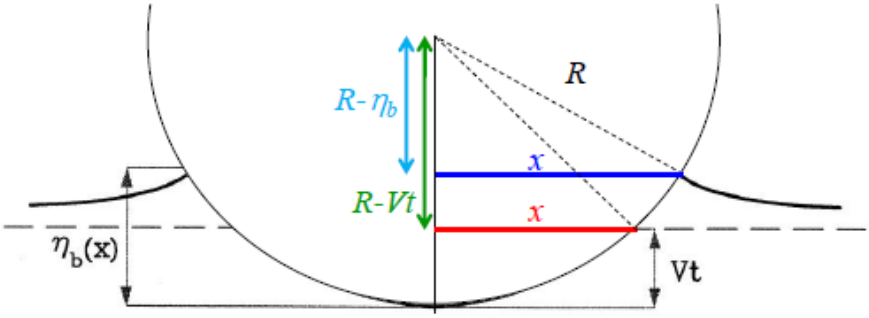

Figure 2. 7 2D circular cylinder [22].

From the geometry, we have the relation

$$x^2 + (R - Vt)^2 = R^2 \Rightarrow c(t) = \sqrt{2VtR - (Vt)^2} \tag{36}$$

Since the impact time t is very small, t^2 can be neglected. The wetted surface can be approximated as

$$c(t) \approx \sqrt{2VtR} \tag{37}$$

Extra attention should be taken that Wagner's method couldn't be applied to water exit phase since that the intersection points cannot be found. This is a consequence of the free-surface condition $\phi=0$. It implies that the fluid accelerations are no longer dominant and gravitational acceleration cannot be neglected. [22]

2.3.3 Von Karman's method

In contrast with Wagner's method, Von Karman's method doesn't account for the uprise of the water when determining the wetted length. *c(t)* is only determined by the geometrical intersection between the body surface and the undistributed water surface. [22]

Slamming happens when relative vertical displacement satisfy the relationship below

$$\eta_R = \eta_B(x,t) - \zeta + d(x) < 0 \tag{38}$$

where,

d(x) is the wetdeck height above the calm water.

ζ is the wave elevation, expressed by

$$\zeta = \zeta_a \sin(\omega_e t - kx) \tag{39}$$

$\eta_B(x,t)$ is the vertical body motion, including both rigid body motions and global hydro-elastic vibrations. However, here, it is determined by the rigid body motion assuming no global hydro-elastic vibrations:

$$\eta_B = \eta_3 - x\eta_5 \tag{40}$$

Compared with Wagner's method, Von Karman's method can be applied to water-exit phase. However, how exact the solution is depends on the duration T_d of the sum of the water entry and exit phases relative to a characteristic time. In addition, the slamming force VdA_{33}/dt is often neglected in water exit phase when using Von Karman method. [4]

2.3.4 Slamming loads and pressures

The dead-rise angle β and relative impact velocity V_R (the relative liquid-structure velocity at the impact) are two important parameter for slamming loads [22]. It is written in section

2.3.1 that most slamming induced effects accounted for are on the bases of small dead-rise angle. When the dead-rise angle β is not small, slamming pressures can be used in a static structural response analysis to find local slamming-induced stresses.

Numerical results based on the similarity solution by Dobrovol'skaya (1969) for water entry of rigid wedges with constant entry velocity was presented by Zhao and Faltinsen (1993) for $20^{\circ} < \beta < 81^{\circ}$ [4]. When $\beta <\approx 20^{\circ}$, the pressure distribution is concentrated close to the spray root with pronouncedly peaked. In this case, measurement of slamming pressure requires high sampling frequency and small pressure gauges. When $\beta > 45^{\circ}$, the maximum pressure occurs at the apex (or keel). The smaller β is, the more sensitive slamming loads are to β. The larger β is, the more uniformly spaced the impact pressure. [4]

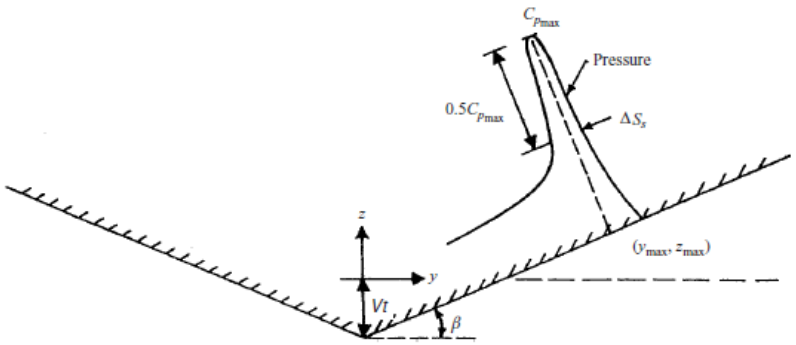

Figure 2. 8 Slamming pressure [4]

In general, for blunt geometries, one must not overemphasize the importance of the peak pressures. In extreme conditions, the maximum slamming induced stress is not affected by the high pressure peaks. Thus, one concern is on the pressure integrated over certain area as long as hydroelasticity are neglected. Hydroelasticity is taken into consideration when the slamming duration is smaller or comparable to the highest wet natural period of the structure.

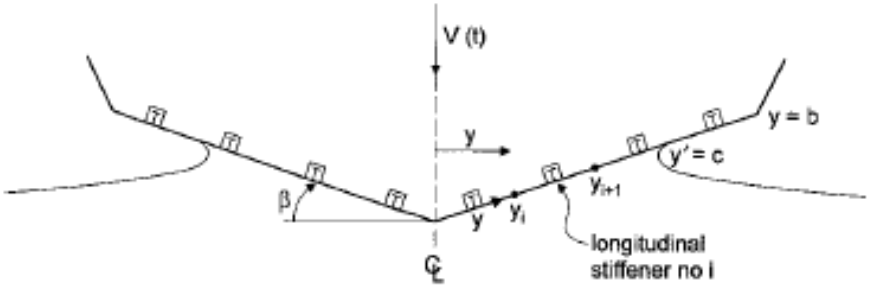

Figure 2. 9 Water entry of a wedge-shaped elastic cross section [4].

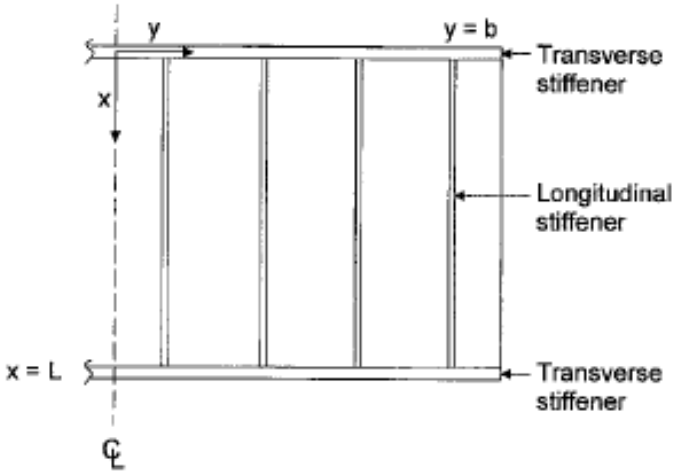

Figure 2. 10 Stiffened plating consisting of plate and longitudinal stiffeners [4].

Take the local rigid body shown in Figure 2.9 and Figure 2.10 for an example, assume that the transverse frame is much stiffer than the longitudinal stiffener. Then the resulting stresses in the longitudinal stiffener are relative more important and of interested. In Figure 2.10, the x-direction represents the longitudinal direction of a ship. The instantaneous slamming pressure is almost the same between two transverse frames. Thus the averaged slamming pressure between two transverse frames y_i and y_{i+1} is approximated. This average pressure vary with time and the largest one is of most concern. The average pressure from y_i to y_{i+1} has the largest value when $c = y_{i+1}$. The Wagner's method is applied here. And this largest value can be obtained from Eq. (26), (35) [4]

$$p_{av}^{max} - p_a = 0.5\rho V^2 \frac{\pi}{tan\beta}\left(\frac{y_{i+1}}{y_{i+1} - y_i}\right) \times \left(\frac{\pi}{2} - sin^{-1}\left(\frac{y_i}{y_{i+1}}\right)\right) \qquad (41)$$

Take a high speed ship with a flat horizontal transverse cross-section wetdeck in long-crested head sea waves as instance, the water surface at the initial impact position can be described by the incident waves. Besides, the flow caused by slamming can be assumed

two-dimensional in the longitudinal cross-sectional plane of the ship [4]. If Wagner's method is applied, multiply the Eq. (27) by the wetdeck breadth *B*. In addition, replace *V* by the constant relative impact velocity V_R, and use Eq. (37) for the expression of *c(t)*. Then the initial slamming force is obtained

$$F_3 = 2\rho\pi V_R^2 RB \tag{42}$$

However, if the water hits initially at the forward end of the deck, there will be a small angle α between the free surface and the deck surface [4]. This means that there is no slamming force initially. The slamming force increases later and is affected by the angle α. Similarly, the slamming force to the vessels with wedge-shaped transverse cross-section wetdeck is smaller than with horizontal transverse cross-section wetdeck. The ship with a ramp bow can decrease the likely to occur slamming.

3 Dynamic Response Analysis

3.1 Seakeeping response analysis

There are several methods to calculate the seakeeping response of a floating structure. For instance, 2D strip theory method, 3D Boundary Element Method (BEM), full 3D volume of fluid (VOF) method and smooth particle hydrodynamics (SPH) method [30].

A 3D structural finite element model is established for analysis. In this thesis, seakeeping response for complex 3D natural modes and other dynamic response such as acceleration and stress at every wetted element of the 3D-FE model need to be calculated. The 3D-BEM method is more suitable to be coupled to a 3D FEM. The 2D strip theory can also be used to calculated hydrodynamic coefficient. It is more accurate than 2D strip theory method for zero speed problem. However, both these two methods are not accurate enough for forward speed problem. Thus 3D BEM method and 2D strip theory can be used in this analysis.

The calculation of seakeeping problem can be performed in both the frequency domain and the time domain. The frequency domain method is less time consuming. The time domain method needs more time for calculation but accounts for large displacement in response. Thus, for non-linear loads and transient impulsive loads induced response analysis, it is more convenient to use the time domain method. Hydrostatic coefficient and Froude-Krylov forces are necessary in calculation for predicting the internal loads of the ship. It is better to include non-linear radiation and diffraction loads, however, this is currently difficult to compute completely in the time domain. Thus, the linear radiation and diffraction coefficients calculated in the frequency domain are used to compute these forces in the time domain.

3.2 Nonlinear analysis

3.2.1 Nonlinear behavior

Structural analysis, including the finite element method, is based on the following principles:

- Equilibrium (expressed by stresses)
- Kinematic compatibility (expressed by strains)
- Stress-strain relationship

So far, the analysis has been based on the assumptions that

- Displacements are small
- The material is linear and elastic

When the displacements are small, the equilibrium equations can be established with reference to the initial configuration. Moreover, this implies that the strains are linear functions of displacement gradients (derivatives).The linear elastic stress-stain relationship corresponds to Hooke's law.

There are three nonlinear conditions:

- Geometrical nonlinear behavior
- Material nonlinear behavior
- Boundary nonlinear behavior

When the ultimate strength of structures that buckle and collapse is to be calculated, the assumptions about small displacements and linear material need to be modified. If the change of geometry is accounted for, when establishing the equilibrium equations and calculating the strains from displacements, a geometrical nonlinear behavior is accounted for. For slamming induced response analysis, large displacements may occur for high speed vessel which encounters large impact loads. In this thesis, the results to whether large displacement is accounted for can be analyzed and compared. Typical nonlinear geometrical behavior related to thin plate/shell is shown in Figure 3.1.

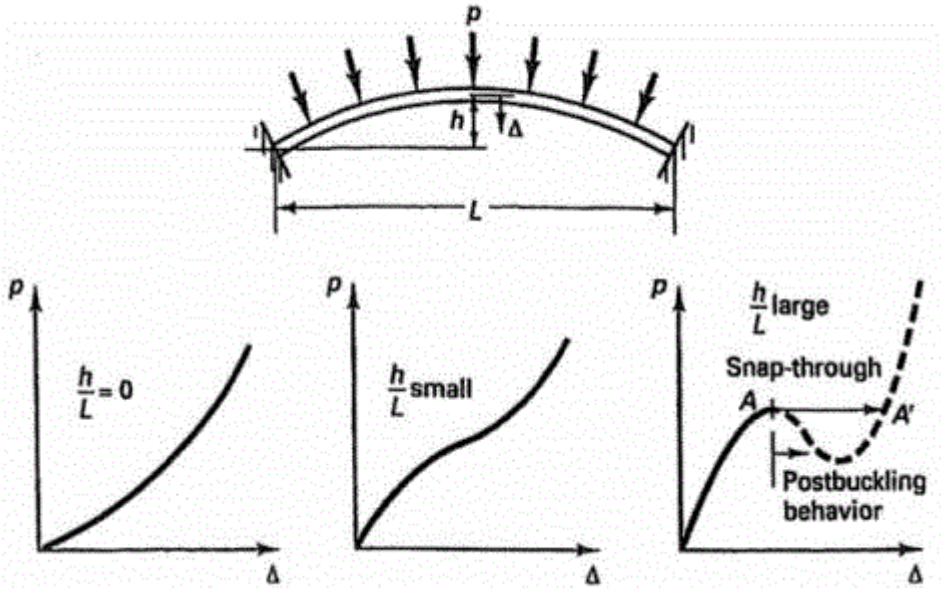

Figure 3. 1 Response of a thin plate/shell (e.g. due to water pressure or explosion pressure) [31]

Analogously, material nonlinear behavior is associated with nonlinear stress-strain relationship, which occurs when the stress exceeds a limit level. The nonlinear material behavior can be shown in Figure 3.2.

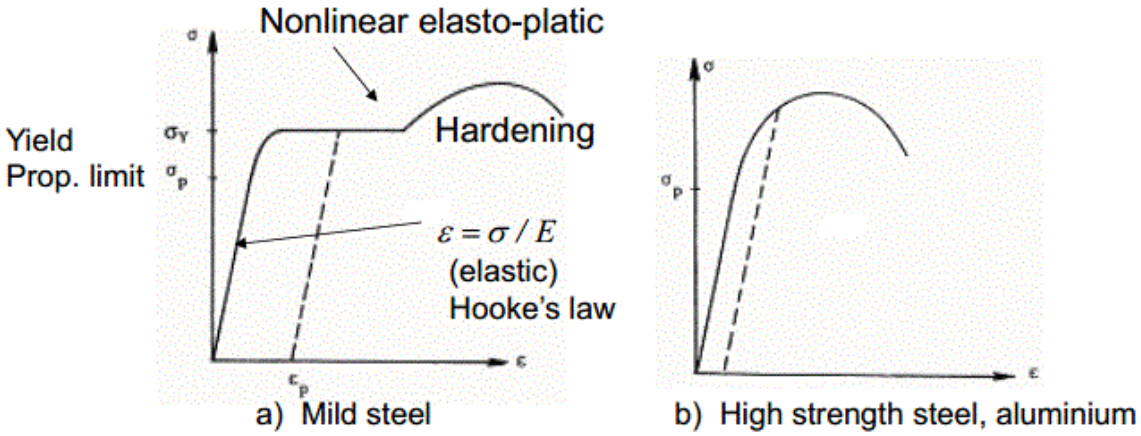

Figure 3. 2 Stress-strain curves for metals [31]

Finally, boundary nonlinear behavior occurs when a large displacement leads contact. The displacements and stresses of the contacting bodies are usually not linearly dependent on the applied loads.

However, nonlinear material behavior and nonlinear boundary behavior are not considered in this thesis.

3.2.2 Techniques solving nonlinear problems

There are three types of methods solving nonlinear problems.

The first one is the load incremental method, which is also called Euler-Cauchy method. The incremental method provide a solution of the nonlinear problem by a stepwise application of the external loading. For each step, the displacement increment is determined. The total displacement is obtained by adding displacement increments. The incremental stiffness matrix is calculated based on the known displacement and stress condition before a new load increment is applied and is kept constant during the increment. For load increment No. (m+1), the expressions are shown:

$$\begin{aligned} \Delta\mathbf{R}_{m+1} &= \mathbf{R}_{m+1} - \mathbf{R}_m \\ \Delta\mathbf{r}_{m+1} &= \mathbf{K}_I(\mathbf{r}_m)^{-1}\Delta\mathbf{R}_{m+1} \\ \mathbf{r}_{m+1} &= \mathbf{r}_m + \Delta\mathbf{r}_{m+1} \end{aligned} \tag{43}$$

The initial condition $\mathbf{r_0=0}$. In this way, the load may be incremented up to the desired level. The accuracy may be increased by reducing the load increment. The method is illustrated for a single degree of freedom in Figure 3.3.

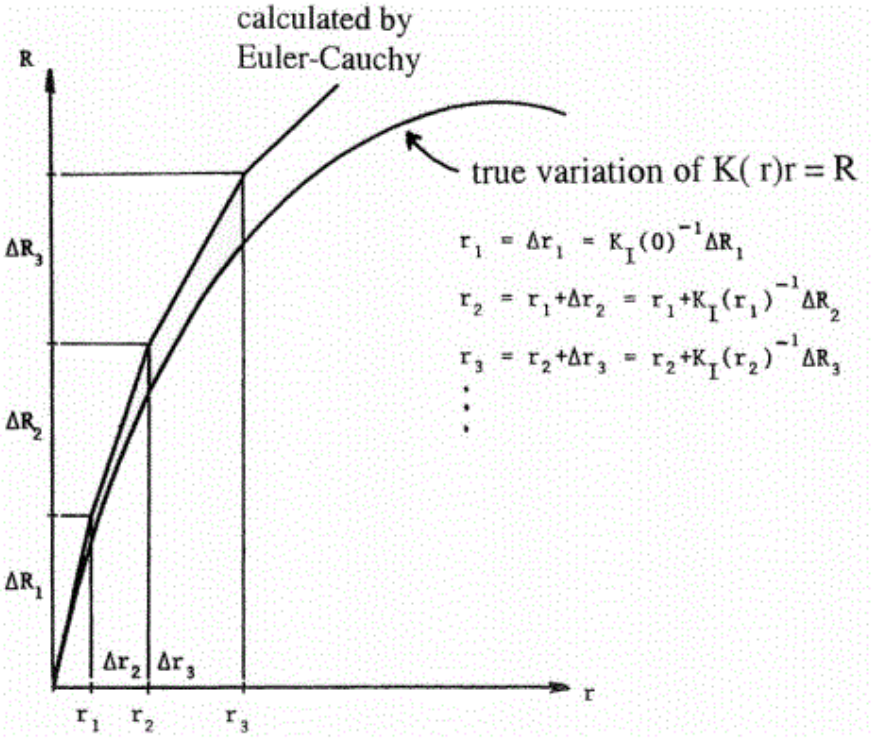

Figure 3. 3 Euler-Cauchy incrementing [31]

The second method is the Newton-Raphson method, which is the most frequently used iterative method for solving nonlinear structural problems. The method for a single d.o.f system is illustrated in Figure 3.4.

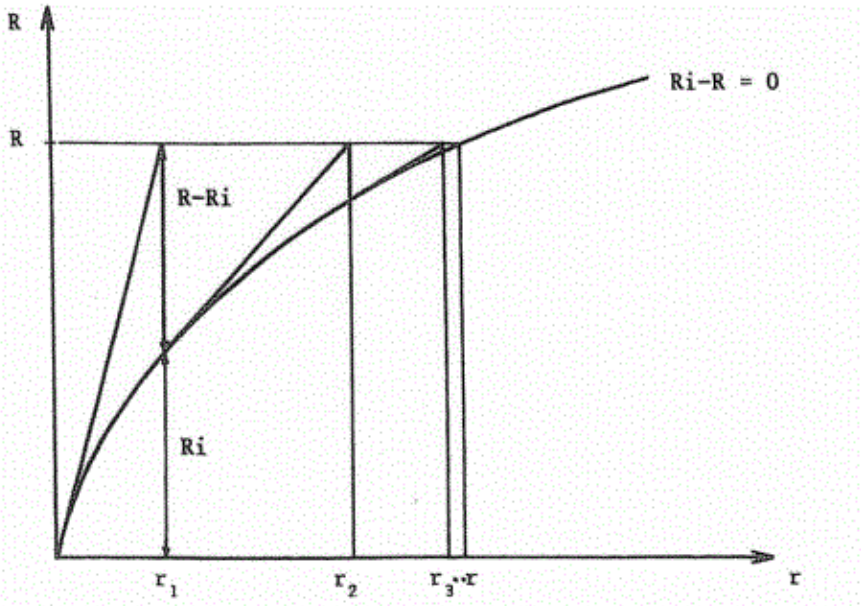

Figure 3. 4 Newton-Raphson Iteration [31]

The iteration formula is expressed:

$$\mathbf{r}_{n+1} - \boldsymbol{r}_n = \Delta \boldsymbol{r}_{n+1} = \boldsymbol{K}_1^{-1}(\boldsymbol{r}_n)(\boldsymbol{R} - \boldsymbol{R}_{int}) \tag{44}$$

This needs that $\Delta \boldsymbol{r}_{n+1}$ to be solved for each step and is time-consuming. By uploading $\mathbf{K_I}$ less frequently, reduced efforts are needed, which forms the modified Newton-Raphson iteration.

The third method is the combined method of incremental and iterative methods. The external load is applied in increments and in each increment equilibrium is achieved by iteration. The method is illustrated in Figure 3.5.

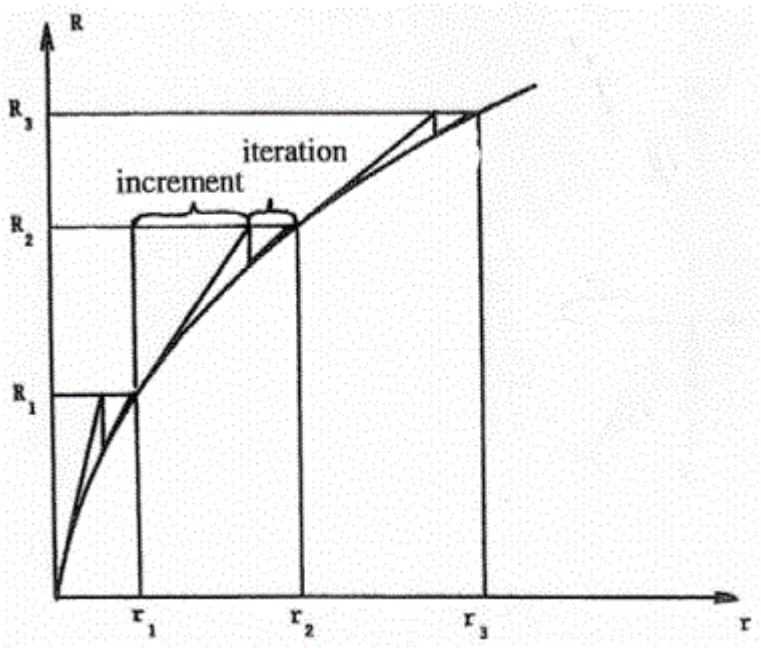

Figure 3. 5 Combined incremental and iterative solution procedures [31]

3.3 Whipping vibration analysis

The basic method of dynamic analysis is to solve the general equation of motion, which is given by:

$$m\ddot{x}(t) + c(x,\dot{x})\dot{x}(t) + k(x,\dot{x})x(t) = F(t) \tag{45}$$

For slamming induced response analysis, Eq. (45) usually needs to be solved in time domain with a given impact load history. However, it is not easy to estimate a force history in reality using numerical tools. Model tests are to be preferred. [8]

The magnitude of hull whipping response mainly depends on the strength and location of the slamming impulse. The important input is the shape of the slamming force history and the ratio of the duration of the load history to the natural period of the relevant hull girder vibration. In fact, time domain analysis needs to be avoided for its complicated and time consuming. Sometimes, quasi-static analysis could be used instead. Then the dynamic amplification magnification factor (DAF) is used to estimate the dynamic response in quasi-static analysis. If the slamming load history can be approximated by one of the standard shapes shown in Figure 3.6, and the maximum response is the main concern, the solution can be found from Figure 3.6 without solving Eq. (45). [8]

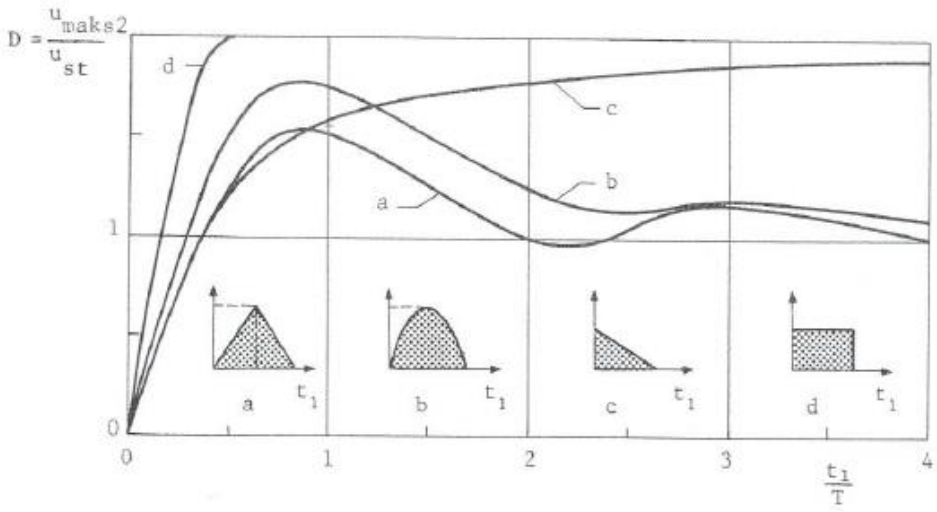

Figure 3. 6 Dynamic amplification factors for 4 different impulse shapes [8].

If the shape of the impulse is not known in detail, but the ratio of the load duration to the natural period is small enough, the response can also be found without solving Eq. (45) by using the unit impulse response function [8].

The coupling between low frequency deflections due to waves and the high frequency elastic hull vibrations is not included in the DAF. The coupling effect can only be obtained by considering the hydrodynamic wave and slamming pressures simultaneously, as well as applying the resulting pressure duration history to the structural response model. Thus, there are two different terminologies exist. The term '1-way coupling' refers to the method that hydrodynamic and structural response analysis performed independently. The term '2-way coupling' refers to the procedure when hydrodynamic and structural response analysis performed simultaneously, i.e. a hydro-elastic analysis is performed. [9]

Also the calculation of ship motions, wave loads and slamming pressures can be performed by different methods. A combination of methods used in the hydrodynamic and structural analysis of hull whipping vibrations is shown in Table 3.1.

Table 3. 1 Alternative methods/models used in the hydrodynamic and structural analysis of hull whipping vibration [9]

Hydrodynamic Excitation Load Analysis		**Coupling**	**Structural Response Analysis**
Ship Motions & Wave Pressures	**Slamming Pressures**		
A Non-linear 2D strip methods	**A** Analytical acc. impact and momentum theory	**A** decoupled	**A** FE Timoshenko beam reflecting vertical vibration modes
	B Non-linear 2D strip methods	**B** 1-way	**B** FE beam reflecting vertical, torsional and horizontal modes
B 3D potential Flow BEM methods	**C** 3D potential flow BEM methods	**C** 2-way	**C** 3D FE model
	D 3D RANSE methods		**D, E, F** Modal coordinates deduced from **A**, **B** and **C**, respectively

3.4 Modal methods

The seakeeping response of a ship is the combination of the rigid-body motion and the flexible response of the structure. For most linear wave-induced problems, the structure deformations are small, which allows to exclude the flexible structural response in calculation. The structural response can be computed after the rigid-body seakeeping calculation. However, this results in not fully account for all hydro-elastic effects.

The slamming induced response problem is in fact the hydro-elastic problem, which is easier solved by using generalized modes. All degrees of freedoms are described by generalized mode shapes, including rigid-body modes and flexible modes. The flexible modes are added to six rigid-body modes for hydro-elastic calculations. The flexible modes of the ship in this thesis can be presented in the following analysis, the pictures in Chapter 5.1.The concept of generalized modes can be used for both single ships and multi-body ships for hydro-elastic calculations. The rigid modes are added to each ship.

The calculation on base of generalized modes is in fact the modal approach, which is a common method to calculate the dynamic response of structures. A number of pre-calculated elastic modes are used to describe the structural response. The natural modes of the ship structure are the basic modes to be used, while, artificial mode shapes may also be used.

For an unconstrained structure in air, flexible response is considered to have no influence on the loading of the structure. Thus, the rigid-body response and the dynamic response of the structure can be solved separately. The natural modes computed by this uncoupled method are called dry natural modes. For the floating structure in water, hydro-elastic effects should be accounted for. It is necessary to solve the dynamic response using both the rigid-body modes and flexible modes simultaneously since that the hydrodynamics couple the rigid-body and flexible modes. This coupled calculation is hydro-elastic calculation. The natural modes computed in this way are called wet natural modes. It is necessary to use the hydro-elastic method when the flexible motions influence the loading of the structure.

A direct coupling between the seakeeping code and the structural solver is avoided by using the modal approach [30]. The dry mode shapes are calculated by a structural solver and these mode shapes are transferred to the hydrodynamic mesh. The wet mode shapes include the effect of added mass and hydro-static stiffness on the modal response and can be used to obtain resulting stresses, bending moments, motions, etc.

The natural modes of the ship structure are calculated using the finite element method. There are two alternative FE methods. The first one uses a 1D beam model of the ship structure. For simple calculation of global bending moment, it is easy to create a beam model of the ship structure. However, for more complex response calculation such as the response including torsion modes, it is not available to use the 1D beam model. The second method is a coupling with commercial 3D-FEM. The 3D FE models are available for complex response calculation. However, it requires more effort and time to create a 3D-FE ship model than a 1D beam model of the ship.

Only the global structural response can be calculated by the modal approach since that only a limited number of modes are needed. In case of local structural response calculation, it is necessary to transfer the dynamic loads on the structure and calculate the structural response within the structural program [30]. The local structural response can only be computed by using 3D-FE method. Thus, the seakeeping, slamming and internal loads of a selected event are transferred to the FEM program, which is used to solve the structural response.

3.4.1 Dry natural mode analysis

First, we simply consider the unconstrained structure in air and get dry mode shapes. The decoupled method neglecting the influence of hydro-elasticity is used.

Euler beam model is used in the analysis, assuming that no plastic deformation caused by this load levels. The model is shown in Figure 3.7.

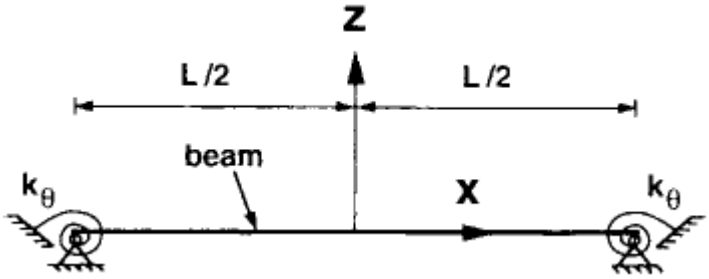

Figure 3. 7 Coordinate system used for local hydroelastic analysis of beam of length L. k_θ is the spring stiffness of spiral springs at the beam ends [4].

The beam equation of motion is expressed as

$$M_B \frac{\partial^2 w}{\partial t^2} + EI \frac{\partial^4 w}{\partial x^4} = p(x, w, t) \tag{46}$$

where

w is the deflection of the beam,

x is the longitudinal coordinate with *x = 0* in the middle of the beam,

t is the time-variable,

p is the hydrodynamic pressure as a function of beam deflection, x-coordinate and time-variable. In the free vibration mode analysis, *p* is equal to zero,

M_B is the structure mass per length square and is assumed constant,

EI is the bending stiffness per length width and is assumed constant.

The boundary conditions at the ends of the beam are expressed as

$$w(x, t) = 0 \qquad \text{at } x = \pm L/2 \tag{47}$$

$$\frac{k_\theta}{EI} \frac{\partial w}{\partial x} \pm \frac{\partial^2 w}{\partial x^2} = 0 \qquad \text{at } x = \pm L/2 \tag{48}$$

Eq. (47) means that the deflection is zero at beam ends. In the whole structure, this implies that this beam is less stiffener than the adjacent structure and is restrained by the adjacent structure. In the Eq. (48), k_Θ is the spring stiffness, $\partial \mathrm{w}/\partial \mathrm{x}$ is the slope of the beam. $k_\theta \cdot \partial \mathrm{w}/\partial \mathrm{x}$ represents the restoring moment of the spring at the left end of the beam, while the restoring moment of the spring at the right beam end has a negative sign. The second term in Eq. (48) is proportional to the beam bending moment $-EI\partial^2 w/\partial x^2$. Eq. (48) satisfies the requirement that the continuity of the bending moment at the rotational springs at the beam ends. If $k_\Theta = 0$, there is no bending moment at the beam ends, which means that the connection between the beams are hinge. If k_Θ is infinite, the slope of the beam ends is zero, which implies the clamped boundary condition. [4]

If the added mass distribution is similar to the structural mass distribution, the dry normal modes are a good approximation of the wet normal modes. Thus we first study the dry mode condition. When the solution is expressed in terms of dry normal modes ψ_n, that is,

$$w(x,t) = \sum_{n=1}^{\infty} a_n(t)\psi_n(x) \tag{49}$$

The eigenfunctions ψ_n are found by setting $p = 0$ in Eq. (46) and assuming a solution of the form $exp(i\omega_n t)\psi_n$, where ω_n are dry natural frequencies corresponding to the nth eigenmode ψ_n. This gives

$$-\omega_n^2 M_B \psi_n + EI\frac{d^4\psi_n}{dx^4} = 0 \tag{50}$$

Assuming that the load on the beam is symmetric about $x=0$, thus only the modes symmetric about $x=0$ is considered here.

Solutions of Eq. (50) can be expressed as

$$\psi_n = B_n \cos p_n x + D_n \cosh p_n x \tag{51}$$

where

$$p_n^4 = \frac{M_B \omega_n^2}{EI} \tag{52}$$

We find equations for ω_n, B_n and D_n by requiring that ψ_n satisfies the same boundary conditions as w, that is Eq. (47) and (48). We cannot determine B_n and D_n, only know how

B_n and D_n depend on each other. The hinged boundary condition is used here, which implies that $k_\Theta = 0$. Besides, $w = 0$, $\partial^2 w/\partial x^2 = 0$. This gives the mode shapes:

$$\psi_n = B_n \cos(p_n x) \tag{53}$$

with $p_{n+1}L/2 = \pi/2 + n\pi$, $n = 0, 1, 2, 3, \ldots$

Further, it has been shown by experiments that the first mode shape, i.e. n =1, has the dominant contribution. Thus, we mainly need to study the mode

$$\psi_1 = B_1 \cos(p_1 x) \tag{54}$$

where

$$p_1 \frac{L}{2} = \frac{\pi}{2} \tag{55}$$

Introducing Eq. (55) into Eq. (45), the lowest dry natural frequency is obtained

$$\omega_1 = \left(\frac{EI}{M_B}\right)^{1/2} \left(\frac{\pi}{L}\right)^2 \tag{56}$$

Other dry eigenvalues are expressed as

$$\omega_n = \left(\frac{EI}{M_B}\right)^{1/2} \left(\frac{(2n-1)\pi}{L}\right)^2 \tag{57}$$

Ψ_n is normalized by setting $B_1 = 1$, and then the beam deflection is expressed as

$$w(x,t) = a_1(t) \cos p_1 x \tag{58}$$

3.4.2 Wet natural mode analysis

However, the dry mode analysis is not applicable for real seakeeping problems. Slamming process contains the effect of the surrounding fluid on the dynamic response. Thus, wet mode analysis, which is based on the dry mode analysis is needed, including added mass and the hydrostatic-gravitational stiffness.

Assume incompressible fluid with the two-dimensional fluid potential flow theory, and no flow through the beam, which means

$$\frac{\partial \varphi}{\partial z} = \cos p_1 x \qquad \text{on } z = 0, -L/2 < x < L/2 \tag{59}$$

The gravity is neglected due to high oscillation frequency. The high-frequency free-surface condition is

$$\varphi = 0 \qquad \text{on } z = 0, |x| > L/2 \tag{60}$$

Here only a simple solution is needed by averaging *cos p_1x* over the beam length. Thus the Eq. (59) can be written as

$$\frac{\partial \varphi}{\partial z} = \frac{1}{L}\int_{-L/2}^{L/2} \cos p_1 x \, dx = \frac{2}{\pi} \qquad z = 0, -L/2 < x < L/2 \tag{61}$$

The velocity potential on the body is then written as

$$\varphi = \frac{2}{\pi}((L/2)^2 - x^2)^{1/2}, \qquad |x| < L/2, z = 0 \tag{62}$$

Then, when we use Eq. (58) to express the beam deflection, the corresponding velocity potential is expressed as

$$\phi = \dot{a}(t)\varphi(x) \tag{63}$$

The considered problem is linear in $\dot{a}(t)$. The corresponding pressure follows from the Bernoulli equation. Only the pressure terms linear to $\dot{a}(t)$ is considered, that is,

$$p = -\rho \partial \phi / \partial t = -\rho \ddot{a}_1(t) \frac{2}{\pi}((L/2)^2 - x^2)^{1/2}, \qquad |x| < L/2 \tag{64}$$

Substituting *p* and *w* given by Eq. (64) and (58) into Eq. (46) results in

$$\begin{aligned} M_B \ddot{a}_1(t) \cos p_1 x + EI \cdot p_1^4 a_1(t) \cos p_1 x \\ = -\rho \ddot{a}_1(t) \frac{2}{\pi}((L/2)^2 - x^2)^{1/2} \end{aligned} \tag{65}$$

We now use the method provided by Clough and Penzien (1993) to solve *$a_1(t)$*. Multiply the equation above with the first mode *cos p_1x* and integrate between *–L/2* and *L/2*. The final equation can now be written as

$$(M_{11} + A_{11})\frac{d^2 a_1}{dt^2} + C_{11} a_1 = 0 \tag{66}$$

where, M_{11} is the generalized structural mass expressed as

$$\mathrm{M}_{11} = M_B \int_{-L/2}^{L/2} \cos^2 p_1 x \, dx = 0.5 M_B L \tag{67}$$

A_{11} is the generalized added mass expressed as

$$A_{11} = \rho \frac{2}{\pi} \int_{-L/2}^{L/2} ((L/2)^2 - X^2)^{1/2} \cos p_1 x \, dx \tag{68}$$

C_{11} is the generalized stiffness expressed as

$$C_{11} = EI p_1^4 \int_{-L/2}^{L/2} \cos^2 p_1 x \, dx = 0.5 \omega_1^2 M_B L \tag{69}$$

Introduce the initial condition obtained from the structural inertia phase, Eq. (66) is solved satisfying zero initial deflection

$$a_1 = C \sin \omega_w t \tag{70}$$

where

$$\omega_{\mathrm{w}} = \left(\frac{\mathrm{C}_{11}}{\mathrm{M}_{11} + \mathrm{A}_{11}} \right)^{1/2} \tag{71}$$

is the wet natural frequency of the lowest eigenmode.

3.5 Direct integration methods

When solving dynamic equation of motion Eq. (45), the modal method is not the only method. An alternative method is the direct integration method, which is used in ABAQUS.

When solving the dynamic equation of motion, nonlinear structural effects make *k* as a function of *x*. This means that the loading *F* is increased (artificially) or as a function of time. The loading time needs to be sufficiently long so that the inertia and damping forces do not have an effect on the behavior on the static problem that is to be solved.

A finite difference approximation is used when the time derivatives of Eq. (45) ($\ddot{x}$ and $\dot{x}$) are replaced by differences of displacement *x* at various instants of time. The direct integration methods can successfully solve geometrical and material nonlinear problems.

The finite difference methods are called explicit if the displacements at the new time step, *t+Δt*, can be obtained by the displacements, velocities and accelerations of precious time steps.

$$x(t+\Delta t) = f\{r(t), \dot{r}(t), \ddot{r}(t), r(t-\Delta t), \dot{r}(t-\Delta t), \ddot{r}(t-\Delta t), \ldots\} \tag{72}$$

or

$$x_{i+1} = f\{x_i, \dot{x}_i, \ddot{x}_i, x_{i-1}, \dot{x}_{i-1}, \ddot{x}_{i-1}, \ldots\} \tag{73}$$

This is opposed to the implicit finite difference formulations where the displacements at the new time step, *t+Δt*, are expressed by the velocities and accelerations at the new time step, in addition to the historical information at previous steps.

$$x_{i+1} = f\{\dot{x}_{i+1}, \ddot{x}_{i+1}, x_i, \dot{x}_i, \ddot{x}_i, \ldots\} \tag{74}$$

One of the explicit solution methods is the central difference method. The central difference method is based on the assumption that the displacements at the new step, *t+Δt*, and the previous time step, *t-Δt*, can be found by Taylor series expansion.

$$x_{i+1} = x_0(t) + \Delta t\, \dot{x}_i + \frac{\Delta t^2}{2}\ddot{x}_i + \frac{\Delta t^3}{6}\dddot{x}_i + \cdots \qquad (\text{with } x_0(t)=x_i) \tag{75}$$

$$x_{i-1} = x_i - \Delta t\, \dot{x}_i + \frac{\Delta t^2}{2}\ddot{x}_i - \frac{\Delta t^3}{6}\dddot{x}_i + \cdots \tag{76}$$

The terms with time steps to the power of three and higher are neglected. Subtracting Eq. (76) for Eq. (75) yields:

$$x_{i+1} - x_{i-1} = 2\Delta t \dot{x}_i \tag{77}$$

Adding Eq. (76) and Eq. (75) yields:

$$x_{i+1} + x_{i-1} = 2x + \Delta t^2 \ddot{x}_i \tag{78}$$

Rearranging Eq. (77) and Eq. (78), the velocities and accelerations at the current time step can be expressed as:

$$\dot{x}_i = \frac{1}{2\Delta t}\{x_{i+1} - x_{i-1}\} \tag{79}$$

$$\ddot{x}_i = \frac{1}{\Delta t^2}\{x_{i+1} - 2x_i(t) + x_{i-1}\} \tag{80}$$

Finally inserting Eq. (79) and Eq. (80) into the dynamic equation of motion Eq. (45) gives:

$$\begin{aligned}\left\{\frac{1}{\Delta t^2}m + \frac{1}{2\Delta t}c\right\}x_{i+1} \\ = F_i(t) - k\,x_i(t) + \frac{1}{\Delta t^2}m\{2x_i - x_{i-1}\} + \frac{1}{2\Delta t}c\,x_{i-1}\end{aligned} \tag{81}$$

If the mass matrix and damping matrix are diagonal, the equations will be uncoupled, and the displacements at the next time step, $t+\Delta t$, can be obtained without solving simultaneous equations. Then $x_{i(i+1)}$ can be directly, explicitly determined by the response at time t. There is no coupling between displacements, $x_{j(i+1)}$ at the time $t+\Delta t$.

The Eq. (81) is conditionally stable and requires that

$$\Delta t < \frac{2}{\omega_{max}} \tag{82}$$

Where ω_{max} is the highest natural frequency of

$$\det(\mathrm{k} - \omega^2\mathrm{m}) = 0 \tag{83}$$

This maximum frequency is bounded by the maximum frequency of the constituent unassembled and supported elements. When finding the maximum natural frequency of an element, one will see that the time step, Δt, must be short enough that information does not propagate across more than one element per time step. The maximum allowable time step will therefore be limited by a characteristic length, λ_e, of the element and the acoustic wave speed, c.

$$\Delta t < \frac{\lambda_e}{c} \tag{84}$$

Higher order elements yield higher maximum frequencies and should be avoided when doing explicit integration.

The advantages and drawbacks of explicit and implicit method used in ABAQUS will be presented in the following section.

3.6 Dynamic analysis with ABAQUS

There are a number of different computer programs available in the market for dynamic analysis of ships and offshore structures, for instance ABAQUS package, ANSYS, SESAM-DNV package, GL shipload etc. In this project, ABAQUS is used for dynamic analysis.

In Abaqus/Standard, dynamic studies are generally performed using eigenmodes as a basic of calculating. The necessary eigenmodes and eigenvalues are calculated first in a frequency extraction step. Eigenmode extraction can become computationally intensive in case of many modes for a large model. [11]

3.6.1 Eigenvalue Extraction

Frequency extraction procedure is a linear perturbation procedure to calculate the natural frequencies and the corresponding mode shapes of a system. There are three eigenvalue extraction methods: [11]

- Lanczos
- Automatic multi-level substructuring (AMS), an add-on analysis capability for Abaqus/Standard
- Subspace iteration

Lanczos method, i.e. the default eigenvalue extraction method, is used in the current work. It has the most general capabilities with less limitations, however, is slower than the AMS method.

The Lanczos Eigen Solver is an extended version of the Inverse Power Method, where blocks of frequencies are evaluated incrementally [11].

$$[M]([K] - \sigma[M]^{-1})[M]\{\phi\} = \theta[m]\{\phi\} \tag{85}$$

Where σ is a converging shift and Θ is the eigenvalue. A new shift is formed after each convergence. The result is transformed to frequency:

$$\omega^2 = \frac{1}{\theta} + \sigma \tag{86}$$

When dealing with ABAQUS, the maximum frequency of interest or the number of eigenvalues needs to be provided. Abaqus/Standard determines a suitable block size. Another choice is to specify the minimum frequencies, and Abaqus/Standard will extract eigenvalues until either the requested number of eigenvalues has been extracted in the given range or all the frequencies in the given range has been extracted. [11]

3.6.2 Implicit versus explicit dynamic analysis

As has been illustrated in section 3.5, the dynamic motion equation can be solved by direct integration dynamic procedure which is provided in ABAQUS. There are two ways to conduct direct integration.

- Eq. (45) is solved only at discrete time intervals "Δt", instead of any time "t",
- The variation of the displacements, velocities and accelerations are assumed within each time interval "Δt".

It is obvious that the choice criteria on these assumption determines the accuracy, stability and cost of the solution procedure. The choice stands between the using of explicit or implicit time integration method. [13]

Abaqus/Explicit uses the explicit method, i.e. the central difference method, where the displacement equilibrium solution at time "t+Δt" is based on using the equilibrium condition at time "t". Displacements and velocities need to be known at the beginning of an increment, thus the stiffness and mass matrices need no factorization for each increment, which means that each increment is relatively inexpensive compared to the increments in an implicit integration method. The disadvantage of this method is that it cannot be applied in the simulation of static phenomena in case of mass and damping effects neglected. However, since that the explicit integration method is conditionally stable, it requires that the time step "Δt" smaller than a critical value Δt_{cr}. If a time step "Δt" is larger than the critical value Δt_{cr} , the integration is unstable. This critical value can be calculated from the mass and stiffness properties of the complete element. More specifically, in order to obtain a valid solution (in case of no damping):

$$\Delta t \leq \Delta t_{cr} = \frac{2}{\omega_{\max}} \tag{87}$$

where ω_{max} is the highest frequency of the finite element assemblage with "n" degrees of freedom. An approximation to the stability limit is written as the smallest transit time of a dilatational wave across any of the elements in the mesh: [13]

$$\Delta t_{cr} \approx \frac{L_{\min}}{\mathrm{c_d}} \tag{88}$$

where

L_{min} is the smallest element dimension in the mesh,

c_d is the dilatational wave speed in terms of effective Lame's constants.

Abaqus/Standard uses the implicit method, where the equilibrium conditions at time "t+ Δt" is used at the same time with the displacement field. The velocity and acceleration are calculated in terms of displacement by using finite difference expressions. The implicit operator options are unconditionally stable and thus there is no limit on the size of the time step "Δt". Different from the explicit method, the implicit method can be applied to both dynamic and static problems. Besides, explicit method offers fewer element types than implicit method.

The implicit integration procedure is used for the response analysis in the work for the reasons below:

- used for nonlinear dynamic response.
- can be both fully nonlinear or based on the modes of the linear system.
- can be used to study a variety of applications, such as dynamic responses requiring transient fidelity , nonlinearity, involving minimal or moderate energy dissipation, as well as certain type of quasi-static responses.

3.6.3 Time integration methods

In general, the Hilber-Hughes-Taylor time integration is used in Abaqus/Standard unless quasi-static analysis is specified. The backward Euler operator is used for quasi-static analysis. The Hilber-Hughes-Taylor operator is an extension of the Newmark β-method.

Numerical parameters associated with the Hilber-Hughes-Taylor operator are tuned differently for moderate dissipation and transient fidelity applications. [14]

When applying implicit integration procedure, the operator matrix must be inverted and the corresponding dynamic equilibrium equations must be solved for each time step. This solution needs iterative procedure by using Newton's method. Marching through a simulation with a finite time increment size generally introduces same degree of numerical damping, which is different from the material damping. [15]

Default parameters for the Hilber-Hughes-Taylor operator are shown in Table 3.2.

Table 3. 2 Default parameters for the Hilber-Hughes-Taylor operator

Parameter	**Application**	
	Transient Fidelity	Moderate Dissipation
α	-0.05	-0.41421
β	0.275625	0.5
ϒ	0.55	0.91421

The time increment size is specified in the analysis. The analysis terminates if convergence tolerances are not satisfied within the maximum number of iterations allowed.

4 Finite Element Modelling

4.1 Sesam model

In general, the model used in dynamic analysis must reflect the structure's dynamic properties in the frequency range of interest, i.e. the eigenfrequencies and mode shapes. 3D finite element model of a ship hull with local FE mesh refinements is recommended here.

The ship to be analyzed in the work here is owned by Wagenborg which is a multi-purpose cargo/container ship. The bench mark committee has provided all the information about the ship and corresponding sea condition. The lines plan of the ship is shown in Appendix A. The main dimensions are given below:

MAIN PARTICULARS

Length o.a.	:	132.20 m
Length p.p.	:	123.84 m
Length rule	:	123.04 m
Breadth mld.	:	15.87 m
Design draught	:	7.05 m
Depth to maindeck	:	9.65 m
Scantling draught	:	7.05 m
Service speed	:	15 kn
Max. displacement	:	11475 ton

Three-dimensional finite element method is a common method to analyze dynamic response of a ship. In this thesis, the panel model of the ship is originally modelled in Sesam Genie, and then analyzed in HydroD to get added mass and hydrodynamic damping.

The wheelhouse, superstructure and forecastle are not included in the model. The model only contains outer shell hull, inner shell hull and stiffeners. In HydroD, all the relevant environmental load condition and sea state are modelled properly. Properties and sections are not assigned to the model in Genie.

In order to make comparison, three ship models are made. The ships are modelled with no bulkhead, 5 bulkheads and 7 bulkheads. The panel modelS established by Sesam are shown in figures below:

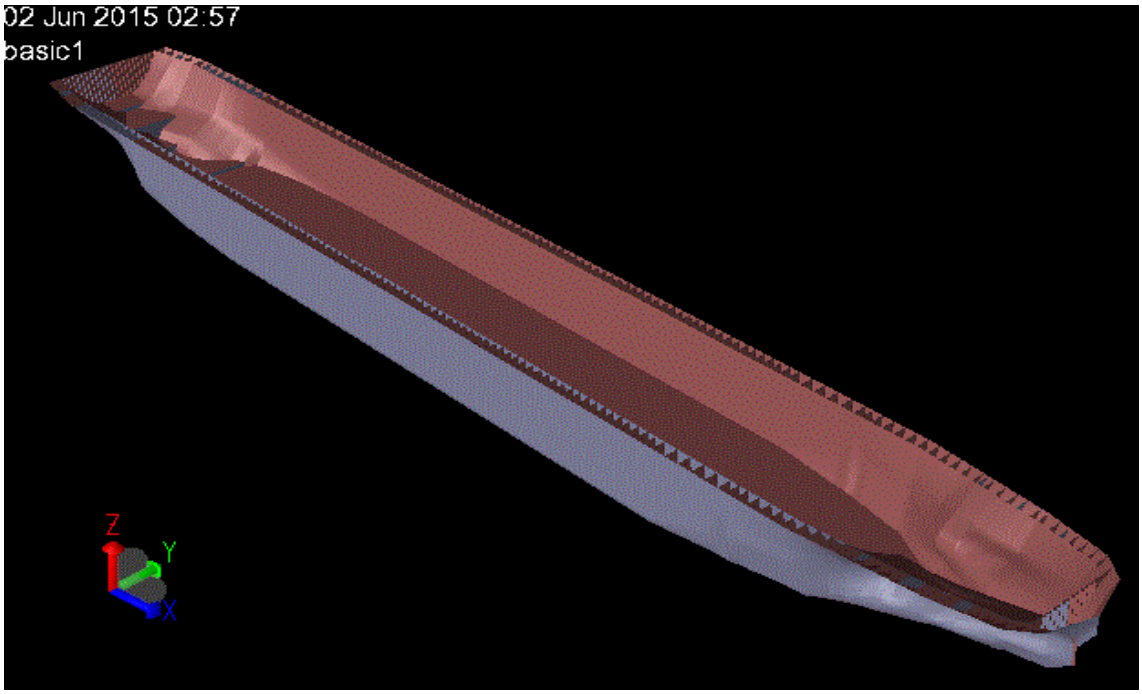

Figure 4. 1 Panel ship model with no bulkhead

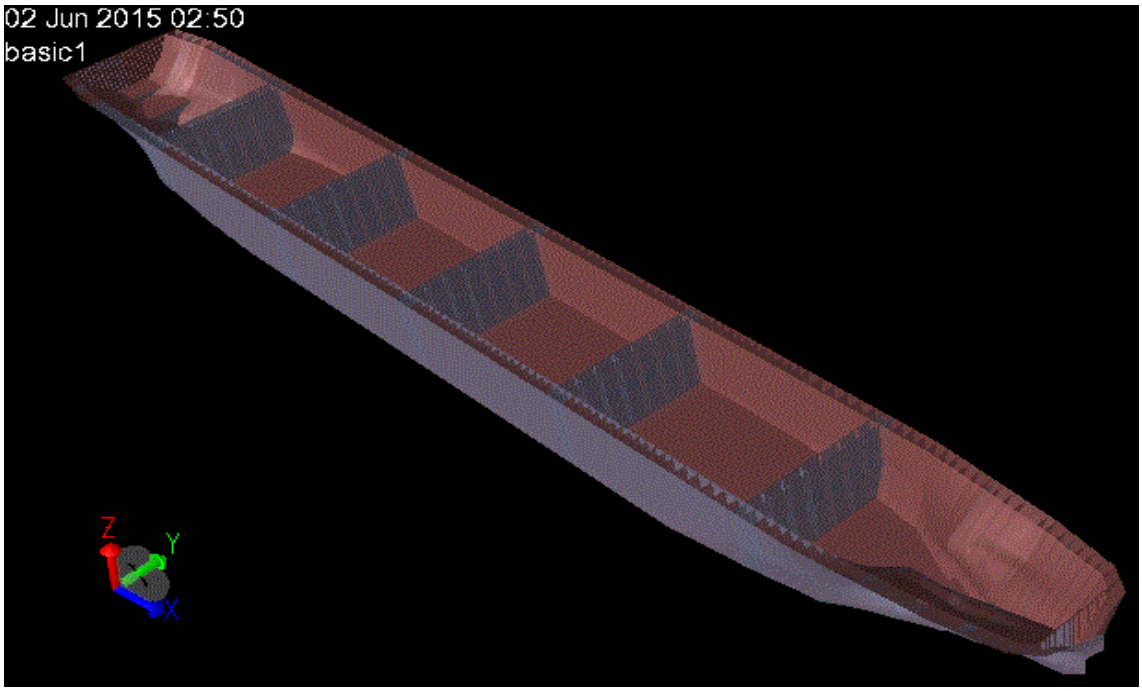

Figure 4. 2 Panel ship model with 5 bulkheads

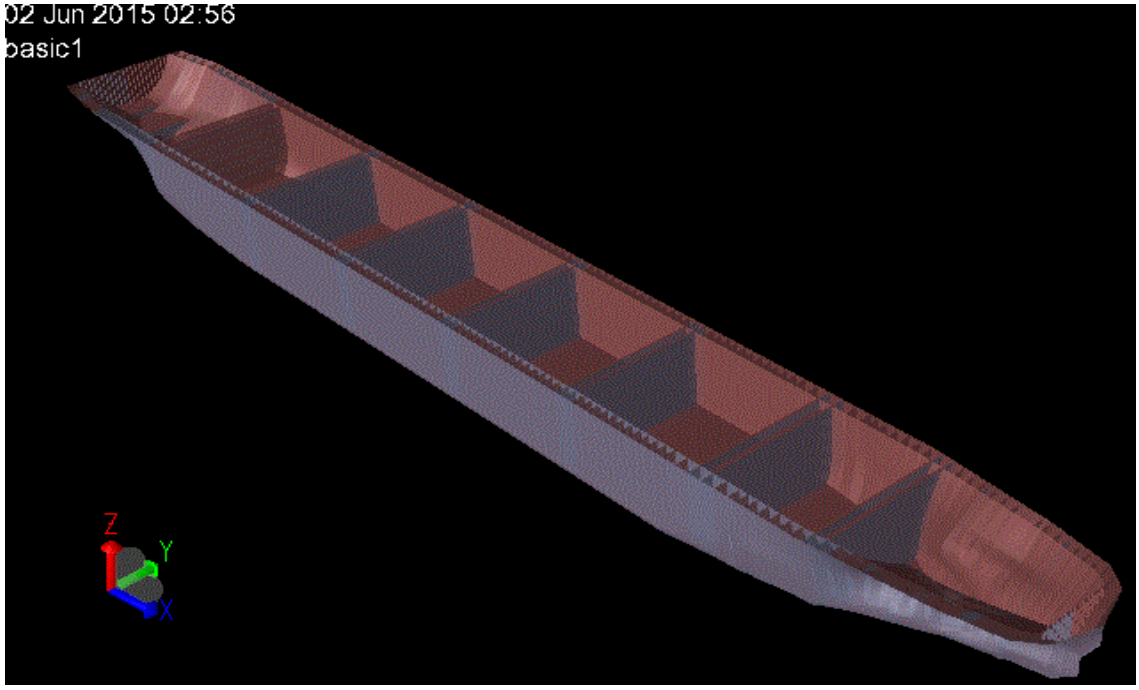

Figure 4. 3 Panel ship model with 7 bulkheads

4.2 ABAQUS model

The panel models made in Genie are imported in ABAQUS for analyzing. The material properties and sections are defined in ABAQUS.

The material for the steel used in the ship is St 42 grade shipbuilding steel and its properties are given below:

- Elasticity modulus = $2.1e^{11}$ N/m^2
- Poisson ratio = 0.30
- Density = 7850 kg/m^3
- Shell thickness = 0.015 m

Mass distribution of the ship is shown in Appendix B. Cargo loading is applied as inertial mass elements distributed along corresponding areas of the ship model.

Slamming is much more likely to occur for the ship in ballast condition than in fully loaded condition. Thus, in this thesis, ballast ship condition is analyzed.

Added mass and hydrostatic stiffness are added to wet mode analysis. As has been explained in Chapter 2, slamming can cause transient heave, pitch and global vertical elastic vibrations. Further it is assumed that the added mass and hydrostatic stiffness in the heave direction is dominated. Thus, added mass is the applied to model the same way as cargo loading and ship mass. Hydrostatic stiffness is imported as linear spring elements at all nodes below the waterline. And when modelling in ABAQUS, the degree of freedom is chosen 3, the spring type is chosen Connect Points to Ground. The axial stiffness is taken equal for each spring element to obtain a uniform buoyancy distribution.

Shell elements are used for model. Conventional S4 and S3 finite element are used for plates in ABAQUS. These elements provide the following characterizes: [11]

- Uniformly reduced integration to avoid shear and membrane locking.
- The element has several hourglass modes that may propagate over the mesh.
- Converges to shear flexible theory for thick shells and classical theory for thin shells.
- S4R is a robust, general purpose element that is suitable for a wide range of applications.

The ABAQUS ship model with 5 bulkheads is shown in Figure 4.4. Other ABAQUS ship models are presented in Appendix C.

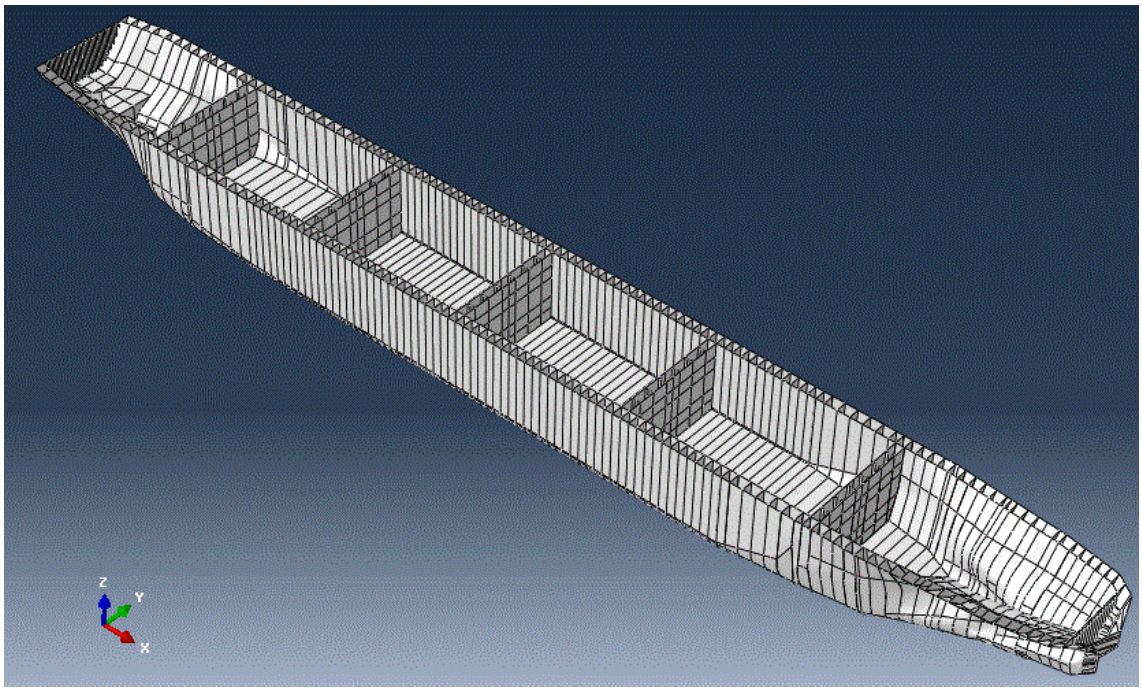

Figure 4. 4 ABAQUS ship model with 5 bulkheads

When meshing the model, structured, quad-dominated element is the first choice, especially for the middle part of ship hull, where the geometry is regular. For other parts, free and tri elements can be chosen. Normally, the degree of fineness of modelling, or mesh size, depends on what kind of response we might expect. In this thesis, global response is of main concern, mesh size needs not to be too small. Mesh size for most part of the ship is defined as 0.8m. The mesh size at the ship bow and stern should be smaller due to the irregular geometry.

- Total number of nodes: 19828
- Total number of elements: 25238
- 23314 liner quadrilateral elements of type S4R
- 1924 linear triangular elements of type S3

The mesh model of ship with 5 bulkheads is shown in Figure 4.5. Other mesh models are presented in Appendix C.

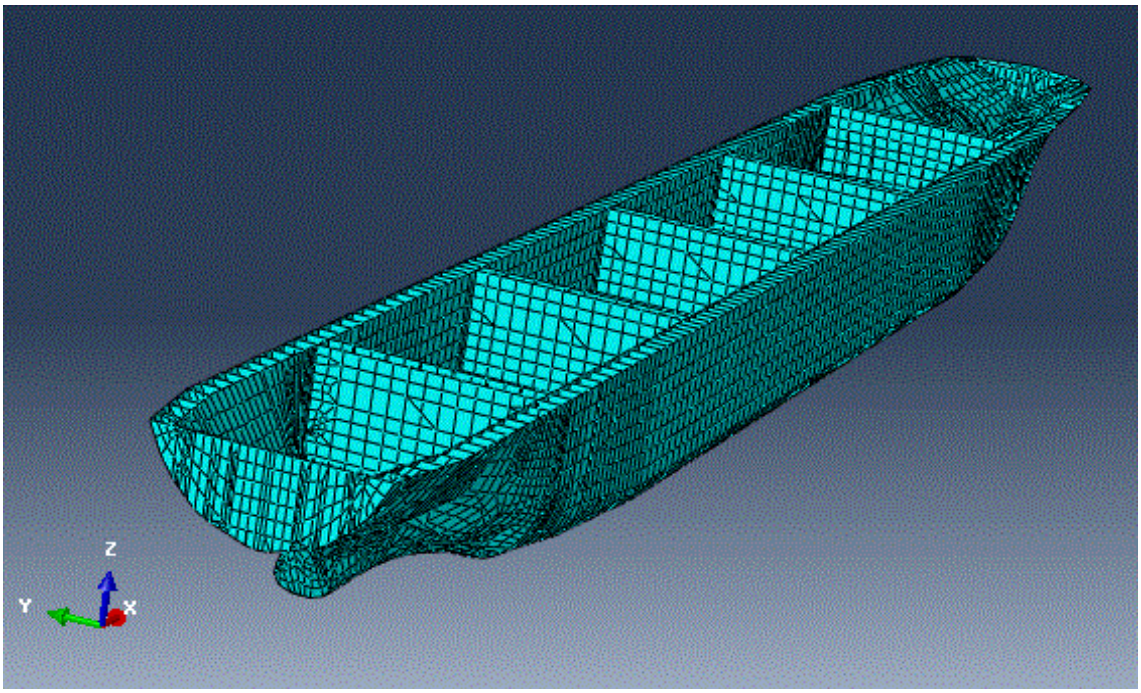

Figure 4. 5 Mesh model of the ship with 5 bulkheads

For natural mode analysis, 'Frquency' is chosen as step type and 'Lanczos' is chosen as eigensolver.

For dynamic response analysis, 'Dynamic, Implict' is chosen as step type. Time period is specified as 5 to get the convergence results. The fixed increment size varies according to the requirement of the results. The fixed increment size influence the analysis time.

Slamming occurs most possibly at the fore part of the ship since that it has the largest relative vertical velocity between the ship and waves. Combination of the heave and pitch motions may lead to the sudden immersion of the forward part of the ship in the water and thus the bottom slamming will occur. The subsequent re-entry of the ship results in impact between the free surface and the bottom. [3]

Hence, loads with different scale and time history are added on the bottom of ship bow in ABAQUS model for analysis. The wave impact loads are added as concentrated force.

5 Results and Analysis

5.1 Natural mode and frequency

Determination of the natural frequencies and mode shapes are very useful to investigate the dynamic behavior of the ship. Linear perturbation analysis is used in this part. Linear perturbation analysis can be performed from time to time during a fully nonlinear analysis by including the linear perturbation steps between the general response steps. The linear perturbation response has no effect as the general analysis is continued. The step time of linear perturbation steps is never accumulated into the total time. [11]

In linear perturbation analysis, the frequency extraction procedure is performed to calculate the natural frequencies and the corresponding mode shapes. First 15 natural modes are requested for the output.

The first 6 mode shapes are rigid body modes which are of no interest. The corresponding mode frequencies are very low. However, if missing or mixing of rigid mode shapes happens, an erroneous FE modeling is implied and check is needed.

5.1.1 Ship model with no bulkhead

Wet natural mode shapes of the ship model with no bulkhead in ballast condition are presented below:

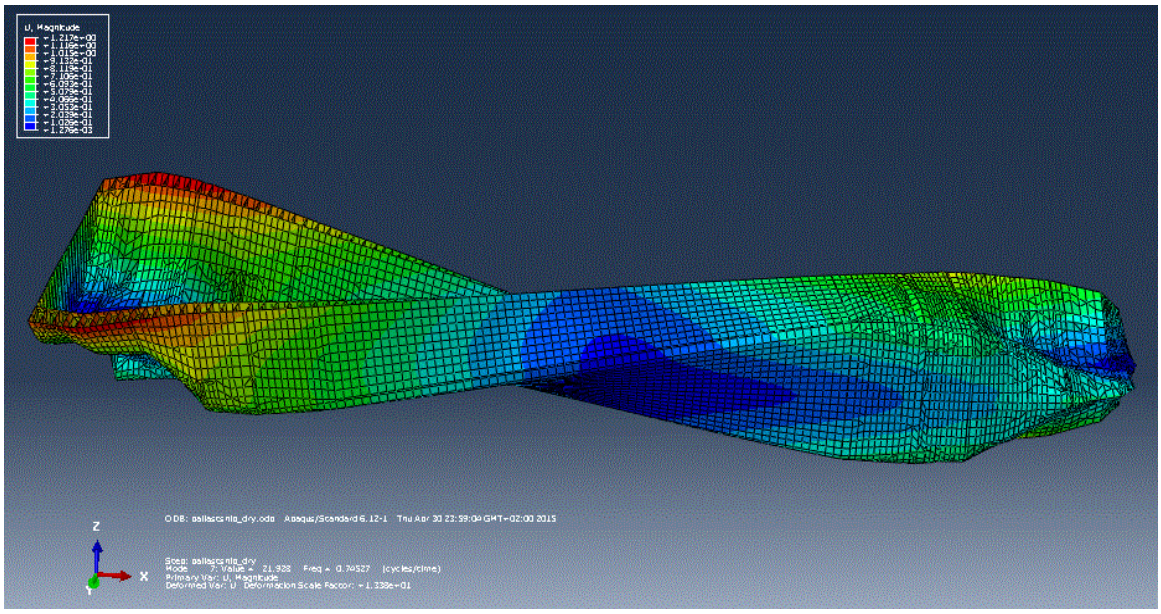

Figure 5. 1 Global torsional mode of the ship with no bulkhead

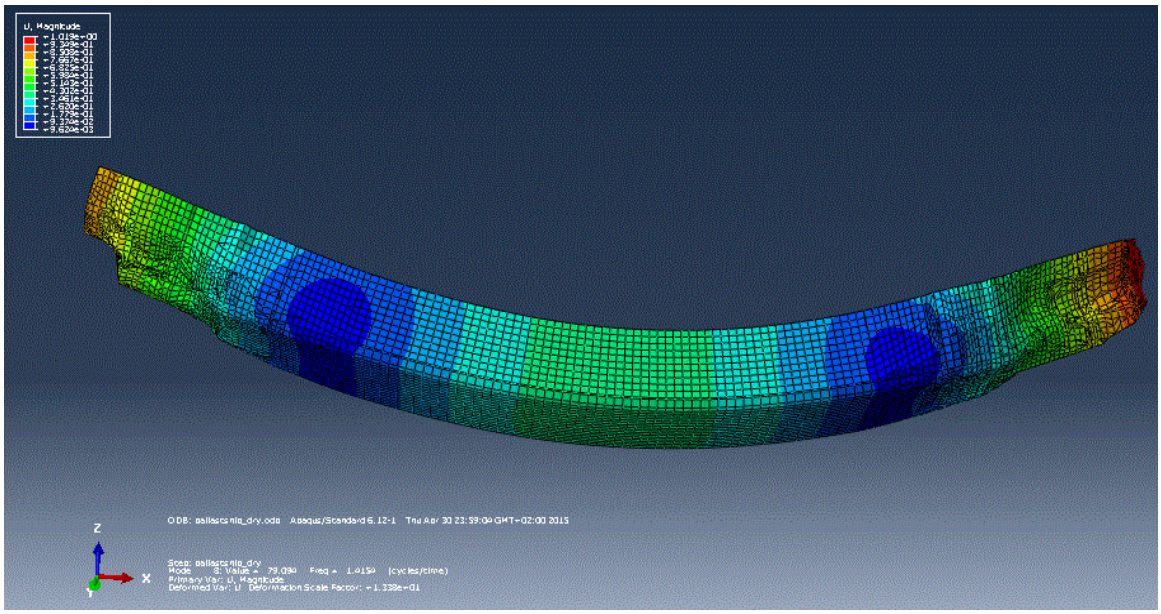

Figure 5. 2 2-node vertical bending mode of the ship with no bulkhead

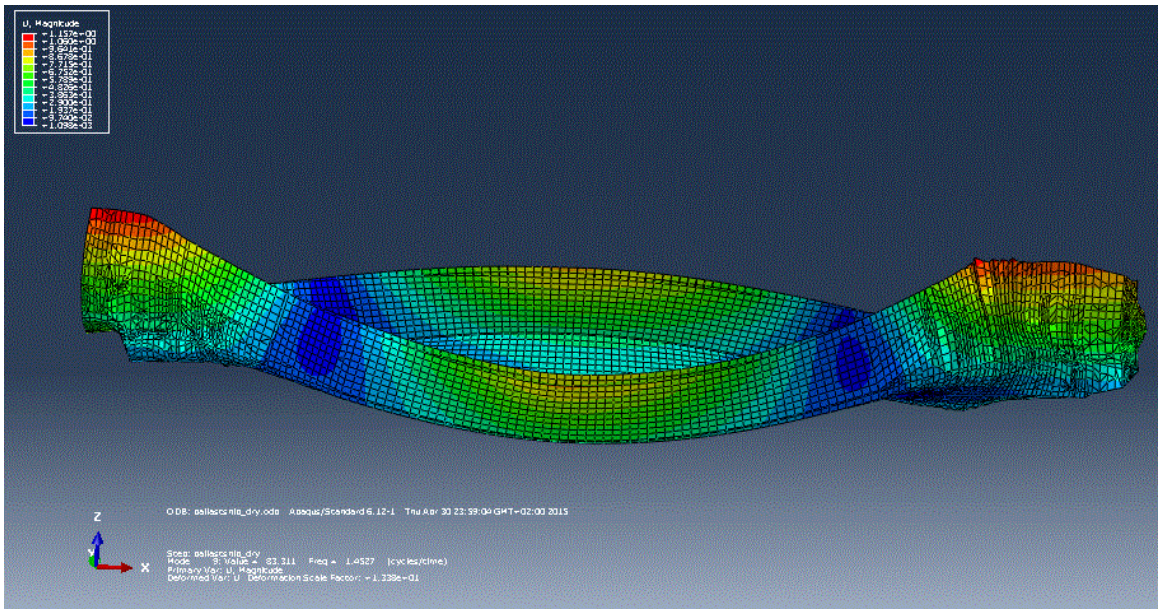

Figure 5. 3 Global torsional and horizontal bending mode of the ship with no bulkhead

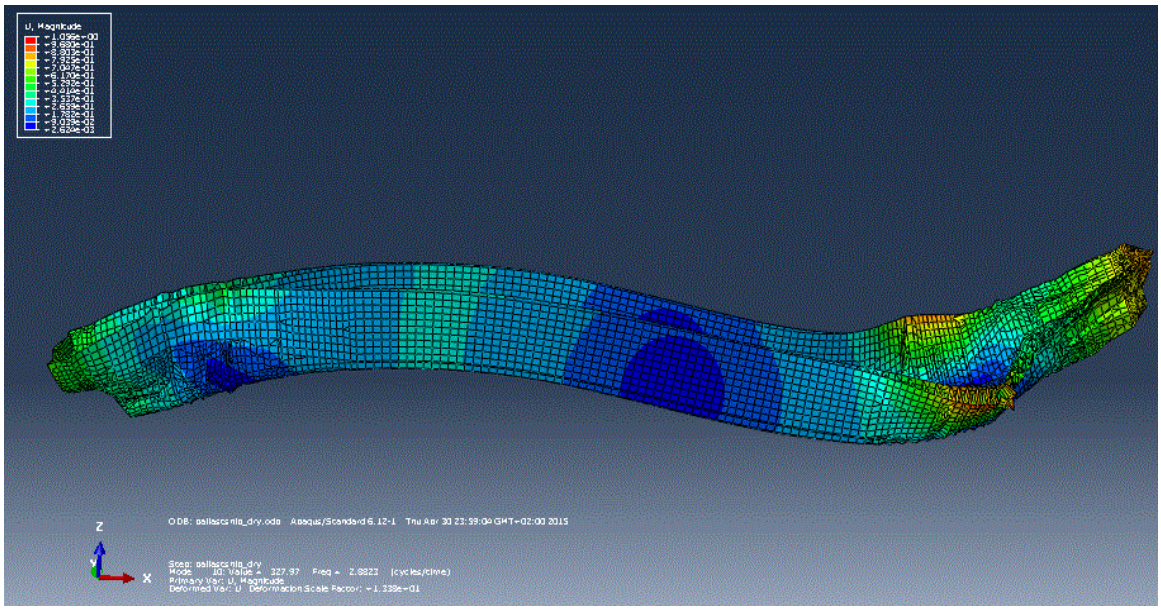

Figure 5. 4 3-node vertical bending mode of the ship with no bulkhead

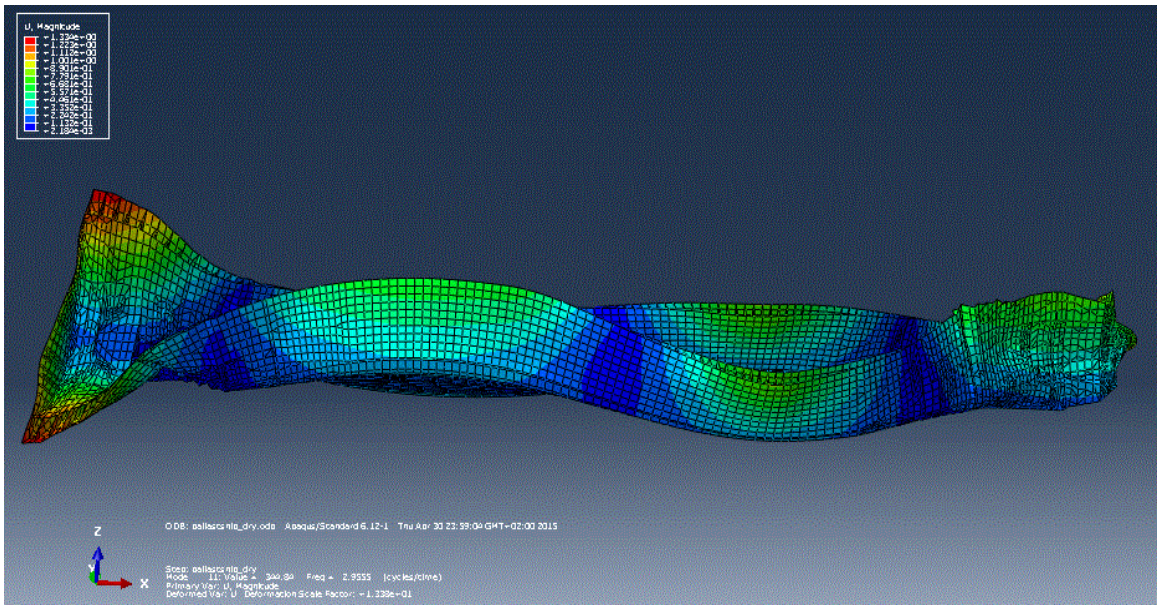

Figure 5. 5 Global torsional and 3-node bending mode of the ship with no bulkhead

For ship with no bulkheads, there are five global flexible modes. Others are rigid-body modes and local flexible modes.

5.1.2 Ship model with 5 bulkheads

Wet natural mode shapes of the ship model with 5 bulkheads in ballast condition are presented below:

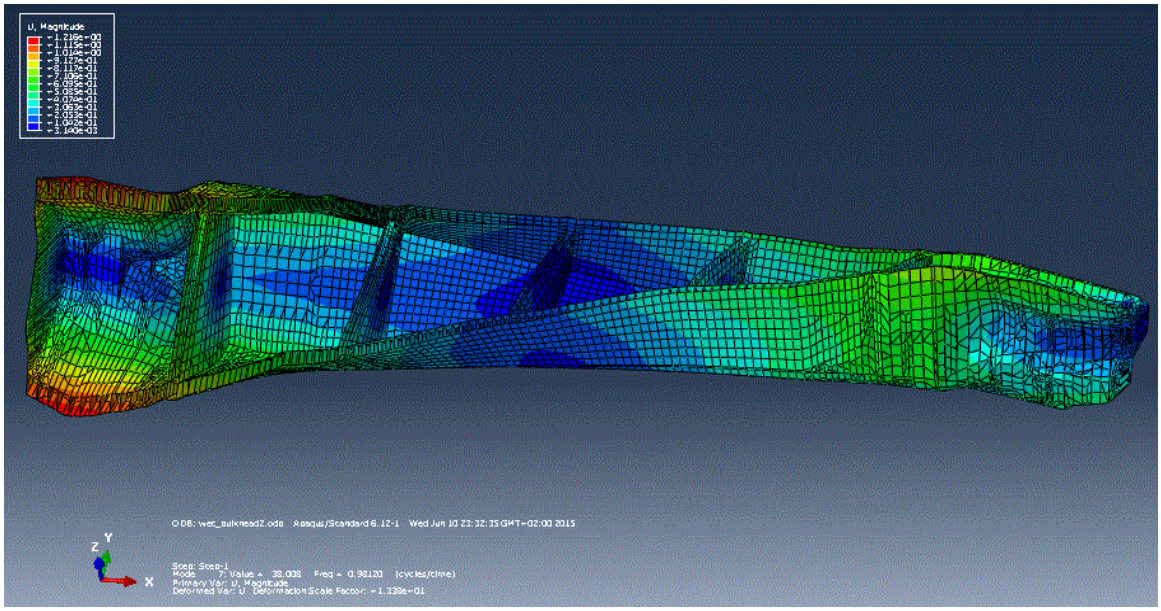

Figure 5. 6 Global torsional mode of the ship with 5 bulkheads

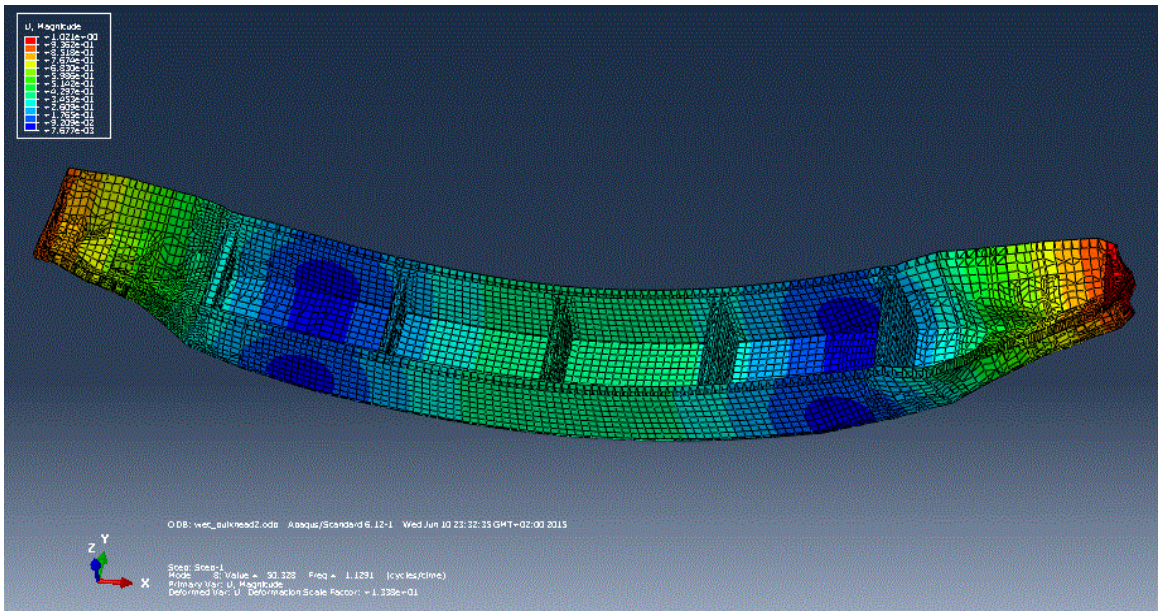

Figure 5. 7 2-node vertical bending mode of the ship with 5 bulkheads

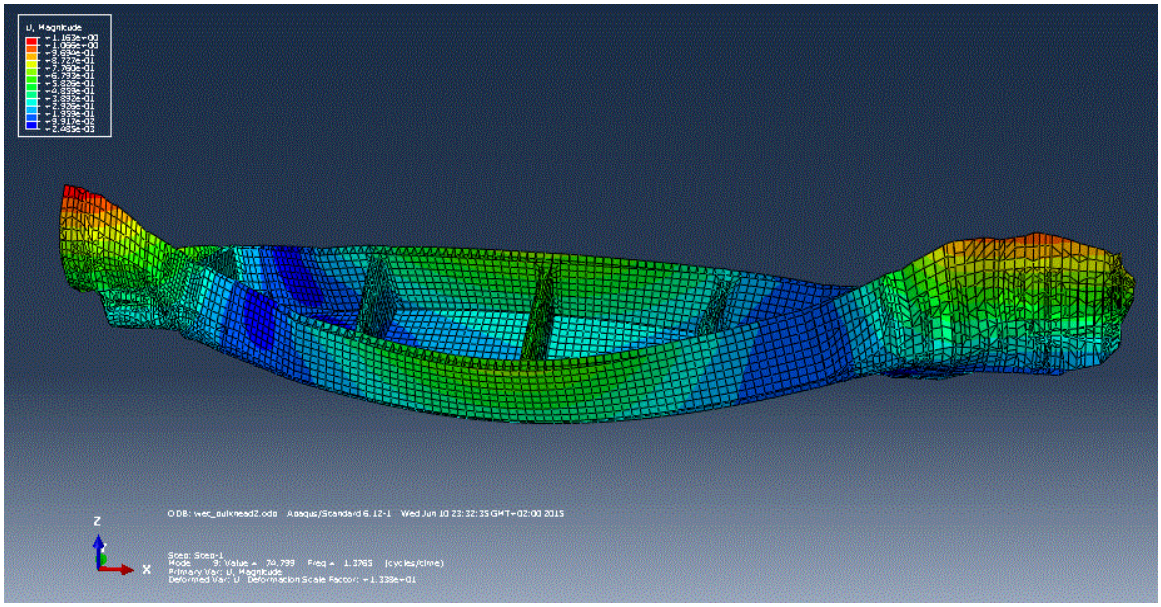

Figure 5. 8 Global torsional and horizontal bending mode of the ship with 5 bulkheads

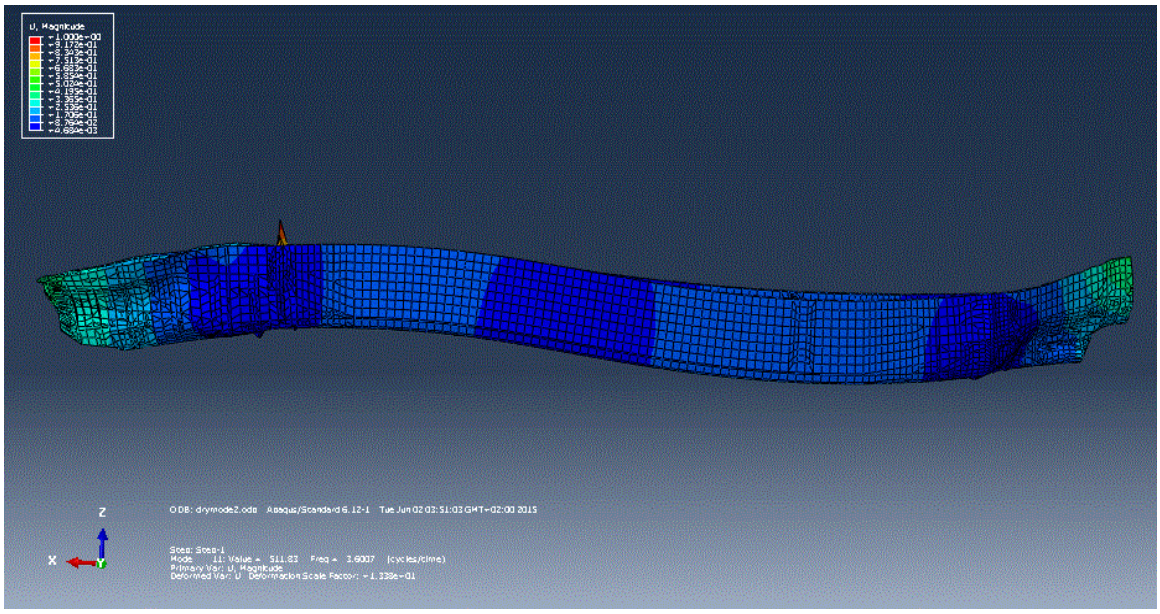

Figure 5. 9 3-node bending mode of the ship with 5 bulkheads

For the ship with 5 bulkheads, there are four global flexible modes. Others are rigid-body modes and local flexible modes.

It is seen from Figure 5.9 that the deformation of 3-node bending mode shape of the ballast ship is not obvious. In comparison, 3-node bending mode shape of the same ship model in lightship condition is analyzed and shown in Figure 5.10.

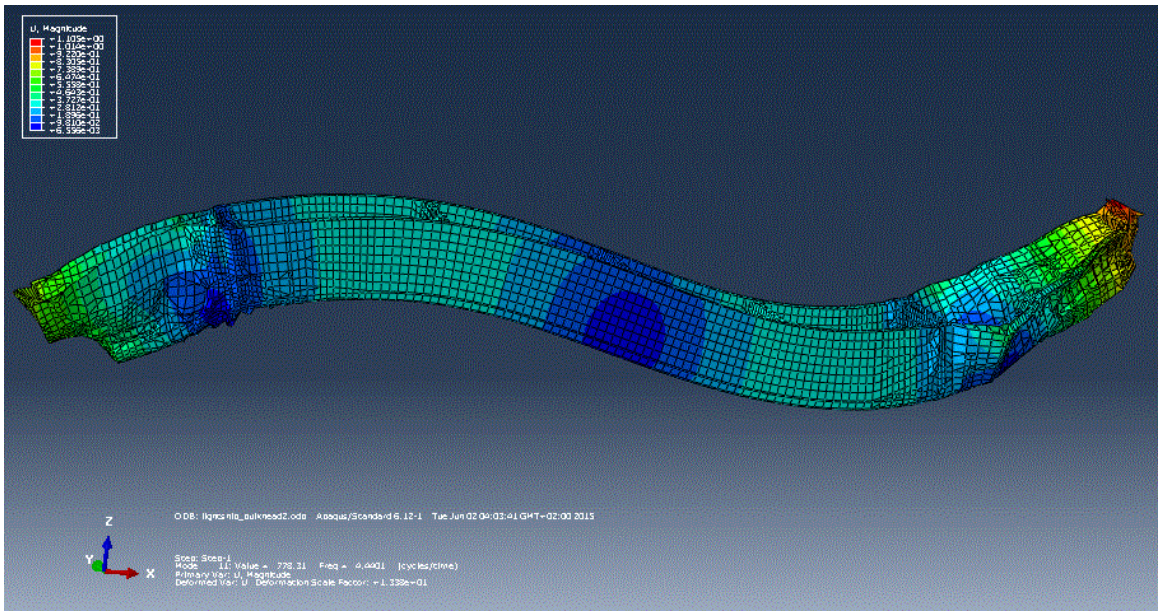

Figure 5. 10 3-node bending mode of the ship with 5 bulkheads (lightship condition)

The deformation in Figure 5.10 is much more obvious than that in Figure 5.9. The difference between ballast ship and lightship is caused by the added mass of fuel and ballast.

5.1.3 Ship model with 7 bulkheads

Wet natural mode shapes of the ship model with 7 bulkheads in ballast condition are presented below:

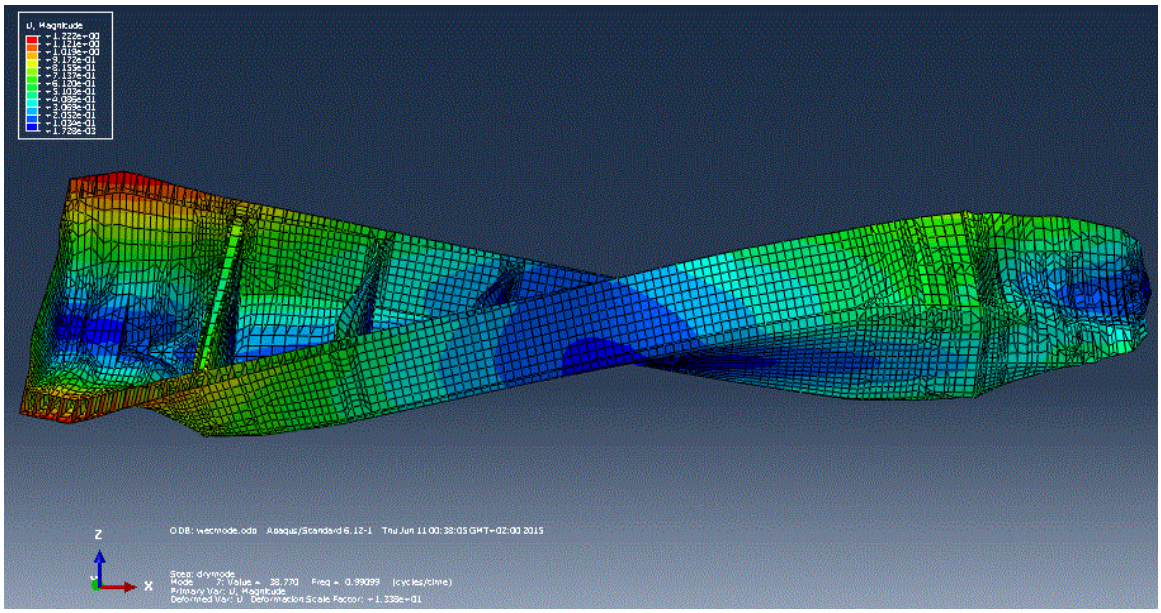

Figure 5. 11 Global torsional mode of the ship with 7 bulkheads

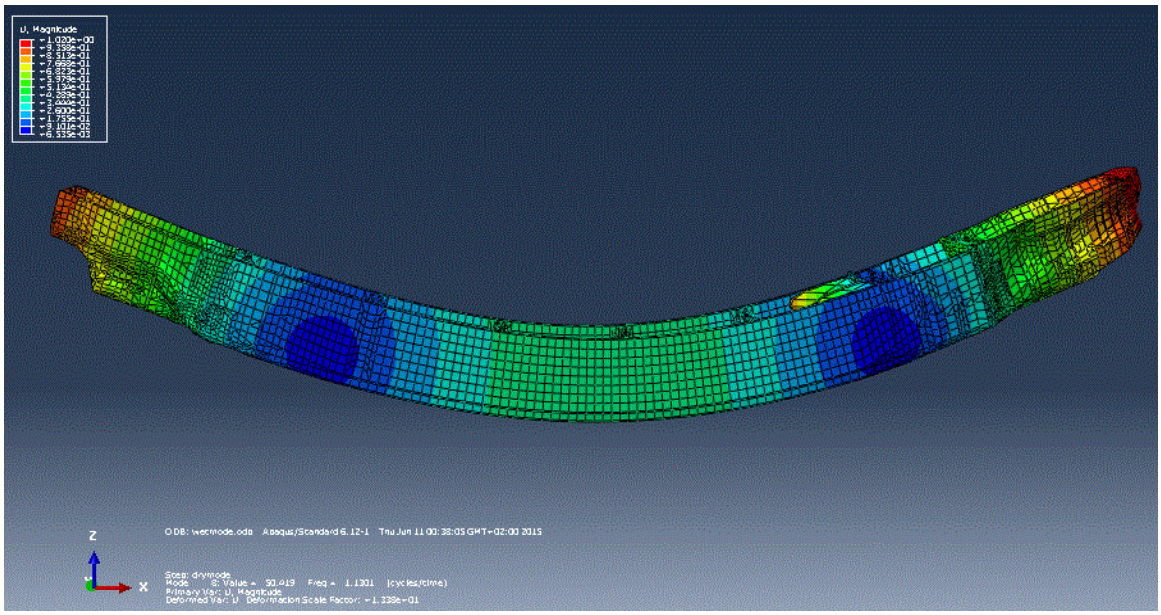

Figure 5. 12 2-node vertical bending mode of the ship with 7 bulkheads

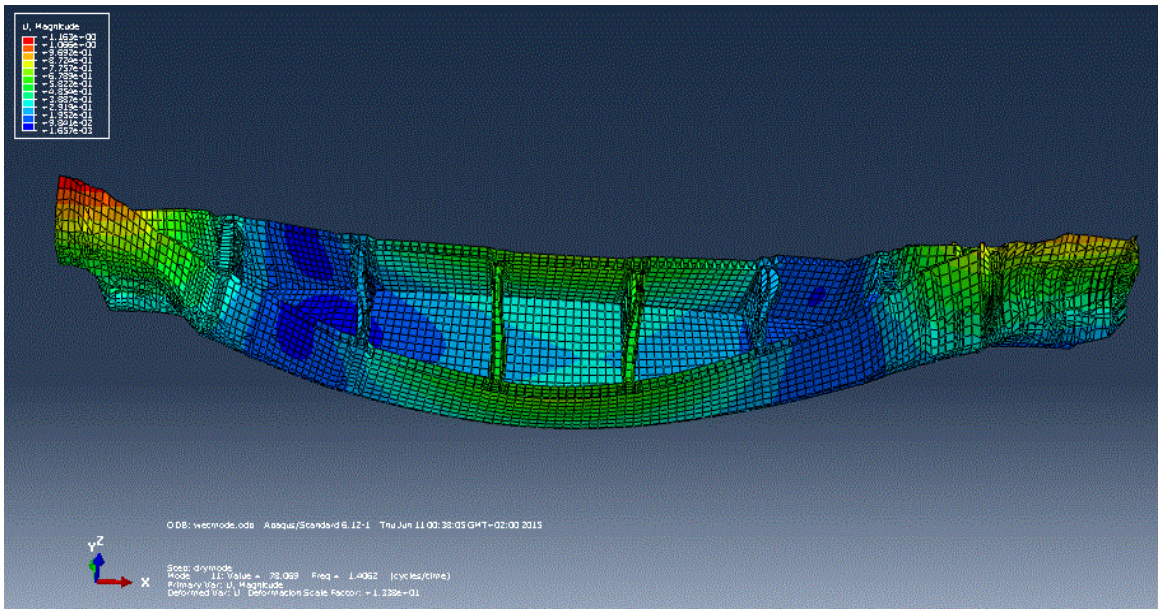

Figure 5. 13 Global torsional and horizontal bending mode of the ship with 7 bulkheads

For the ship with 7 bulkheads, there are three global flexible modes. Others are rigid-body modes and local flexible modes. Comparing to the ship model with no bulkhead and the ship model with 5 bulkheads, four and five global flexible modes are presented separately in the above sections.

In addition, the ship model with 7 bulkheads does not have 3-node vertical bending mode. When comparing the 3-node vertical bending mode for the other two ship models in Figure 5.4 and Figure 5.9 with each other, it is easy to find that the deformation of the ship with 5 bulkheads is much smaller.

The reason for the two phenomenons described above is that the bulkheads increase the stiffness of the ship. Hence, it is more difficult to have global vibrations for the ship with more bulkheads.

It can be concluded that 7 bulkheads are unnecessary for this type of ship. The ship with no bulkhead is also inapplicable. Only the ship with 5 bulkheads is chosen for the following dynamic response analysis.

Examples of local flexible mode shapes of the ship model with 7 bulkheads in ballast condition are presented below:

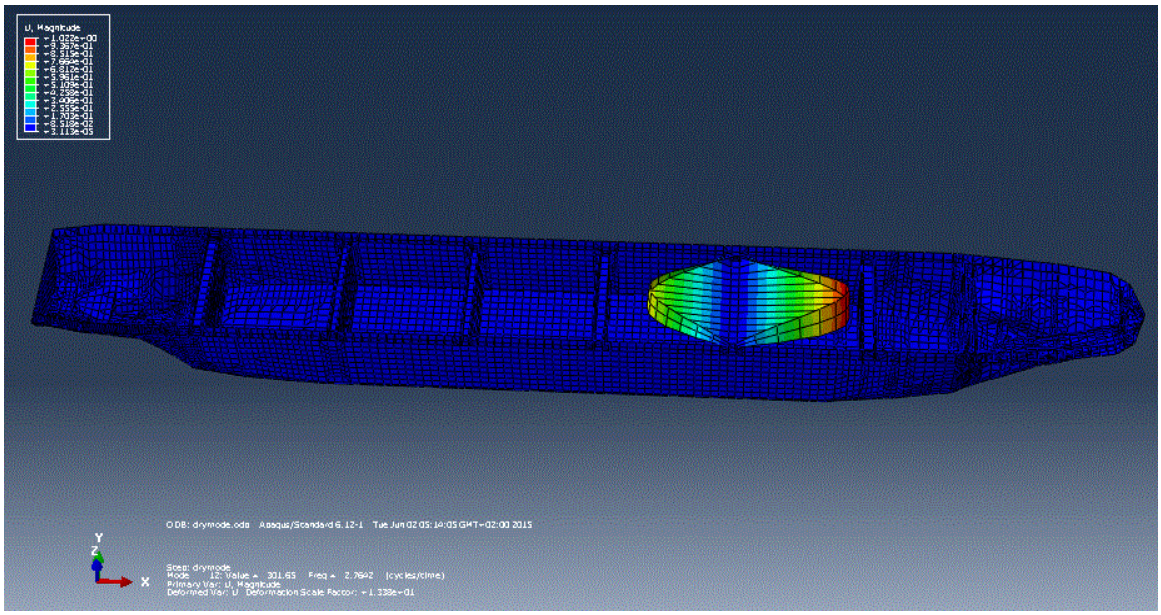

Figure 5. 14 Local vibration mode of the ship with 7 bulkheads

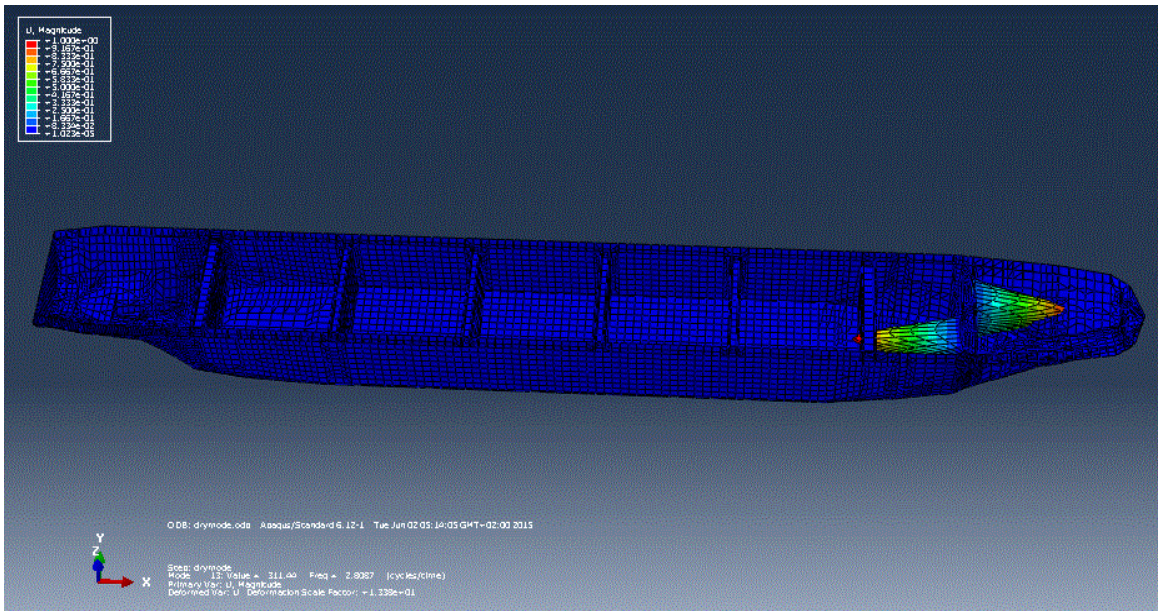

Figure 5. 15 Local vibration mode of the ship with 7 bulkheads

The dry natural mode shapes of different ship models looks quite similar to the wet natural mode, they are not presented here.

5.1.4 Results of natural frequencies

The corresponding natural frequencies for both dry and wet modes for the ship with 5 bulkheads in ballast condition are shown in Table 5.1.

Table 5. 1 Dry and wet natural frequencies (cycles/time) for ship with 5 bulkheads

	dry natural frequency(Hz)	wet natural frequency(Hz)	wet natural period(s)
global torsion mode	1.2718	0.9812	1.0192
2-node vertical bending mode	1.5266	1.1291	0.8857
global torsion and horizontal bending mode	1.8440	1.3765	0.7265
3-node vertical bending mode	3.6007	2.6375	0.3795

By comparing dry and wet natural frequencies in the table above, it is found that the hydrodynamic added mass greatly lower the natural frequency of the structure. The hydrostatic stiffness also has the effect on decreasing the natural frequencies.

Since that the ship model analyzed has the large deck-opening ratio, it has a low rigidity in torsion and the lowest flexible mode should be torsional mode which is also indicated in Table 5.1.

The natural frequency of vertical bending mode is around 1s, which is a useful parameter for the following dynamic response analysis.

The corresponding natural frequencies for both dry and wet modes for the ship with no bulkheads and the ship with 7 bulkheads in ballast condition are shown in Table 5.2 and Table 5.3 separately.

Table 5. 2 Dry and wet natural frequencies (cycles/time) for ship with no bulkheads

	dry natural frequency(Hz)	wet natural frequency(Hz)	wet natural period(s)
global torsion mode	0.73527	0.57995	1.7243
2-node vertical bending mode	1.4154	1.0185	0.9818
global torsion and horizontal bending mode	1.4527	1.0701	0.9345
3-node vertical bending mode	2.8823	2.1071	0.4746
global torsion and 3-node bending mode	2.9555	2.1279	0.4699

Table 5. 3 Dry and wet natural frequencies (cycles/time) for ship with 7 bulkheads

	dry natural frequency(Hz)	wet natural frequency(Hz)	wet natural period(s)
global torsion mode	1.2917	0.9909	1.009
2-node vertical bending mode	1.5243	1.1301	0.8849
global torsion and horizontal bending mode	1.8825	1.4062	0.7111

Compare the natural frequencies of three models, it is easily to found that the ship model with more bulkheads has larger natural frequency.

5.1.5 Bending moment at different natural modes

In this section, three cross-sections are taken at the ship bow, midship and ship stern area for measurement of bending moment.

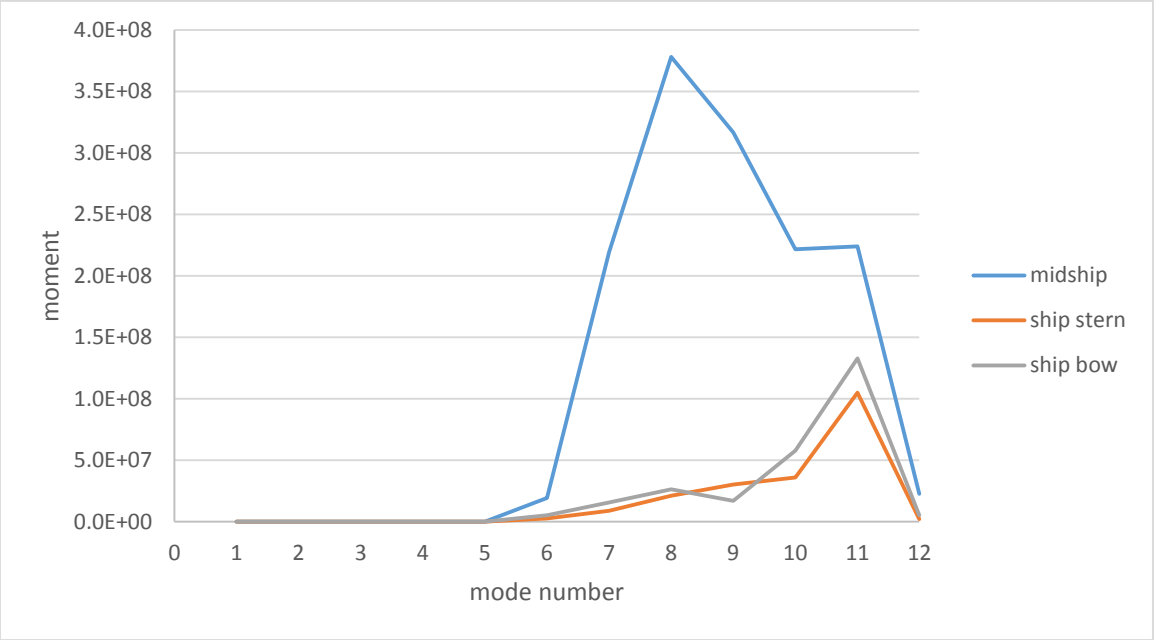

Figure 5. 16 Bending moment of ship cross-sections at different natural modes

It is shown in Figure 5.16 that the maximum bending moment occurs at the midship area. The natural mode number 8 is corresponding to the 2-node vertical bending mode, which has the largest bending moment at the midship. The natural mode number 11 is corresponding to the 3-node bending mode which has the largest bending moment at the ship stern and ship bow area.

5.2 Dynamic response

In the dynamic response analysis, explicit analysis method cannot be used due to the existence of spring element. Here the dynamic implicit analysis is chosen for the second step in ABAQUS. The observed time period is chosen 5s. Time increment is 0.01s. Slamming load is modeled as concentrated load under the ship bow. The magnitude of the slamming load is 560000N. The time series of the slamming load is shown in Table 5.4.

Table 5. 4 Slamming load history

Time (s)	Amplitude (N)
0	0
0.15	1
0.03	0

Figure 5.17 shows a side view of the vessel. The location of the sensors and type are indicated ([S] strain, [A] acceleration, [P]pressure). Time history of different parameters are observed at different ship locations in the following analysis.

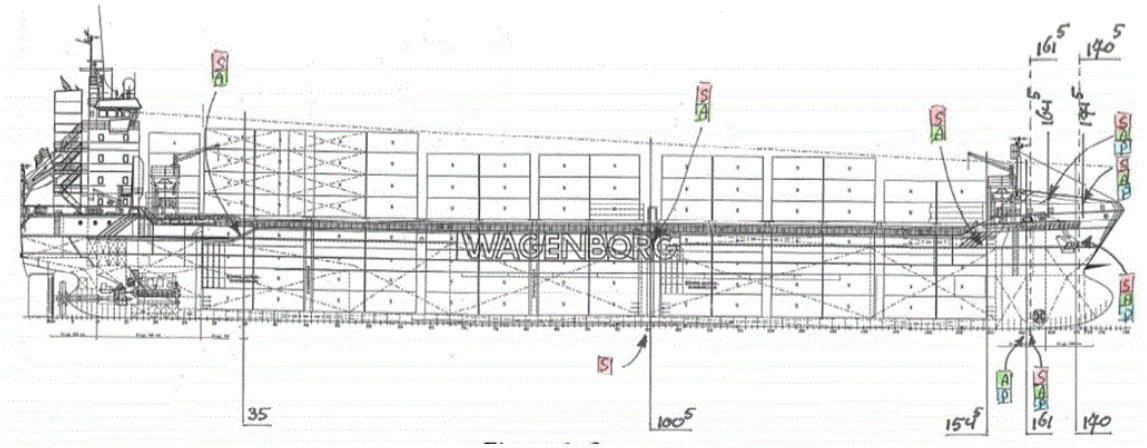

Figure 5. 17 Location of sensors

5.2.1 Displacement time traces

Displacement time traces at different positions along the ship are observed:

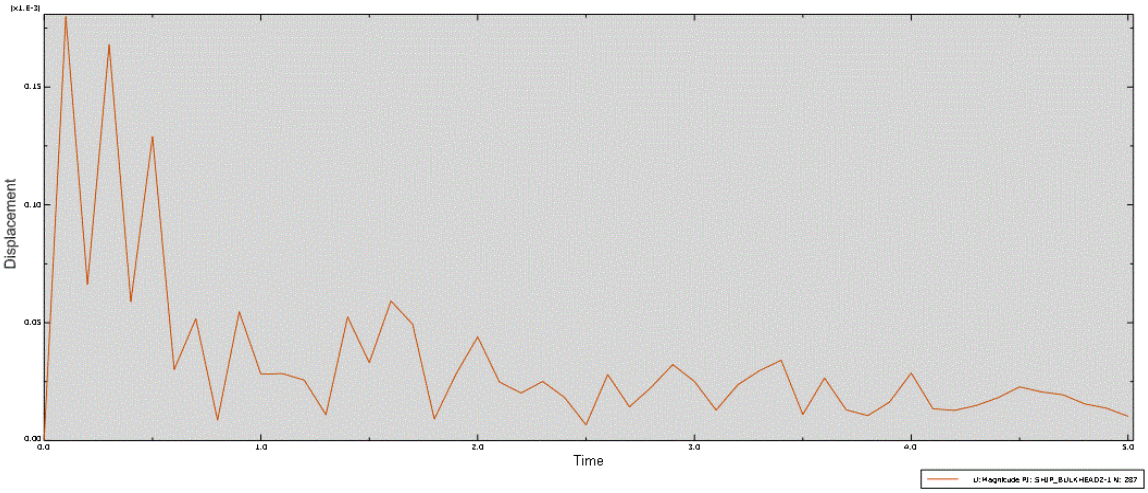

Figure 5. 18 Displacement time trace at ship bow (deck)

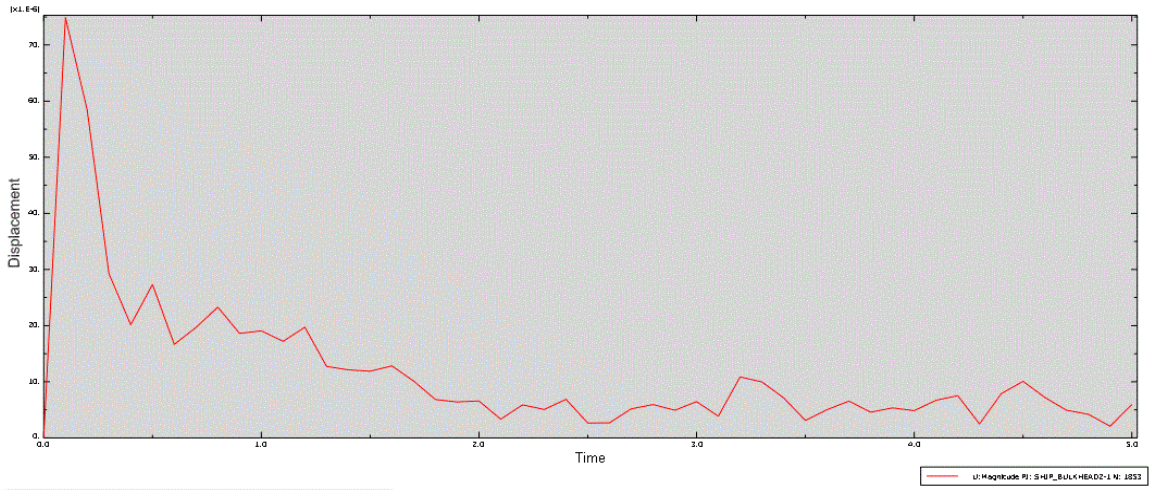

Figure 5. 19 Displacement time trace at ship bow (bottom)

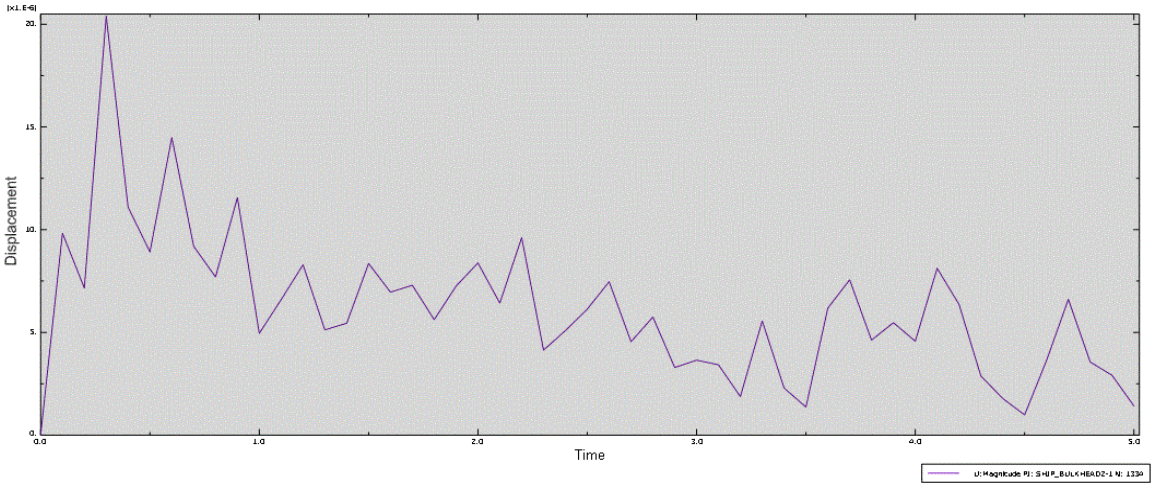

Figure 5. 20 Displacement time trace in midship (deck)

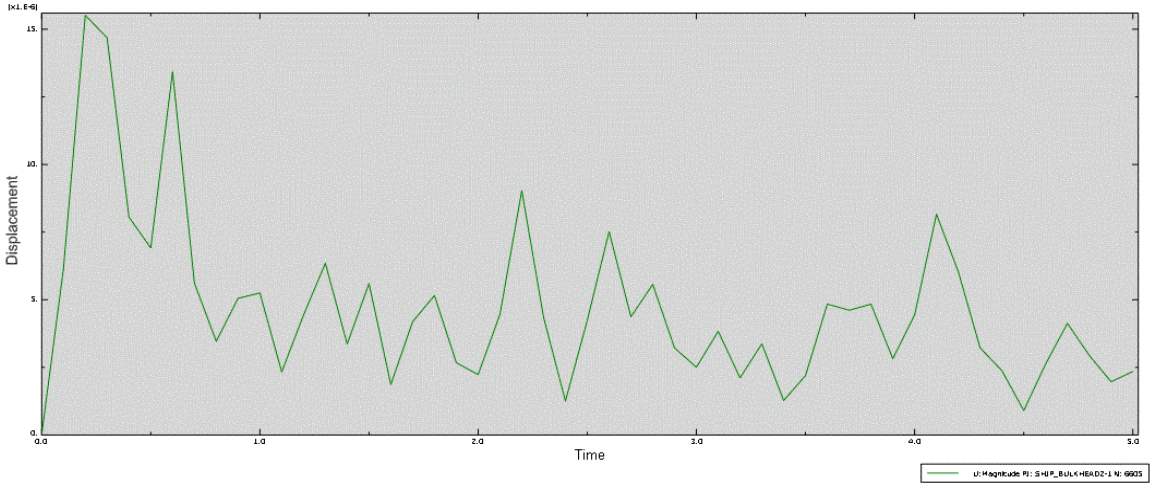

Figure 5. 21 Displacement time trace in midship (bottom)

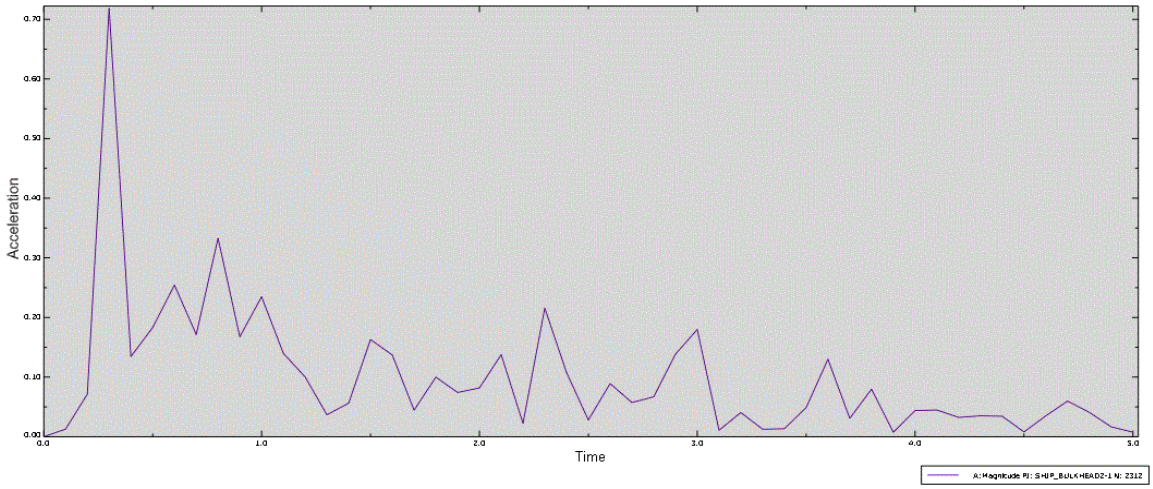

Figure 5. 22 Displacement time trace at ship stern (deck)

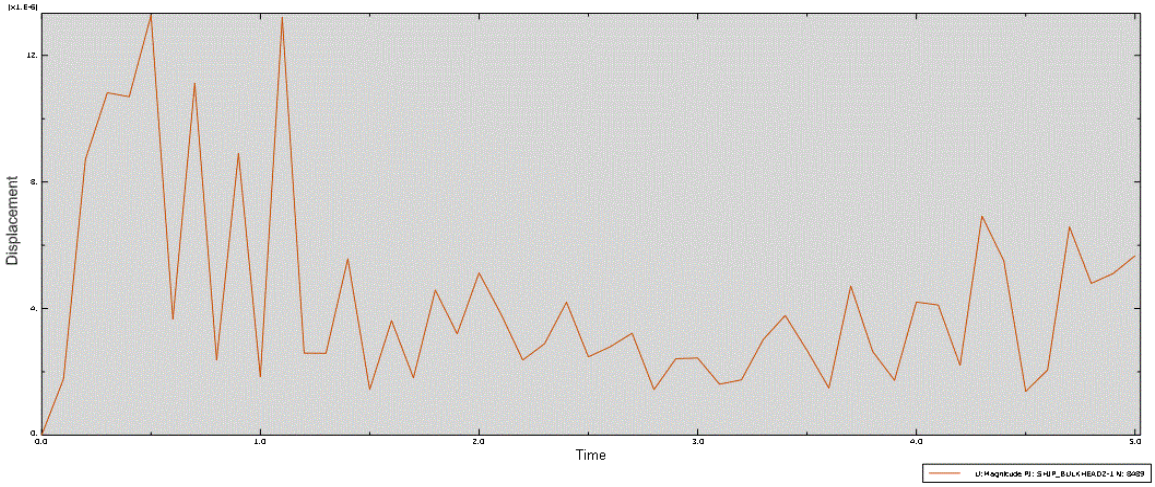

Figure 5. 23 Displacement time trace at ship stern (bottom)

It is observed that displacements convergences as time passes. The displacement at the ship bow convergences best and convergences to zero at last. Comparing displacement time traces on the deck and on the bottom, it is found that the maximum displacement on the deck is the first amplitude, however the maximum displacement on the bottom is usually the second amplitude.

5.2.2 Stress time traces

Stress time traces at different positions along the ship are observed:

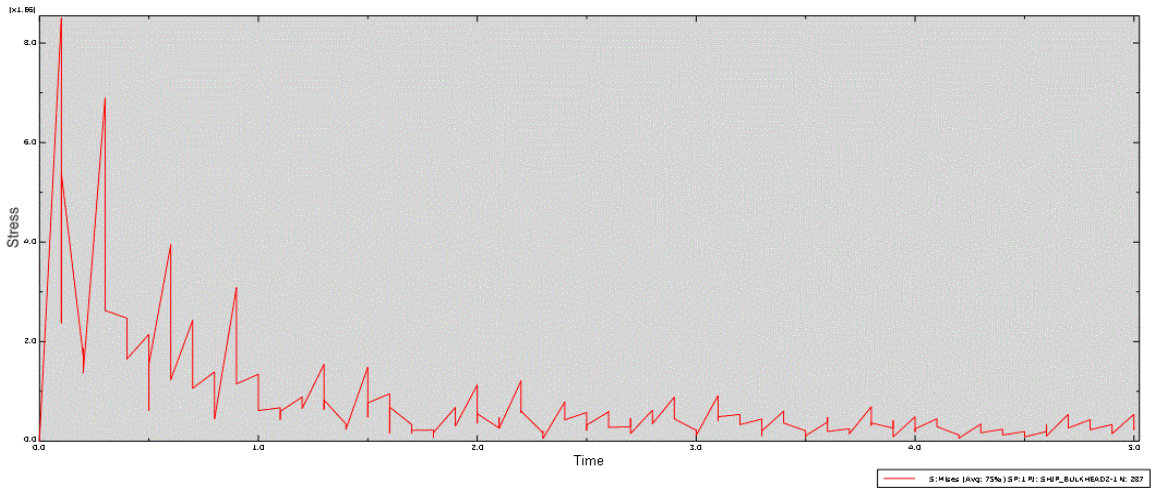

Figure 5. 24 Stress time trace at ship bow (deck)

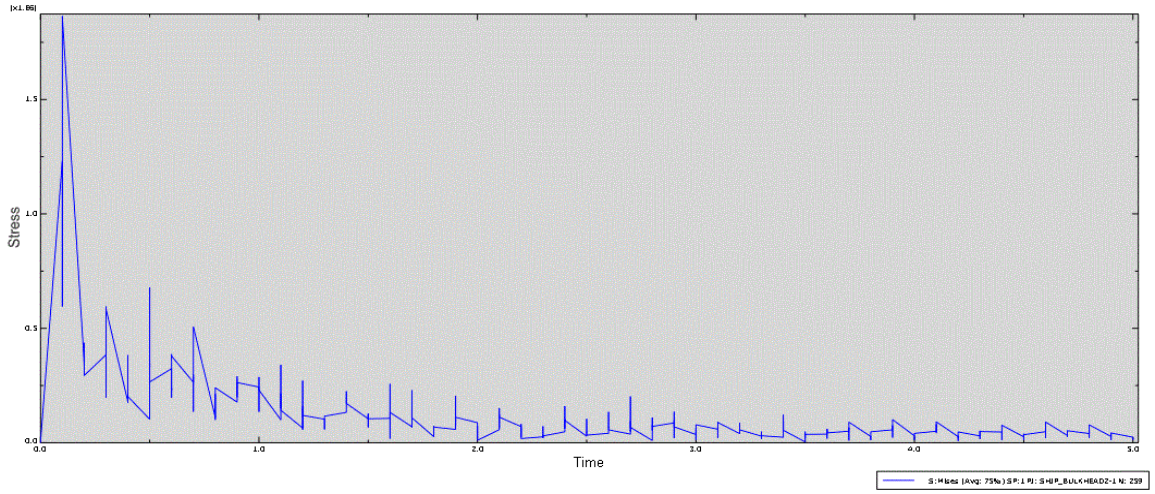

Figure 5. 25 Stress time trace at ship bow (bottom)

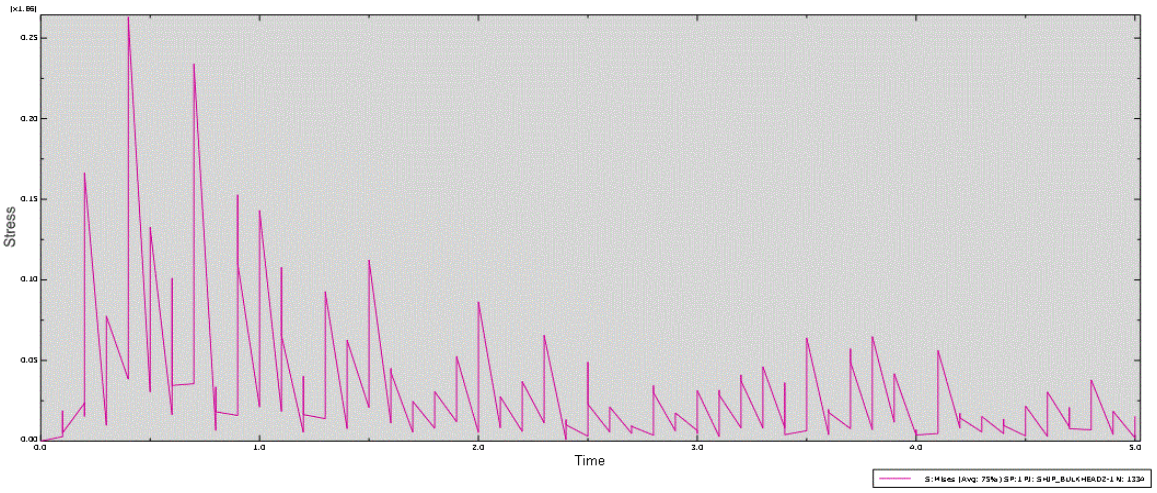

Figure 5. 26 Stress time trace in midship (deck)

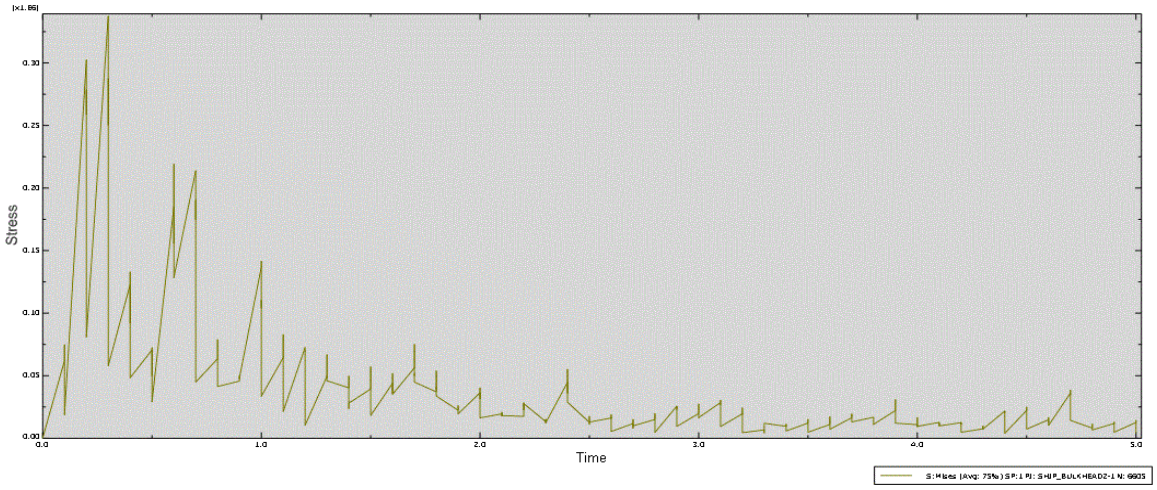

Figure 5. 27 Stress time trace in midship (bottom)

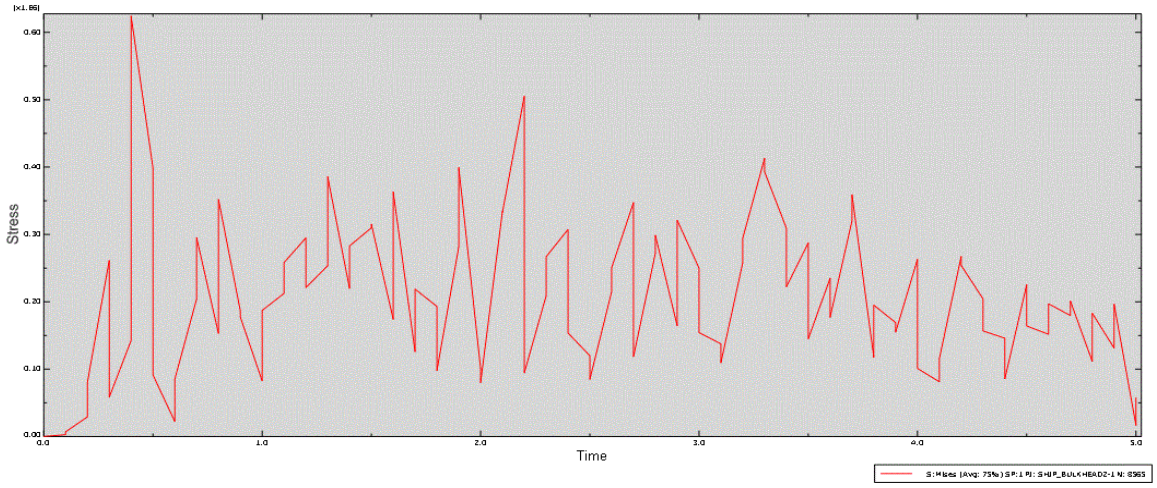

Figure 5. 28 Stress time trace at ship stern (deck)

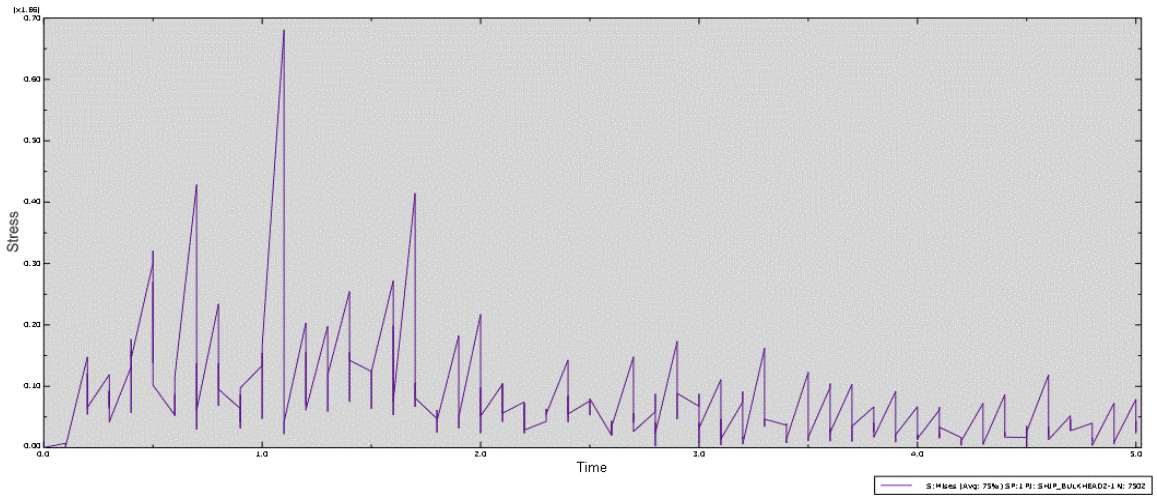

Figure 5. 29 Stress time trace at ship stern (bottom)

The stress of the ship also convergences. The stress on the bottom convergences well to nearly zero. The stress level falls quickly and significantly after slamming occurs,

especially in the fore part area of the ship bottom. There is a significant maximum value during slamming at the ship bow which is presented in Figure 5.24 and Figure 5.25. The maximum stress in the stern area appears a little after slamming occurs. Besides, the stress level does not show significant decrease in the ship stern area. The stress on the deck of ship stern almost stays stable in Figure 5.28.

5.2.3 Strain time traces

Strain time traces at different positions along the ship are observed:

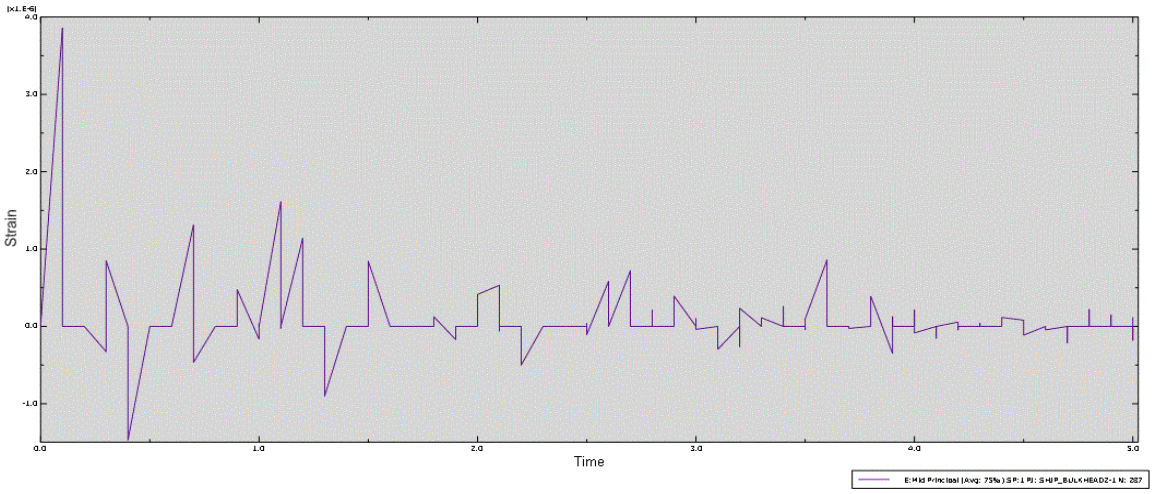

Figure 5. 30 Strain time trace at ship bow (deck)

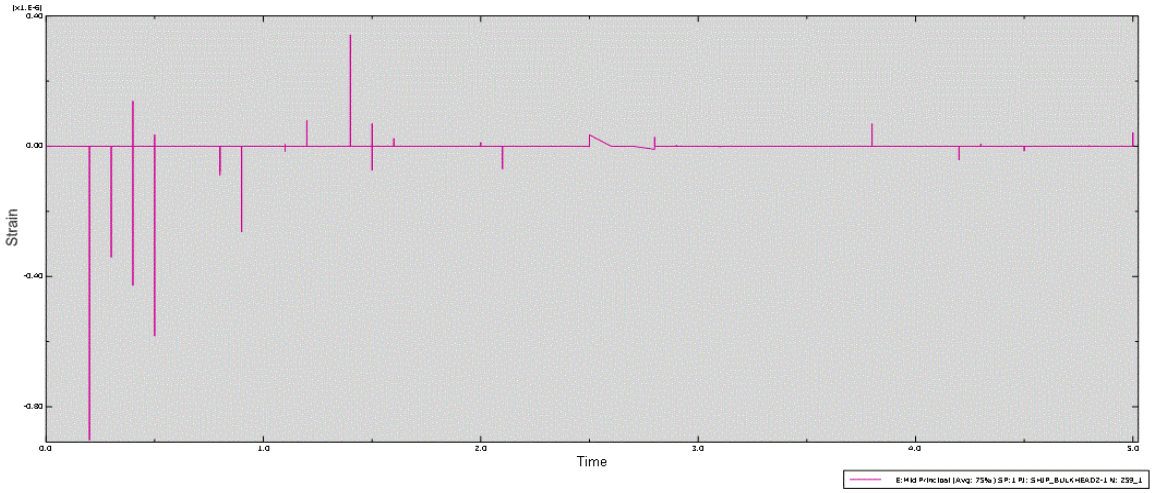

Figure 5. 31 Strain time trace at ship bow (bottom)

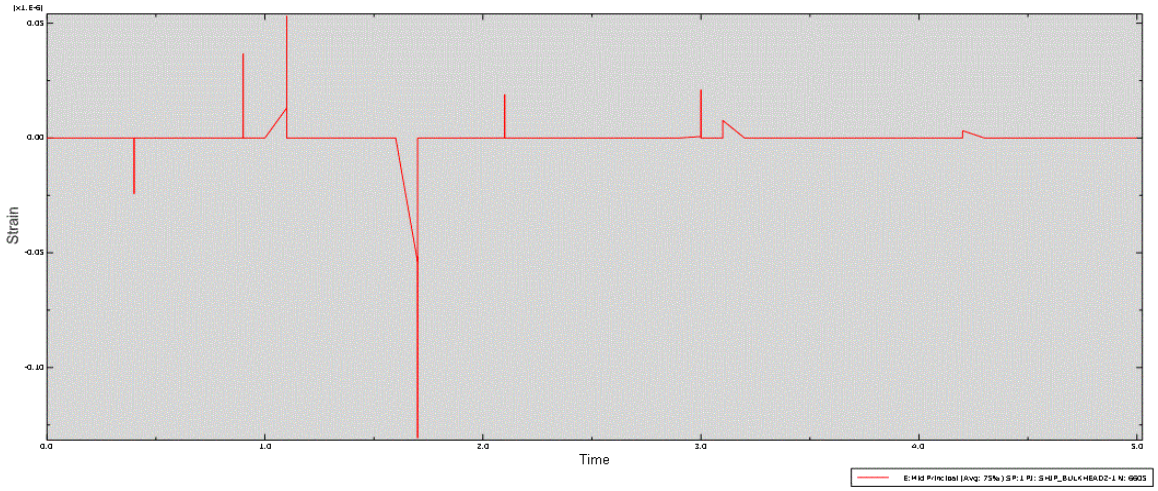

Figure 5. 32 Strain time trace in midship (deck)

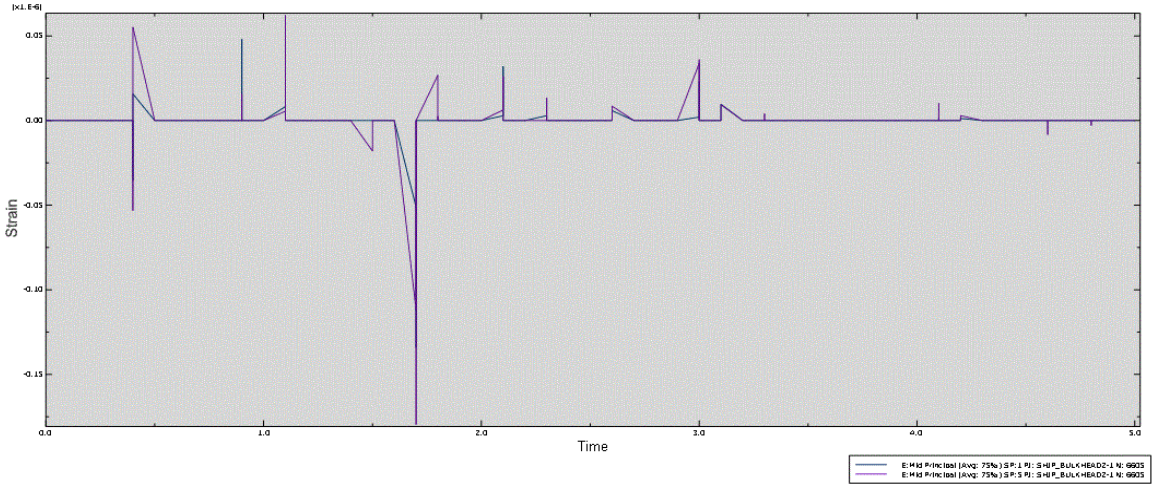

Figure 5. 33 Strain time trace in midship (bottom)

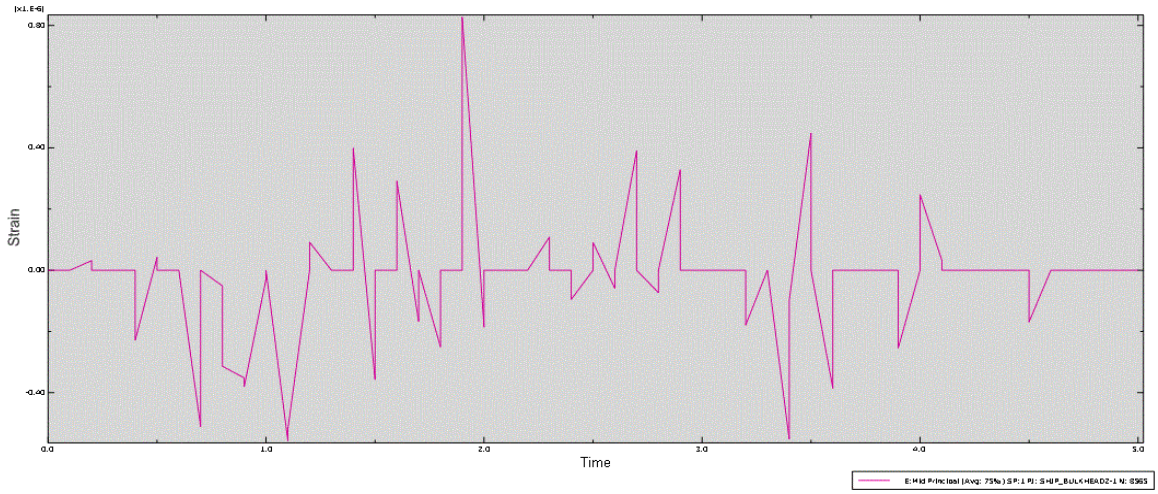

Figure 5. 34 Strain time trace at ship stern (deck)

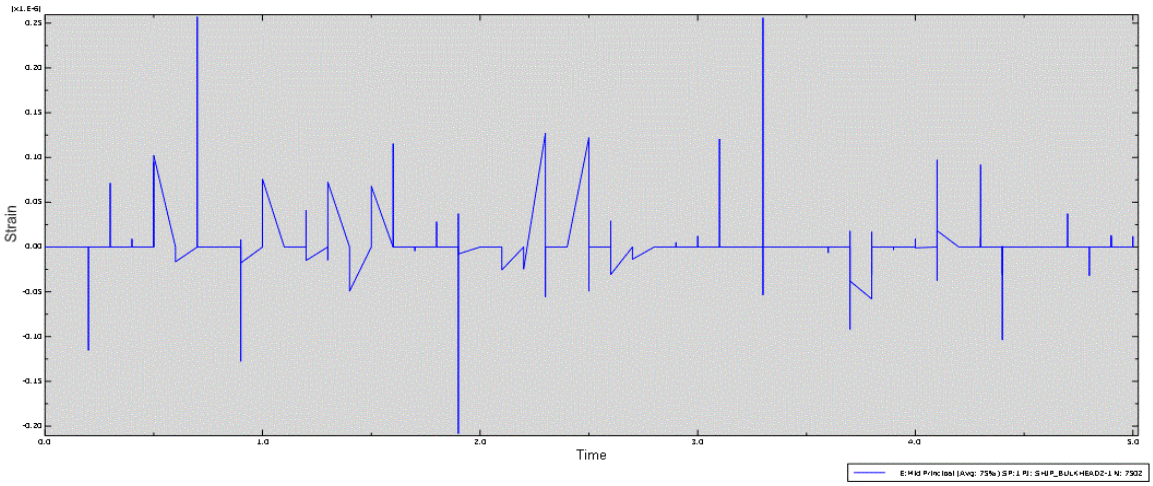

Figure 5. 35 Strain time trace at ship stern (bottom)

It can be shown that there are obvious stress component in both ship bow and stern area. Especially, the largest strain is induced by slamming loads and then damps out at the ship bow. However, there is almost no strain component for most time history in the middle area of the ship. The ship has the largest strain level at ship bow and stern area. This can also be shown in the following figures, which present the strain distribution along the longitudinal axis of the ship bottom at different time instant. In these figures, the origin of x-axis is at the ship stern.

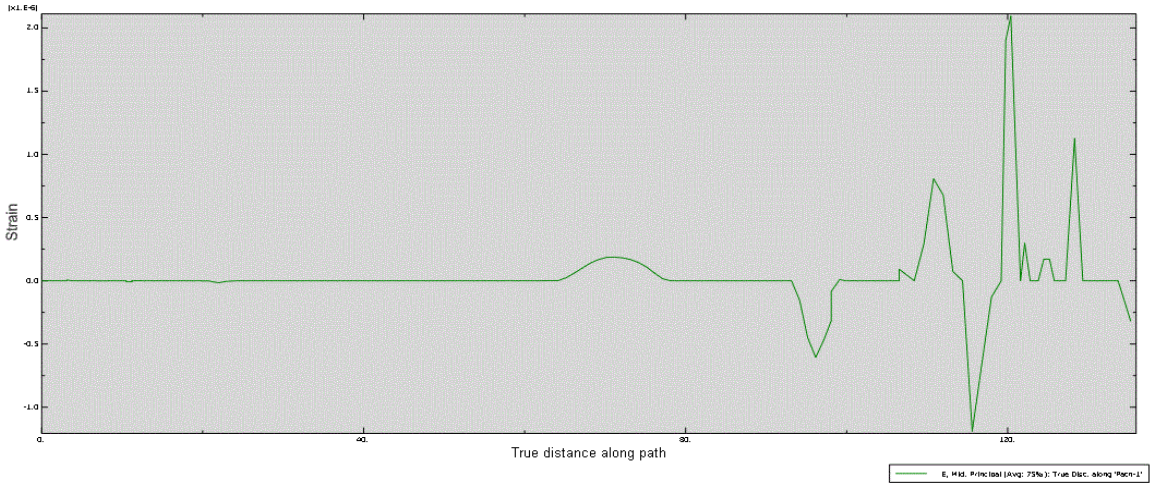

Figure 5. 36 Strain distribution along the longitudinal axis of the ship at t=0.1s

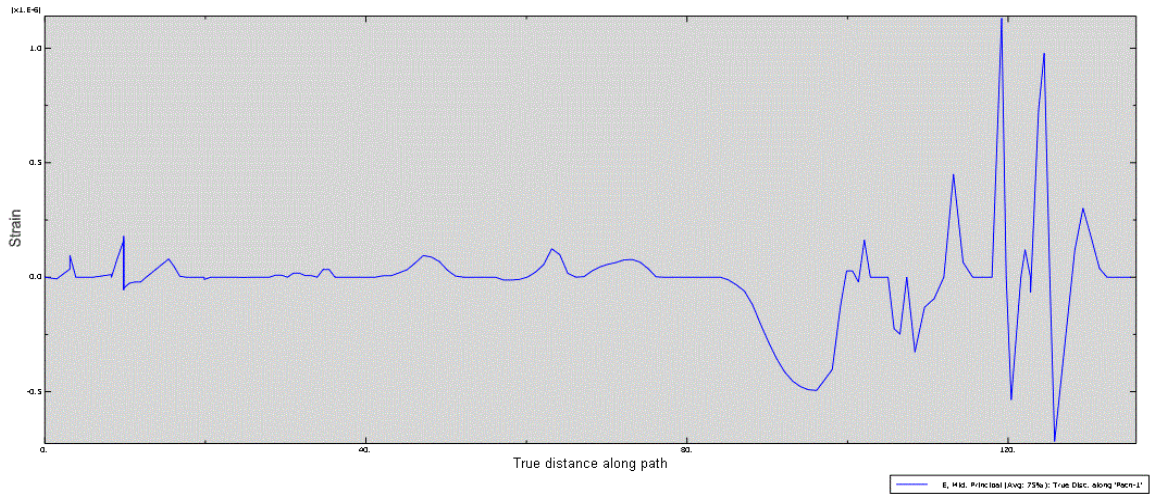

Figure 5. 37 Strain distribution along the longitudinal axis of the ship at t=0.2s

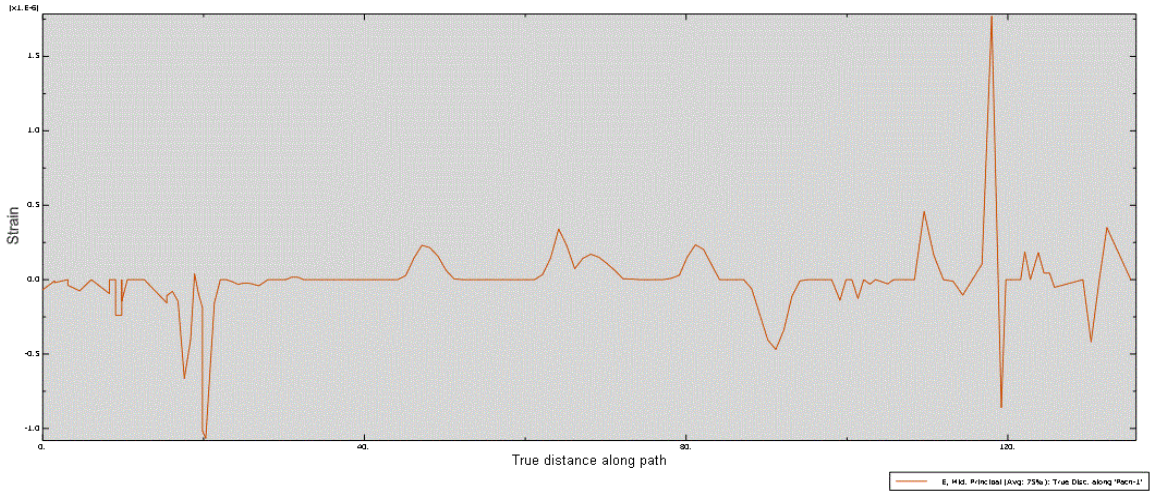

Figure 5. 38 Strain distribution along the longitudinal axis of the ship at t=0.3s

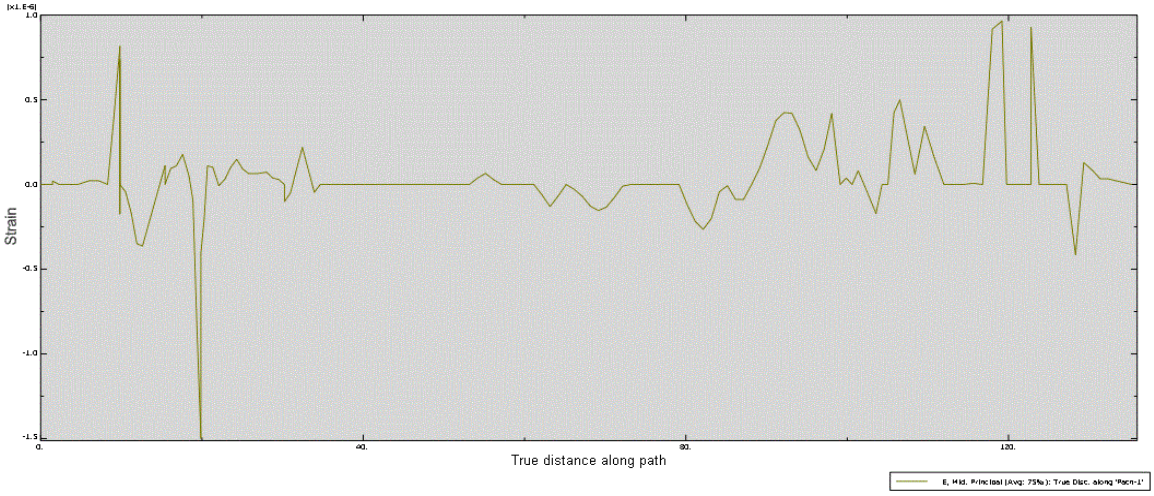

Figure 5. 39 Strain distribution along the longitudinal axis of the ship at t=0.6s

5.2.4 Acceleration time traces

Acceleration time traces at different positions along the ship are observed:

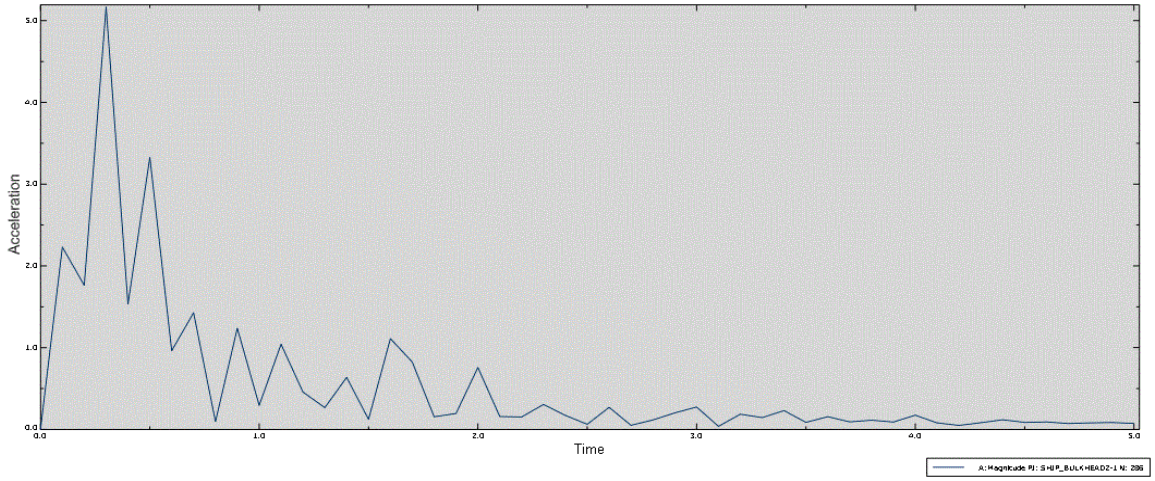

Figure 5. 40 Acceleration time trace at ship bow (deck)

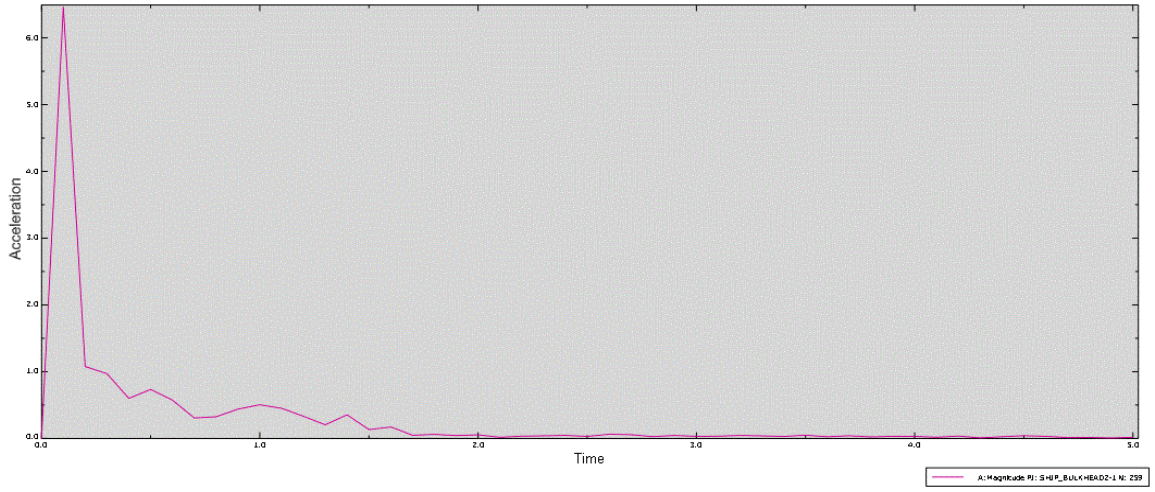

Figure 5. 41 Acceleration time trace at ship bow (bottom)

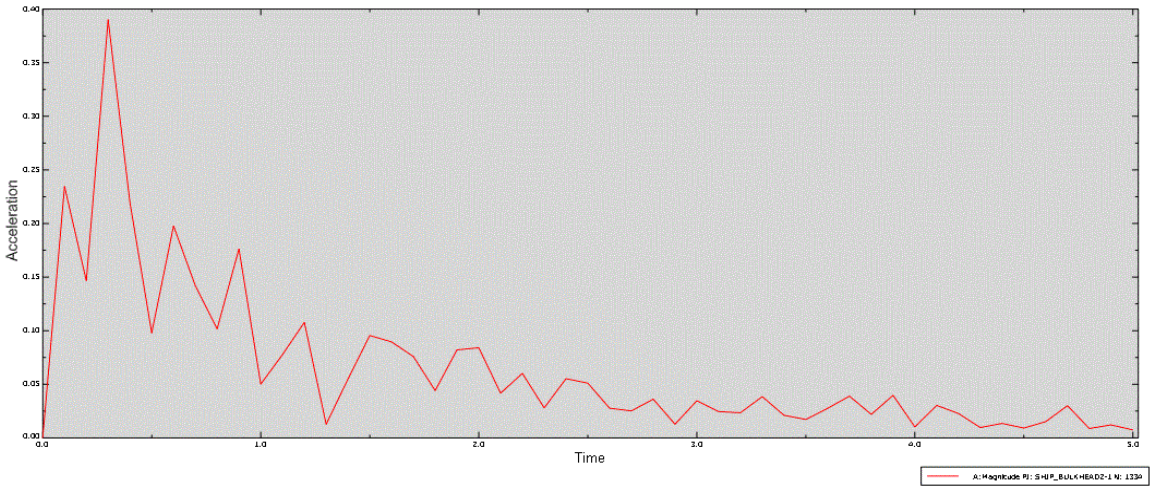

Figure 5. 42 Acceleration time trace in midship (deck)

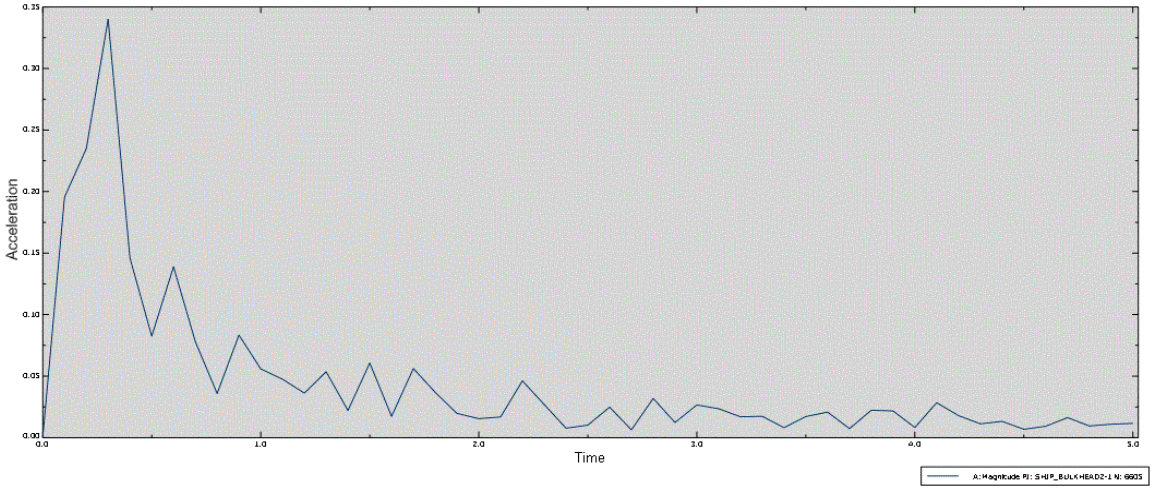

Figure 5. 43 Acceleration time trace in midship (bottom)

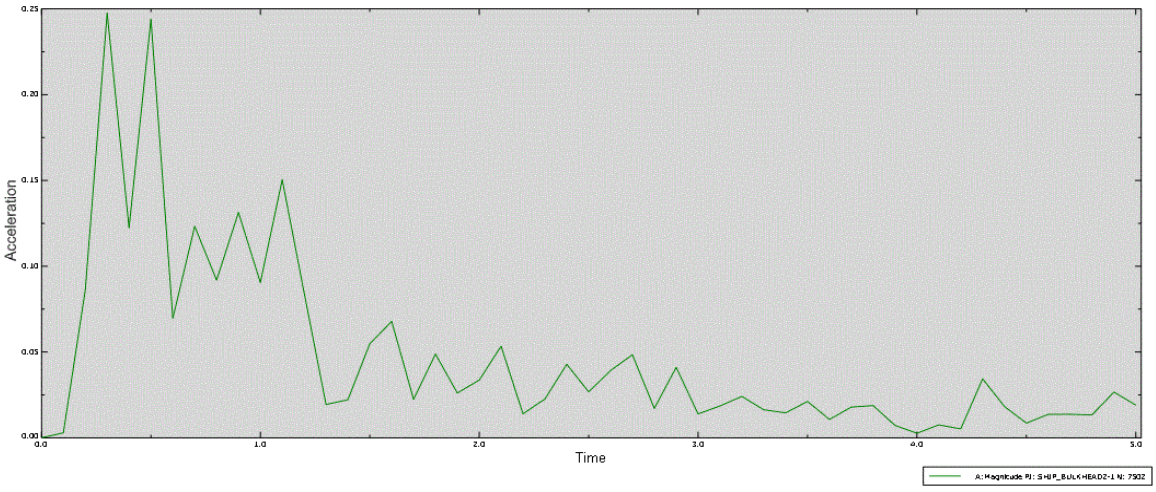

Figure 5. 44 Acceleration time trace at ship stern (deck)

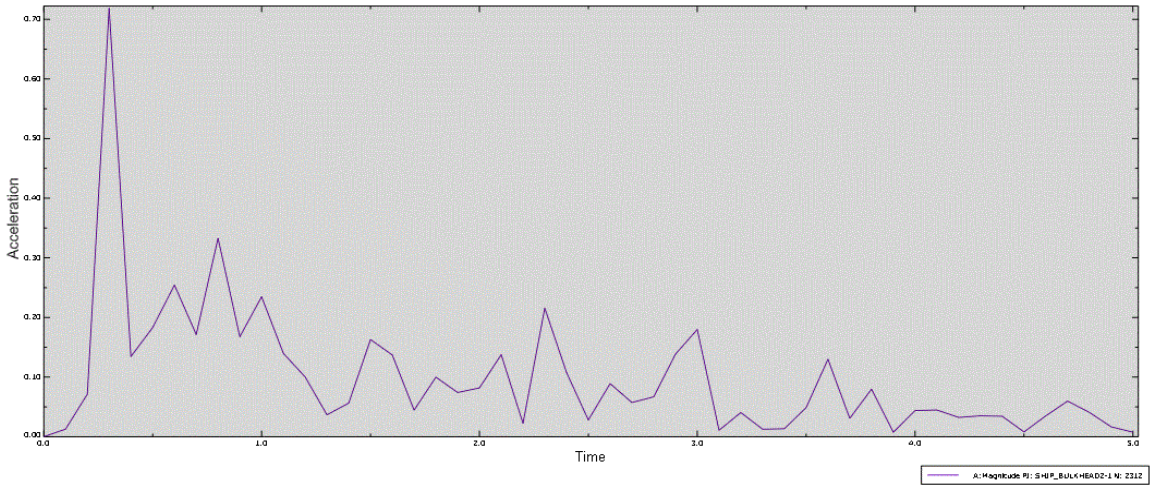

Figure 5. 45 Acceleration time trace at ship stern (bottom)

Acceleration of the ship convergences well as time passes. Especially at the ship bow, it convergence almost to zero. The acceleration damps out more quickly on the bottom than on the deck.

5.2.5 Velocity time times

Velocity time traces at different positions along the ship are observed:

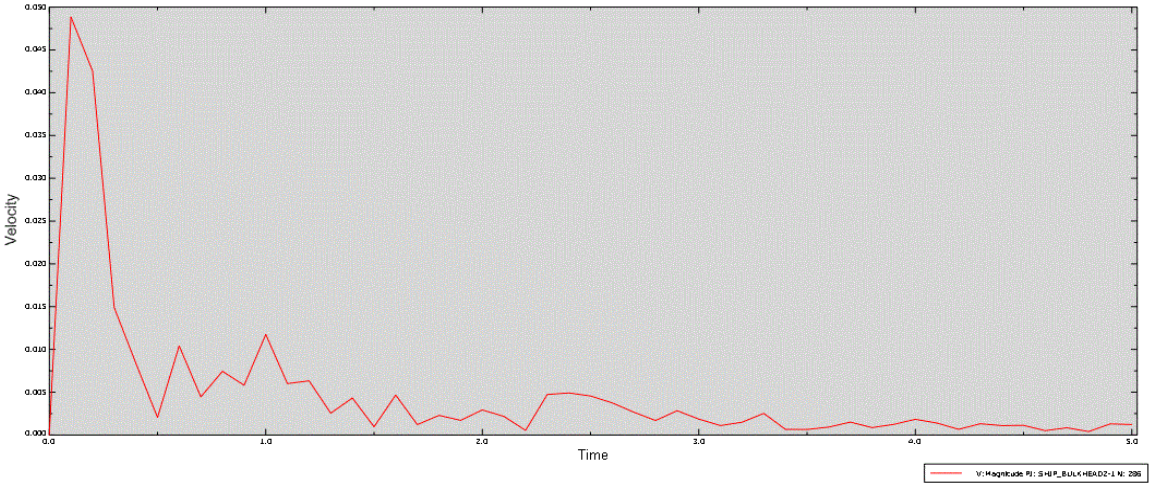

Figure 5. 46 Velocity time trace at ship bow (deck)

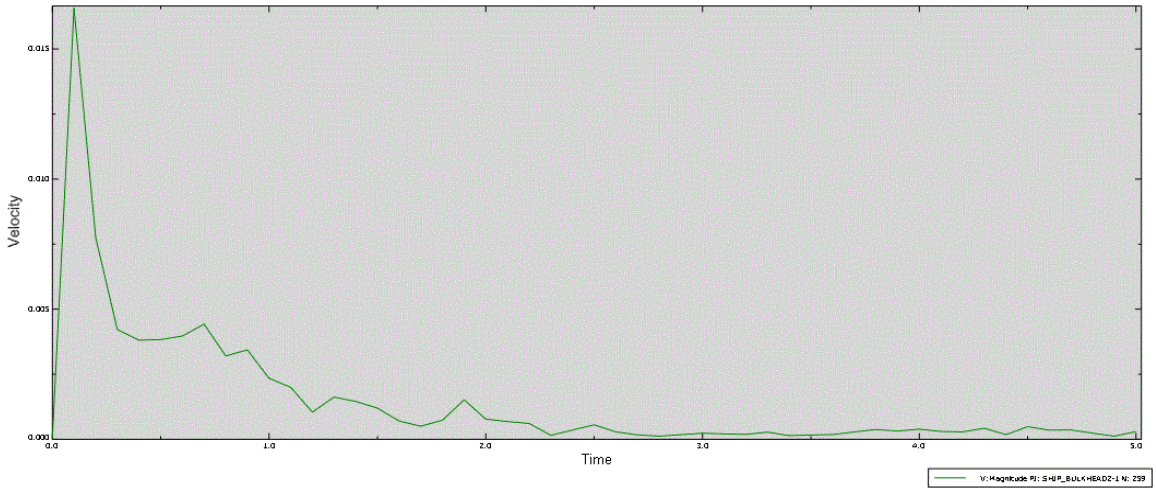

Figure 5. 47 Velocity time trace at ship bow (bottom)

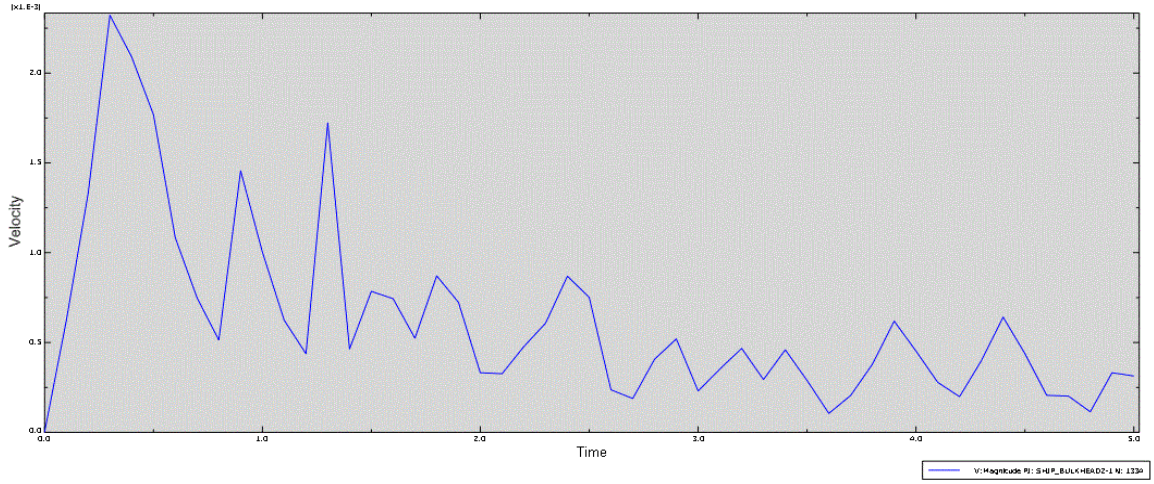

Figure 5. 48 Velocity time trace in midship (deck)

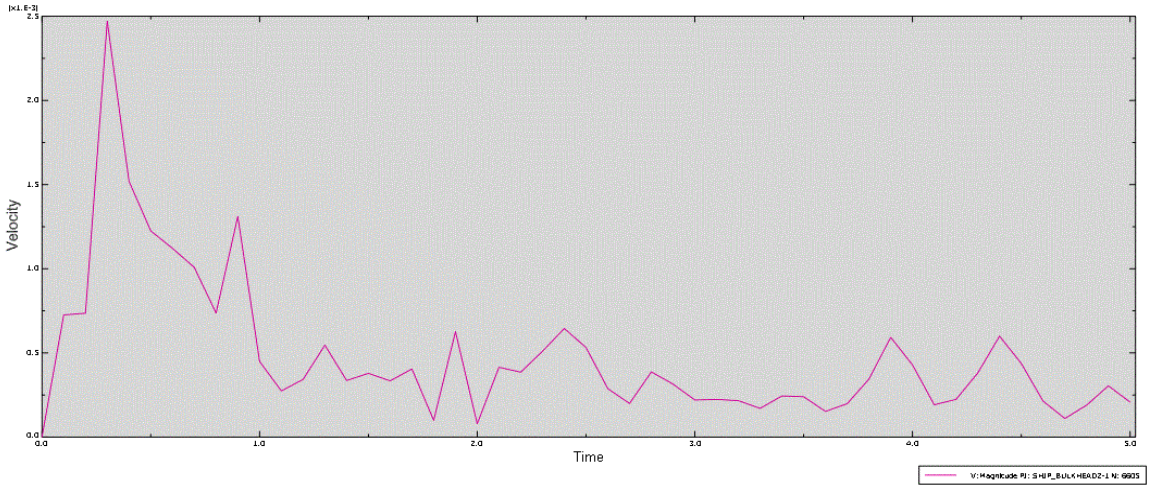

Figure 5. 49 Velocity time trace in midship (bottom)

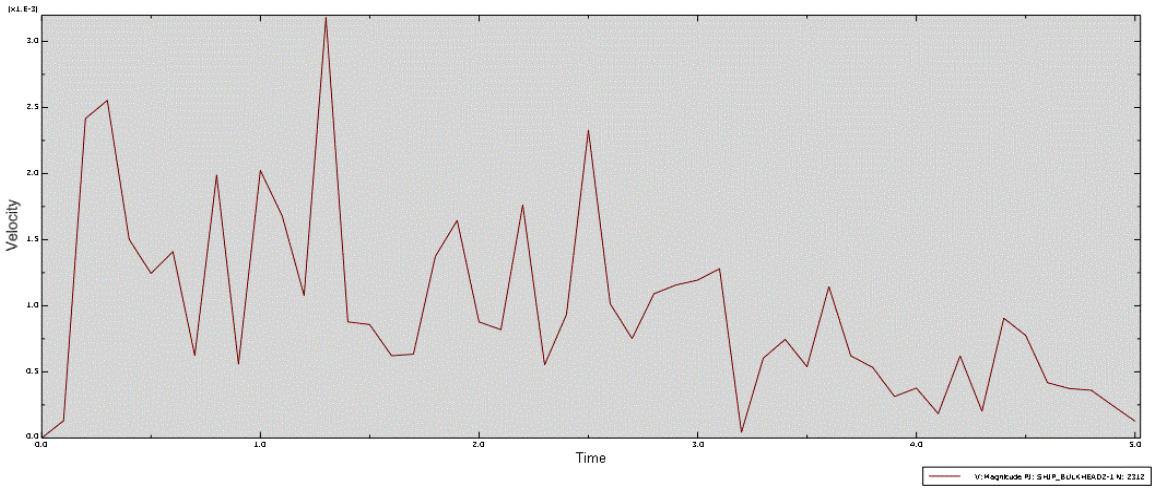

Figure 5. 50 Velocity time trace at ship stern (deck)

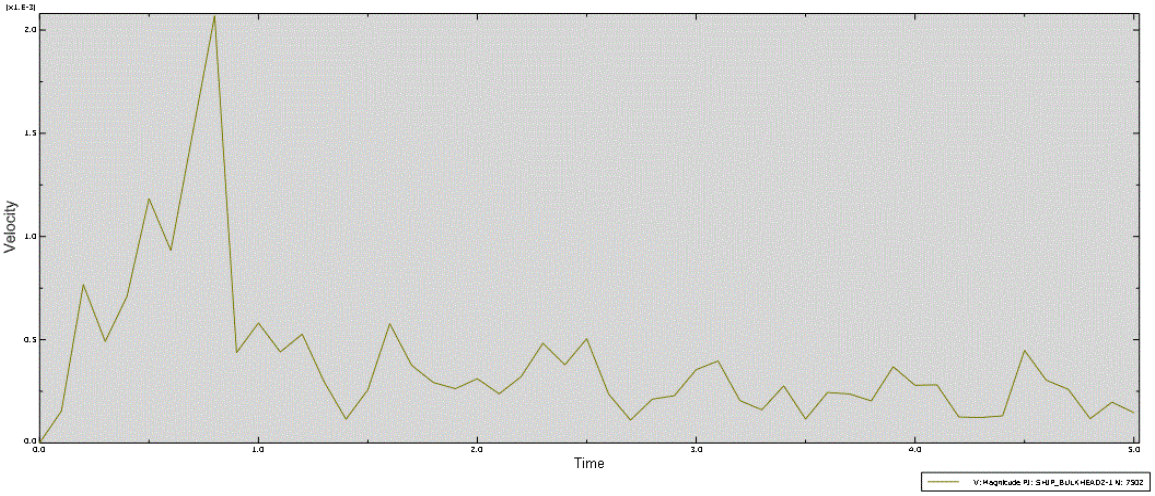

Figure 5. 51 Velocity time trace at ship stern (bottom)

Similar to other parameter time traces, velocity damps out immediately after slamming and convergences to zero at the ship bow area. The maximum velocity at the ship bow is excited when the slamming occurs. The maximum velocity at ship stern appears after slamming occurs. Besides, velocity damps out more slowly at the ship stern than that at the ship bow. It convergences to a value not equal to zero.

5.3 Parametric study

5.3.1 Duration of slamming loads

Normally, the typical duration of local hydroelastic slamming is of the order 10^{-2}s. However, in this this thesis, the duration of slamming loads varying from 0.03s to 1s are analyzed. 5 different time scales of slamming loads are chosen.

The time history of vertical displacement at ship bow in case of different slamming load durations are compared in the figures below:

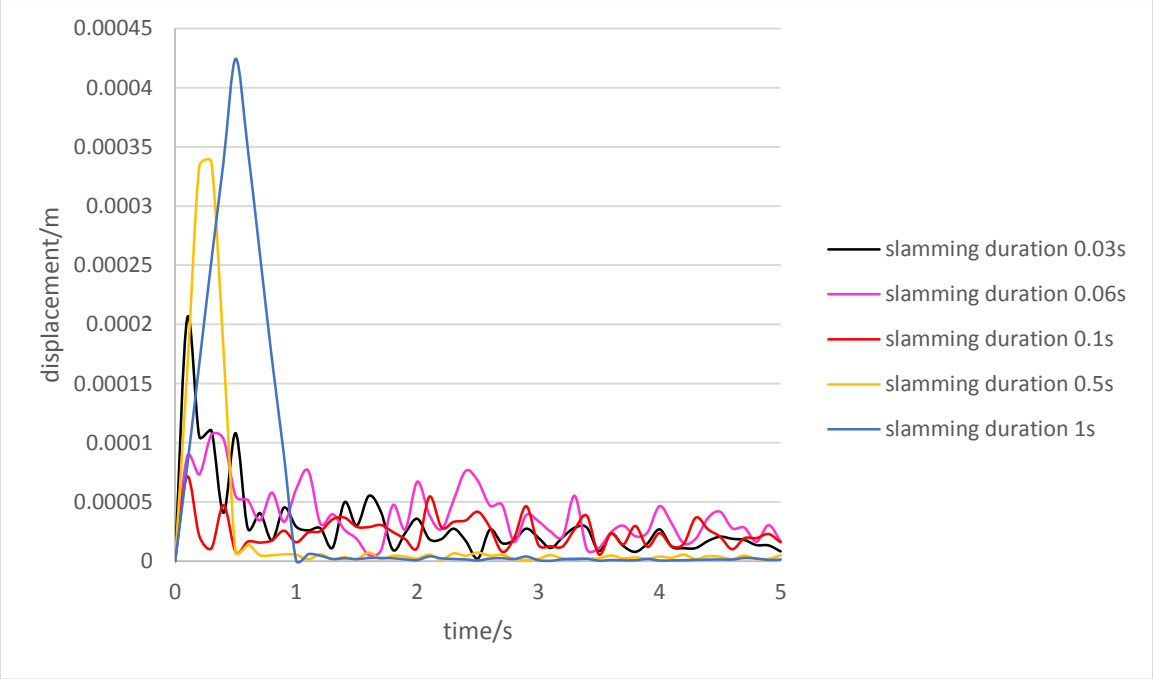

Figure 5. 52 Displacement time trace at ship bow (deck)

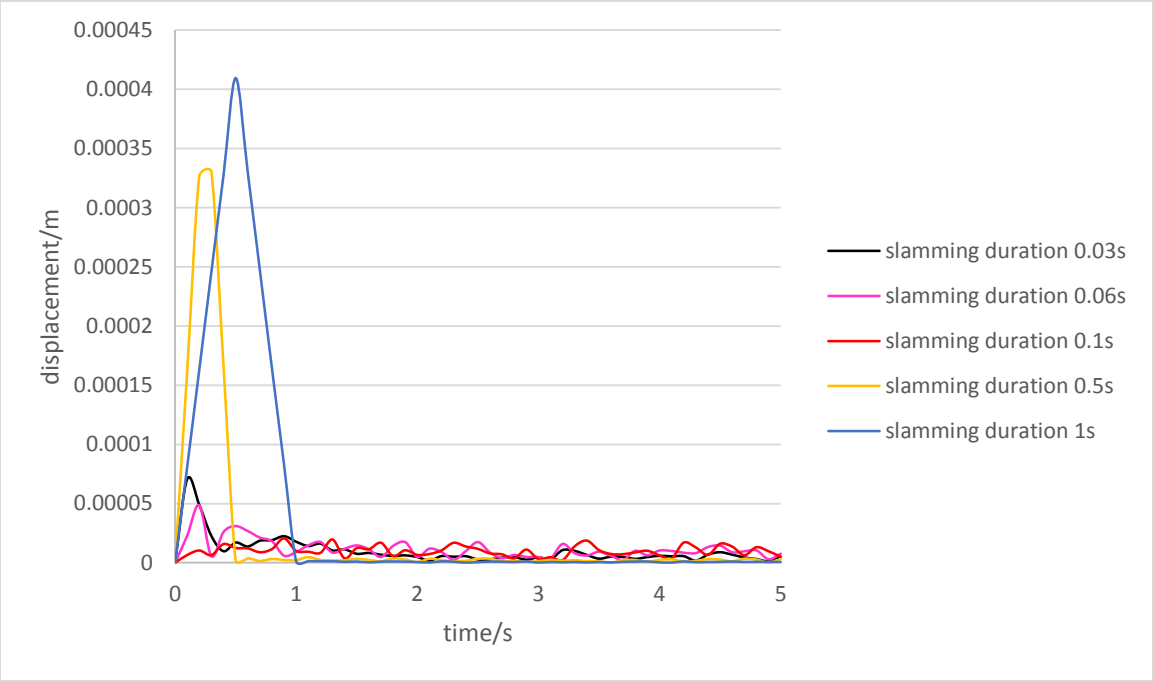

Figure 5. 53 Displacement time trace at ship bow (bottom)

It is shown from the figures above that when slamming duration is 0.5s and 1s, the maximum displacement at ship bow is the largest and much larger than the other cases. One reason is that the 2-node bending natural period is around 0.9s. Resonance may be excited. However, it should be noticed that the response is the smallest when slamming duration is 0.1s.

Energy spectrums of dynamic response in case of different slamming load durations are presented in Figure 5.54. It shows the same trend as displacement time trace.

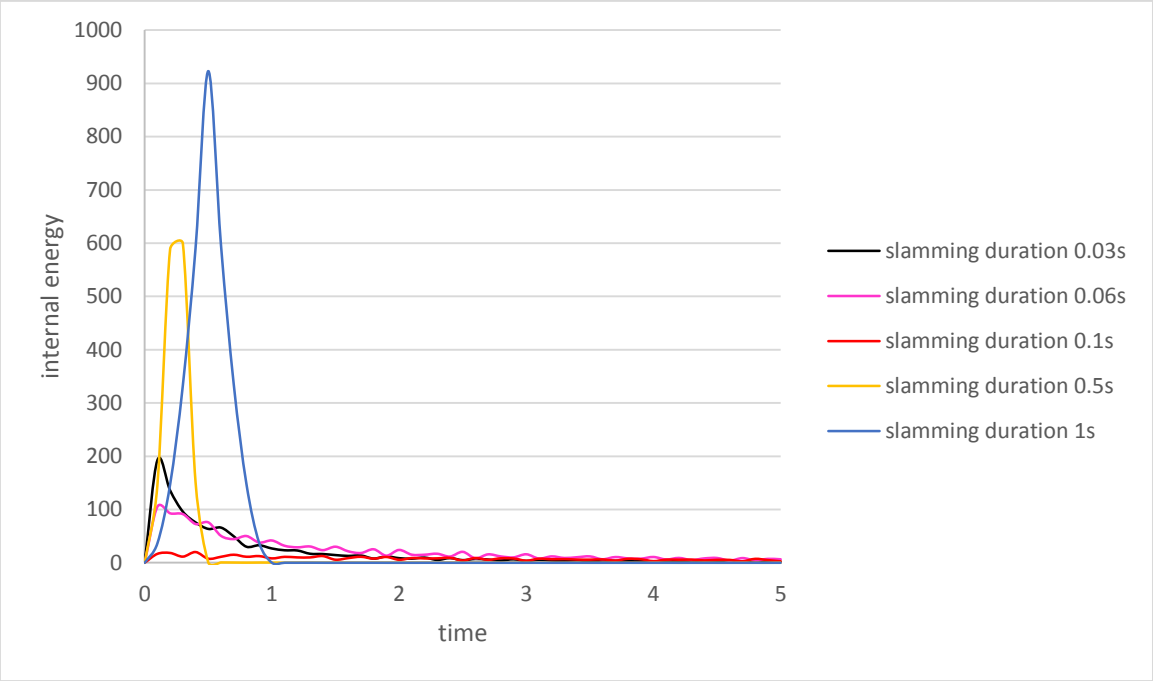

Figure 5. 54 Energy spectrum of dynamic response

5.3.2 Impulse shape of slamming loads

As has been described in Chapter 3.1, there are different impulse shape of slamming loads. In this section, the influence of load pulse shape is analyzed. 5 different load pulse shapes are shown below:

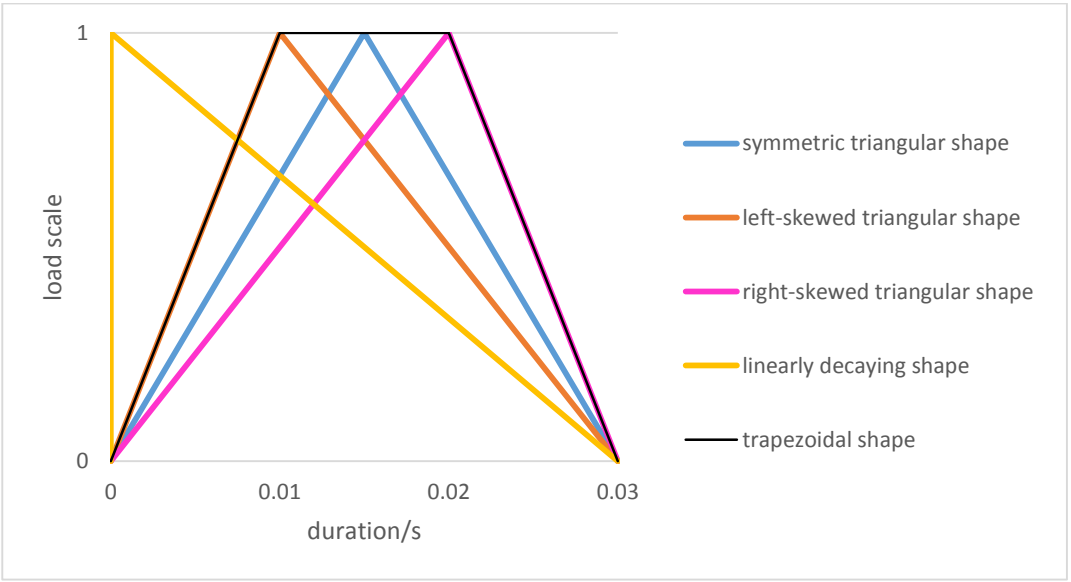

Figure 5. 55 Impulse shape

Time histories of ship bow displacement for different triangular impulse shape are shown below and made comparison with each other.

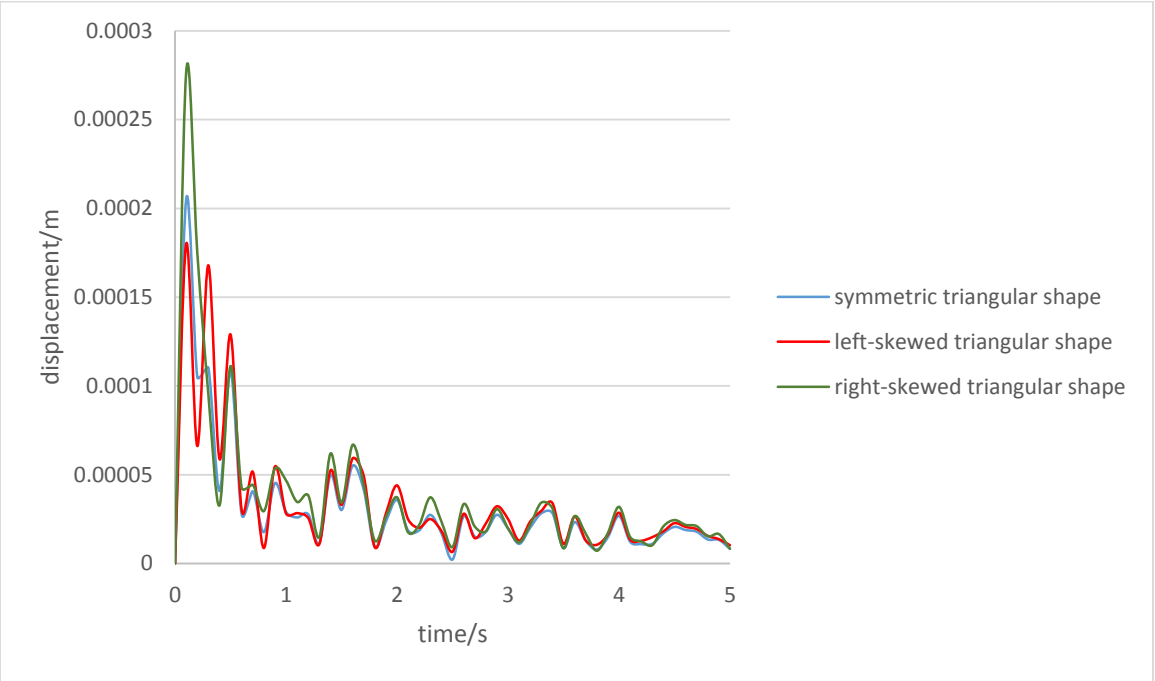

Figure 5. 56 Displacement time trace at ship bow (deck) in case of different impulse shapes

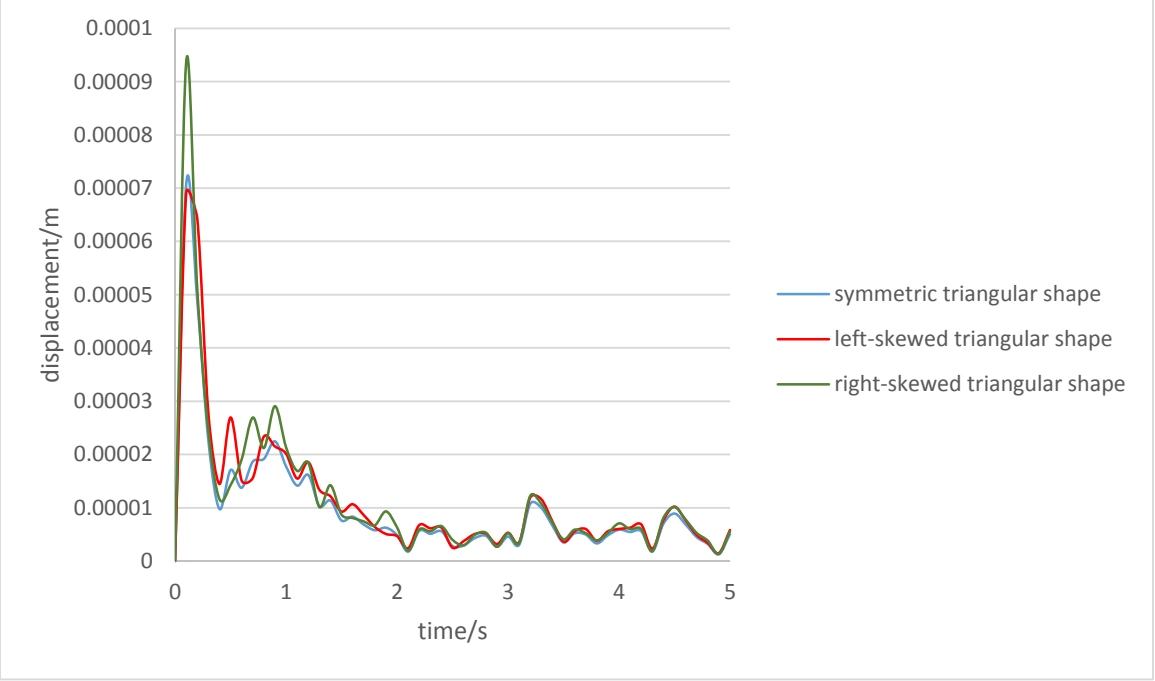

Figure 5. 57 Displacement time trace at ship bow (bottom) in case of different impulse shapes

It is shown from Figure 5.56 and Figure 5.57 that the main difference of ship bow displacement time traces for different impulse shape is the maximum value. The

displacement time trace of right-skewed triangular impulse shape has the largest displacement amplitude. The displacement time trace of left-skewed triangular impulse shape has the smallest displacement amplitude.

Time histories of ship bow displacement for symmetric triangular impulse shape and linearly decaying impulse shape are shown below.

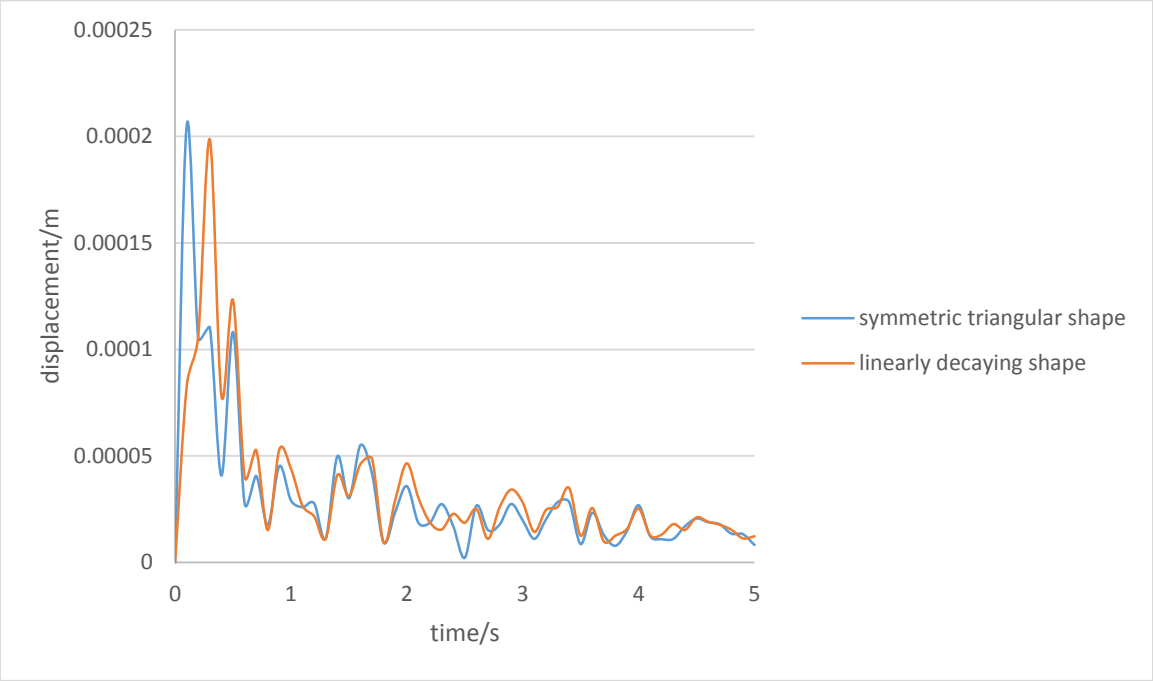

Figure 5. 58 Displacement time trace at ship bow (deck) in case of different impulse shapes

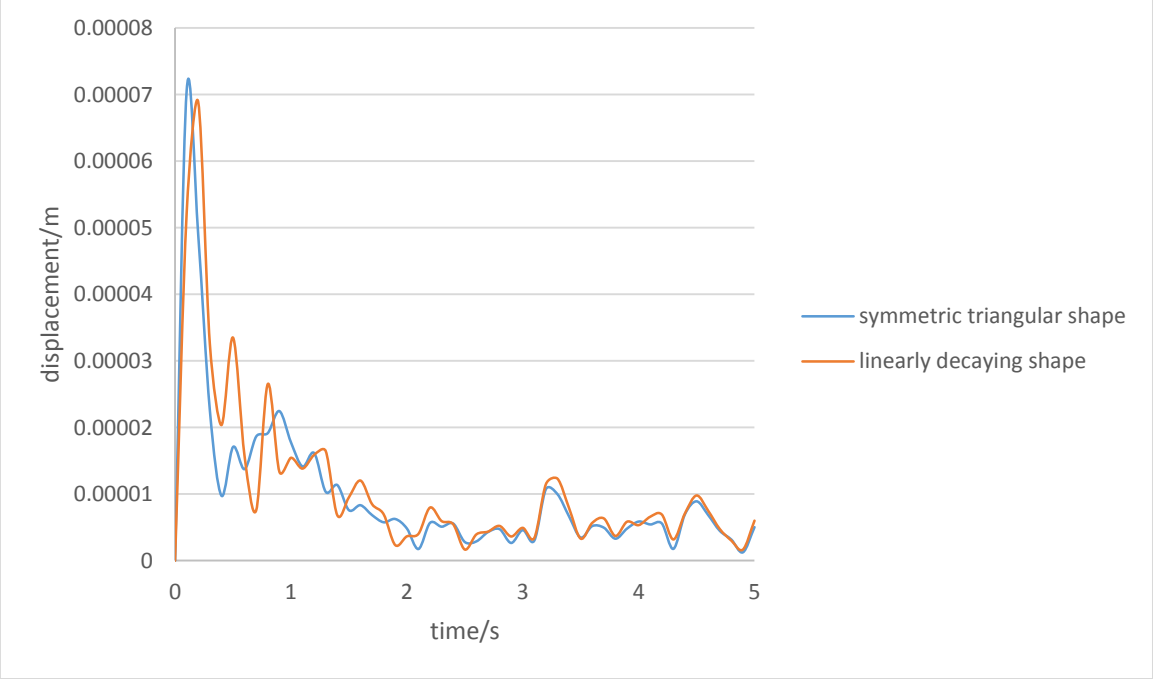

Figure 5. 59 Displacement time trace at ship bow (bottom) in case of different impulse shapes

The maximum displacement at ship bow for two different impulse shapes are almost the same. However, the maximum value for linearly decaying impulse shape occurs a little late and is a bit smaller than the other.

Time histories of ship bow displacement for triangular impulse shape and trapezoidal shape are shown below:

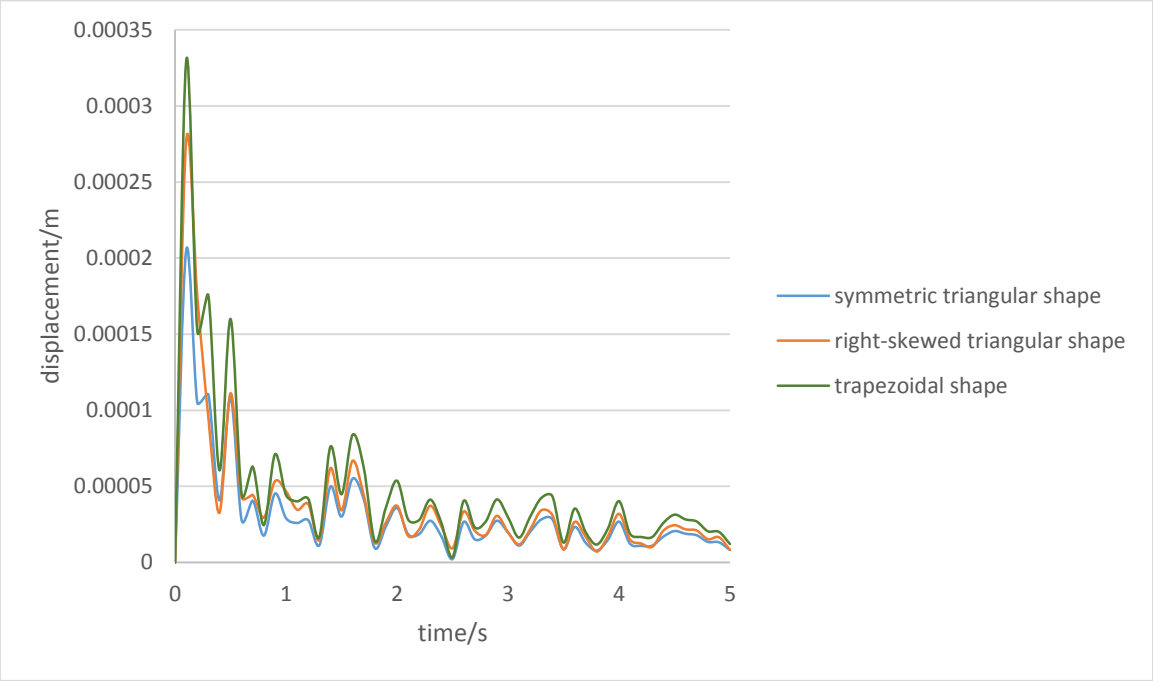

Figure 5. 60 Displacement time trace at ship bow (deck) in case of different impulse shapes

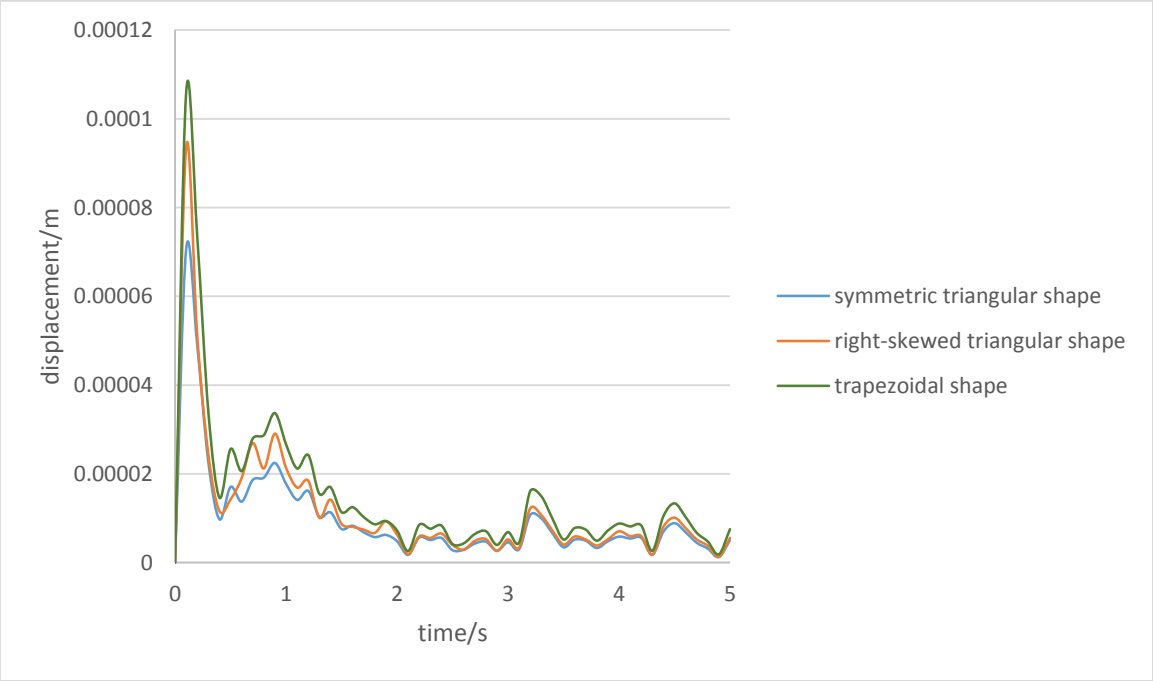

Figure 5. 61 Displacement time trace at ship bow (bottom) in case of different impulse shapes

It is found that the ship has the largest response when slamming load shape is trapezium. This can be understood since that in this case the area under the trapezium curve in Figure 5.55 is the largest.

5.3.3 Mass distribution

In the following sections, the time series of the slamming load is chosen as the one show in Table 5.4. The magnitude of the slamming load is 560000N.

In the analysis before, the ballast, fuel and lightship mass distribution are added according to the real ship mass distribution which is presented in Appendix B. In this section, the model is modified, lightship, ballast and fuel mass are all uniformly distributed along the whole ship and comparison is made related to dynamic response.

The time history of displacement and acceleration at ship bow in different mass distribution cases are presented below:

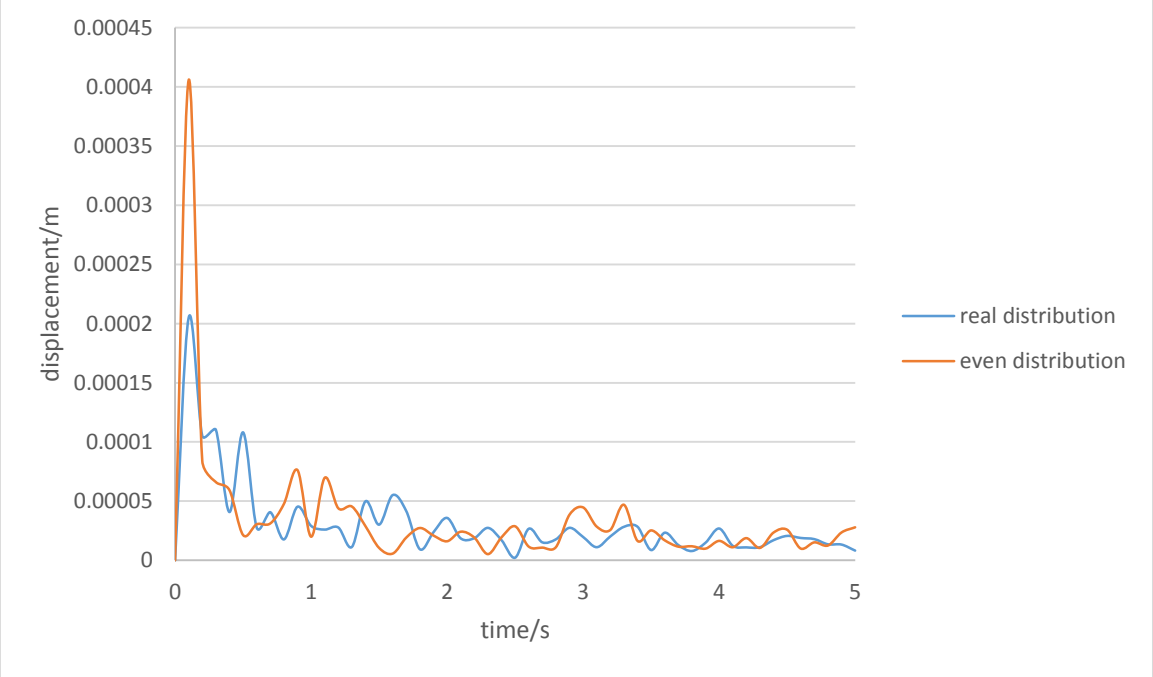

Figure 5. 62 Displacement time trace at ship bow (deck) in case of different mass distribution

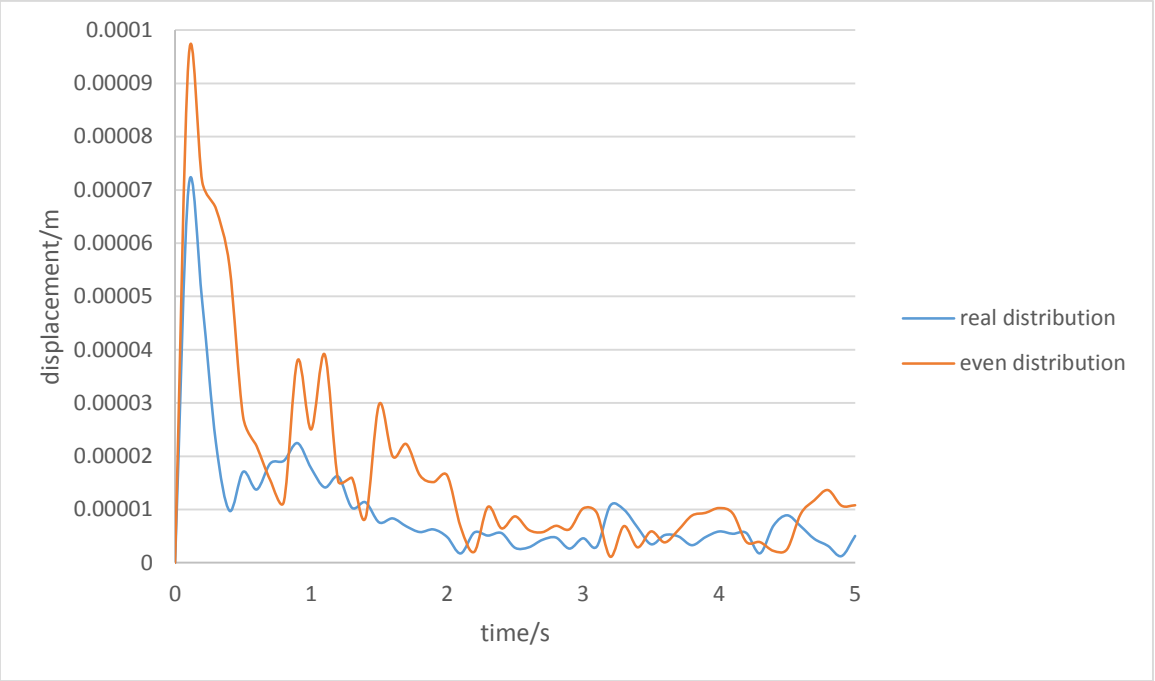

Figure 5. 63 Displacement time trace at ship bow (bottom) in case of different mass distribution

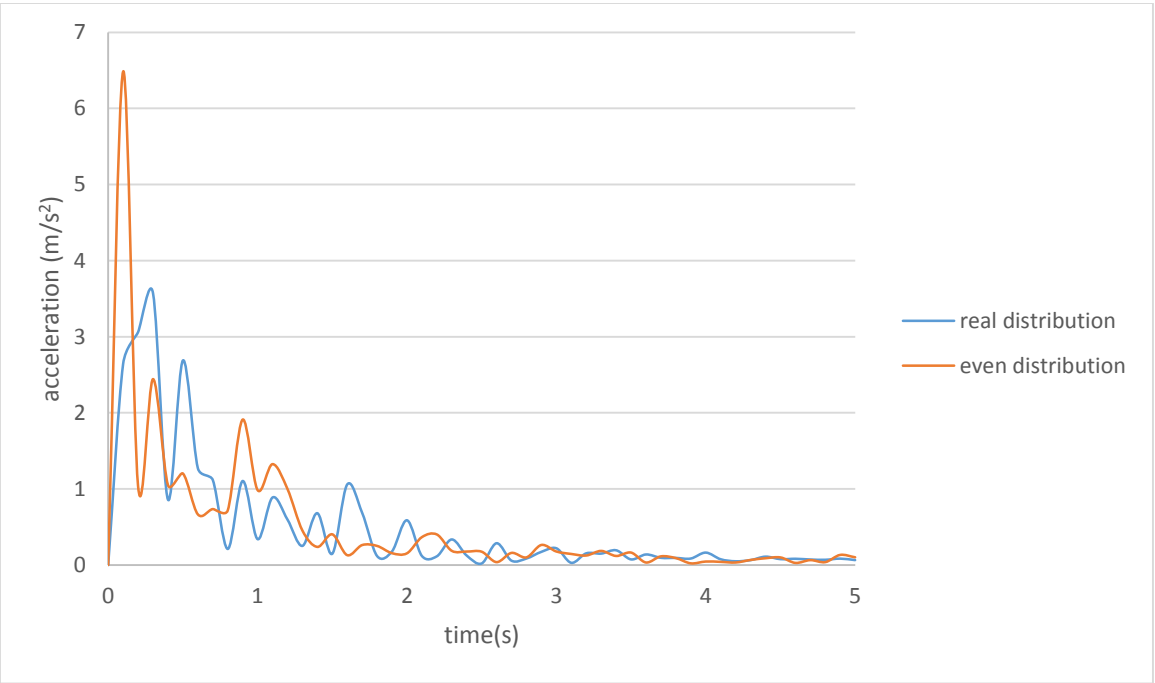

Figure 5. 64 Acceleration time trace at ship bow (deck) in case of different mass distribution

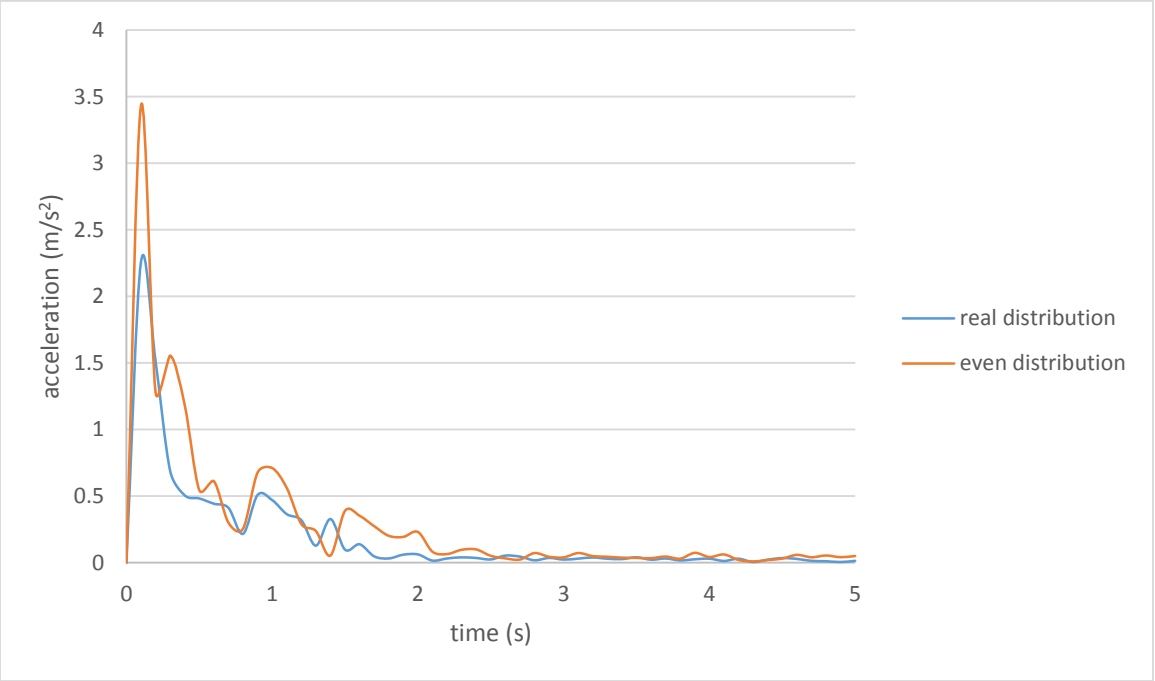

Figure 5. 65 Acceleration time trace at ship bow (bottom) in case of different mass distribution

It is shown that mass distribution has a significant on dynamic response. The dynamic response of the assumed uniform mass distribution is much larger.

5.3.4 Geometrical nonlinear behavior effects

It has been described in section 3.2 that geometrical nonlinear behavior has influence on the response of the structure. In the analysis above, the effect of large deformations is not included. In ABAQUS, the nonlinear effect of large deformations can be included by turning 'Nlgeom' on. In this section, the nonlinear effect of large deformations is analyzed and presented in Figure 5.66 and 5.67.

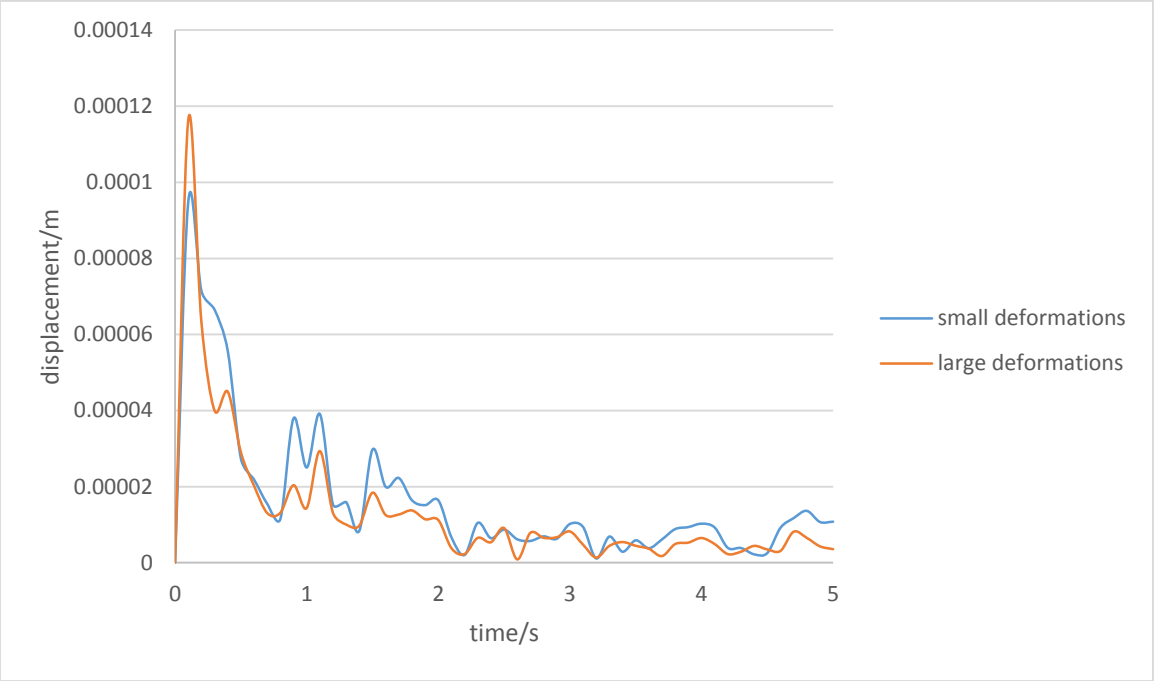

Figure 5. 66 Displacement time trace at ship bow (bottom)

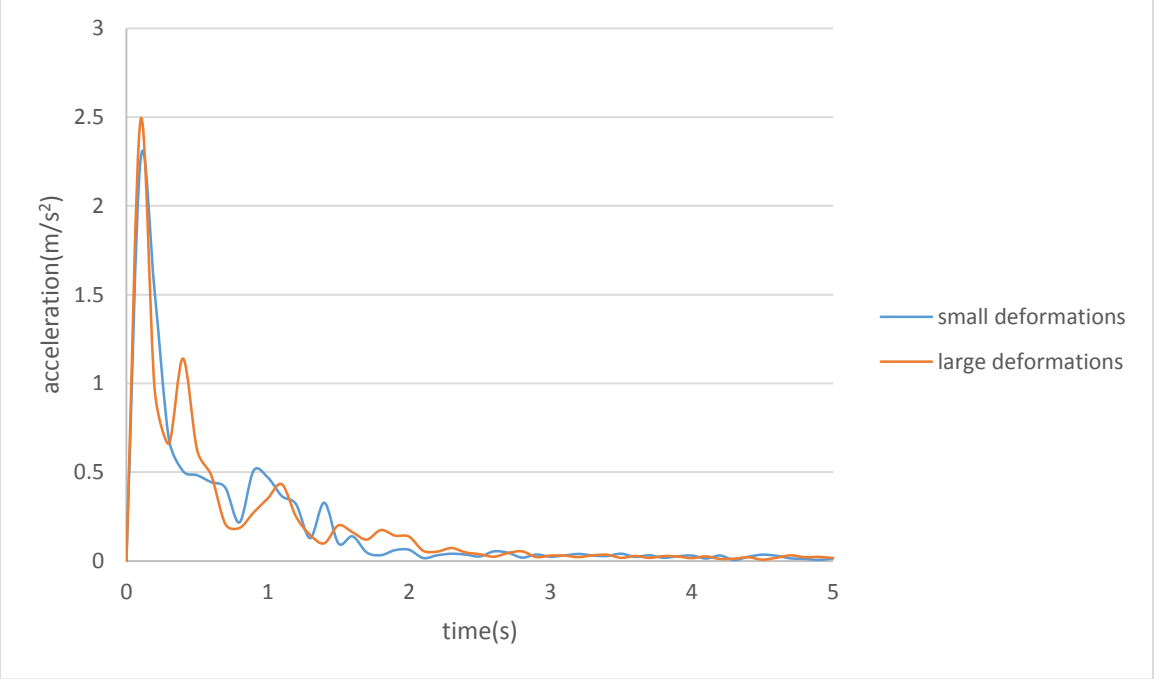

Figure 5. 67 Acceleration time trace at ship bow (bottom)

The displacement and acceleration at the ship bow when accounting for nonlinear geometrical effects are larger. However, the difference is not obvious. Thus, in this load case, the nonlinear effect of large deformations has only a little influence on the dynamic response. It is assumed that when increasing the load magnitude, the nonlinear geometrical behavior may have larger effects.

6 Conclusion

The main objective of this thesis has been to analyze the transient dynamic response of the ship structure induced by slamming loads. A multi-purpose cargo ship owned by Wagenborg is used as the FE model, which is established in Sesam Genie. While, the dynamic analysis is conducted in ABAQUS in this study.

Different types of external loads which act on the ship hull has been described. Corresponding dynamic response analysis has been elaborated with focus on nonlinear analysis and whipping analysis. Dynamic response analysis methods including modal methods and direct integration methods has been discussed. The analysis methods and numerical algorithms used by ABAQUS has also been described.

The ship model with different number of bulkheads are established for comparison. For each ship model, dry and wet natural modes and frequencies are computed. The wet natural frequencies are smaller than the dry natural frequencies due to the influence of added mass and hydrostatic-gravitational stiffness. The critical cross section of the maximum bending moment is the amidship section. When comparing the results of the ship models with different number of bulkheads, it is found that the bulkheads increase the global stiffness of the ship and have significant influence on the natural frequencies. The ship model with 5 bulkheads is chosen as the available model for the following dynamic response analysis.

When conducting dynamic response analysis, the time traces of displacement, velocity, acceleration, stress and strain at different locations of the ship are considered as the dynamic response of the ship. The characteristics of these time traces are presented and analyzed. The response at the ship bow has significant maximum value and damps out after slamming occurs. The time traces of the response at the ship stern may stay stable.

Sensitivity studies with respect to important parameters have been carried out. Firstly, the effects of both time duration and impulse shape of the slamming load have been investigated. The load cases which induce the largest dynamic response have been found. In addition, the analysis of the ship with different mass distributions has been performed. The dynamic response of uniform mass distribution is much larger than that of the real

mass distribution case. Finally, the effect of geometrical nonlinear behavior has been estimated to find little influence on the dynamic response for the chosen load case.

In the future study, major substructures such as deckhouses, superstructures and forecastles are recommended to be modelled. In this case, the results would be more accurate. Besides, local vibrations of the substructures can be analyzed.

Reference

[1] Hadler, J. B., C. M. Lee, J. T. Birmingham, and H. D. Jones (1974). Ocean catamaran seakeeping design, based on the experiences of USNS Hayes. Annual meeting, The Society of Naval Architects and Marine Engineerings.

[2] Ge, C., Faltinsen, O. M., & Moan, T. (2005). Global hydroelastic response of catamarans due to wetdeck slamming. Journal of ship research, 49(1), 24-42.

[3] O.M.Faltinsen, Sea Loads on Ships and Offshore Structure, 1990

[4] Odd M. Faltinsen, Hydrodynamics of High-speed Marine Vehicles, Chapter 8, 2005

[5] Kochin, N. E., Kibel, I. A., Roze, N. V., 1964, Theoretical Hydromechanics, New York: Interscience Publishers.

[6] Zhao, R., Faltinsen,O. M, 1992, Slamming loads on highspeed vessel, In Proc. 19th Symp. on Naval Hydrodynamics, Washington, D.C.: National Academy Press.

[7] Ge, C., 2002, Global hydroelastic response of catamarans due to wetdeck slamming, Dr.Ing thesis, Dept. of Marine Technology, NTNU, Trondheim.

[8] Haver, Sverre K, 2011, Prediction of Characteristic Response for Design Purposes, Statoil

[9] 17th international ship and offshore structure congress 16-21 august, 2009, seoul, korea, Dynamic response committee II.2

[10] 18th international ship and offshore structure congress, 09-13 september 2012, rostock, Germay, Dynamic response committee II.2

[11] ABAQUS/CAE 6.12-1 user manual

[12] Hoque, Md Emdadul (2014). "Dynamic Response of Ship Hull due to Slamming.".

[13] Duni, E., Saponaro, R., Monfrino, G., Caudano, M., Urbinati, F., Spinelli, M., & Antonino, P. (2003). Numerical simulation of full vehicle dynamic behaviour based on the interaction between ABAQUS/Standard and explicit codes. In Abaqus Users' Conference, june Munich.

[14] Hilber, H. M., T. J. R. Hughes, and R. L. Taylor, "Improved Numerical Dissipation for Time Integration Algorithms in Structural Dynamics," Earthquake Engineering and Structural Dynamics, vol. 5, pp. 283–292, 1977

[15] Czekanski, A., N. El-Abbasi, and S. A. Meguid, "Optimal Time Integration Parameters for Elastodynamic Contact Problems," Communications in Numerical Methods in Engineering, vol. 17, pp. 379–384, 2001.

[16] Cunha, A., Caetano, E., Ribeiro, P., & Müller, G. "Dry" and "wet" mode superposition approaches for the hydroelastic analysis of floating structures.

[17] Guedes Soares, C. (1989). Transient response of ship hulls to wave impact. International shipbuilding progress, 36(406), 137-156.

[18] Datta, N. (2010). Hydroelastic response of marine structures to impact-induced vibrations (Doctoral dissertation, The University of Michigan).

[19] Tuitman, J. T., Bosman, T. N., & Harmsen, E. (2013). Local structural response to seakeeping and slamming loads. Marine Structures, 33, 214-237.

[20] Iijima, K., Yao, T., & Moan, T. (2008). Structural response of a ship in severe seas considering global hydroelastic vibrations. Marine structures, 21(4), 420-445.

[21] Bernt J. Leira (2014). Marine structures, 2014.

[22] Marilena Greco (2012). Sea Loads, Lecture Note, NTNU, 2012.

[23] Colicchio, G., Greco, M., Miozzi, M., & Lugni, C. (2009). Experimental and numerical investigation of the water-entry and water-exit of a circular cylinder. In Proceedings of the 24th Int. Workshop on Water Waves and Floating Bodies, Zelenogorsk, Russia, Apr (pp. 19-22).

[24] Seng, S., Pedersen, P. T., & Jensen, J. J. (2012). Slamming And Whipping Analysis Of Ships (Doctoral dissertation, Technical University of DenmarkDanmarks Tekniske Universitet, Department of Naval Architecture and Offshore EngineeringInstitut for Skibs- og Havteknik).

[25] Faltinsen, O. M. (2000). Hydroelastic slamming. Journal of Marine Science and Technology, 5(2), 49-65.

[26] Marine Accident Investigation Branch. Report on the investigation of the structural failure of MSC Napoli English Channel on 18 January 2007. Technical report, 2008.

[27] Han, H. S., & Lee, K. H. (2015). Root cause analysis of the fracture of a sonar window caused by hydrostatic, hydrodynamic, and transient forces around a ship. Engineering Failure Analysis, 48, 218-235.

[28] Rastgar, M., 2002, Investigation of dynamic behavior of floating structures using finite element method, Master Thesis, Department of Civil Engineering, Engineering Faculty, Urmia University, Iran.

[29] Faltinsen, O. M., Landrini, M., & Greco, M. (2004). Slamming in marine applications. Journal of Engineering Mathematics, 48(3-4), 187-217.

[30] Tuitman, J. T. (2010). Hydro-elastic response of ship structures to slamming induced whipping. TU Delft, Delft University of Technology.

[31] T.Moan, 2003, Lecture notes of Advanced Structural analysis.

Appendix A

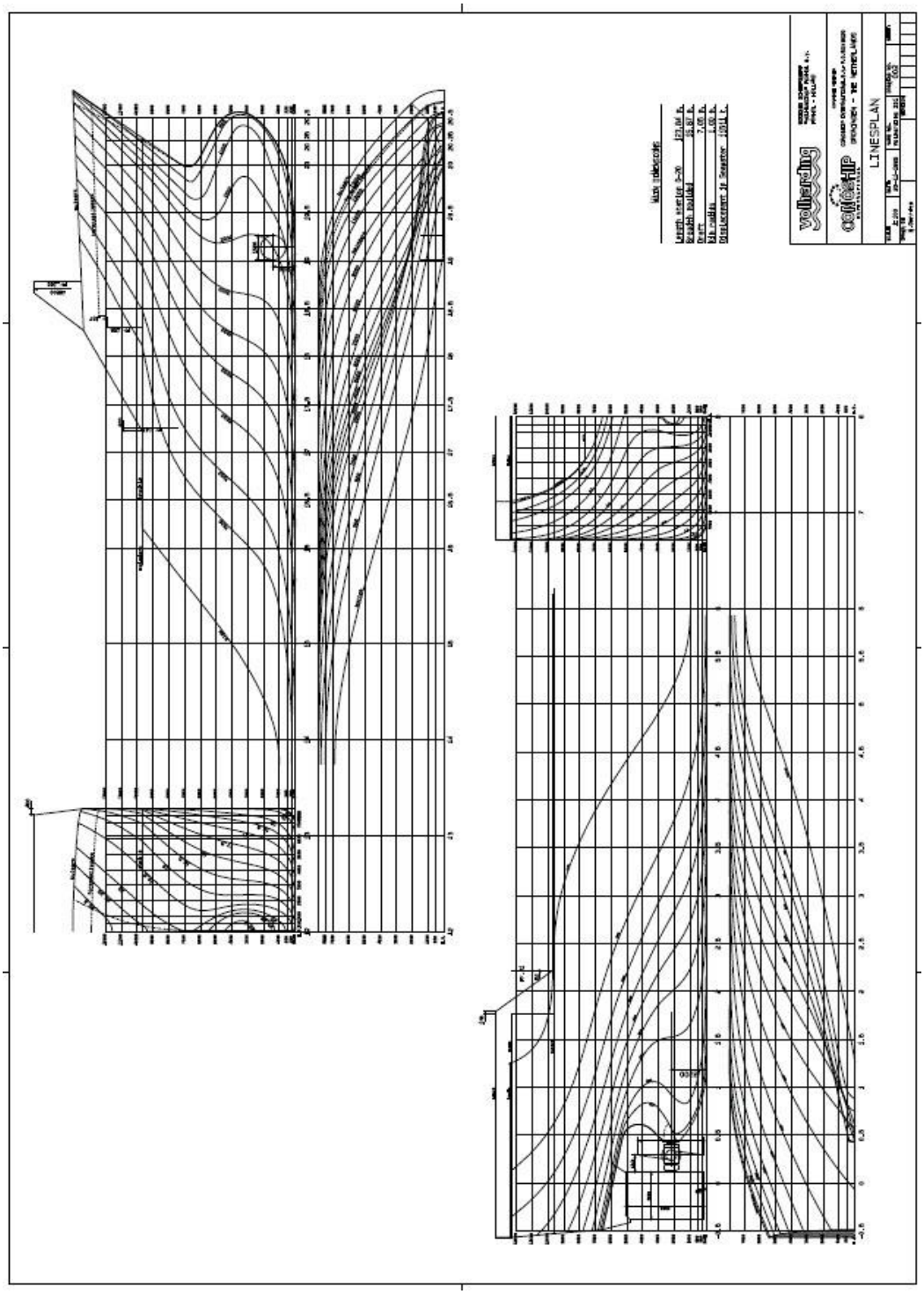

Figure A. 1 Lines plan of the ship

Appendix B

Input data from ISSC Committee II.2 Dynamic Response

The mass distribution of light weight and deadweight are given in this document

Given		
Displacem	98	tons
LCG	61.49	m
Neutral	4.00	m

Lightweig				
Lightweig	29	tons	Check	LSW
LCG	51.88	m	63.525	LCG FA

Compone	Weight	LCG [m]	Start [m]	End [m]	VC	Weight/m	com	com	I_{xx} [kgm^2]	I_{xx} [kgm^2]
Engine	51.0	13.00	10.20	15.45	3.00	9.71	3.00	4.00	157	120070
Engineroo	200.0	13.70	6.00	18.60	2.50	15.87	10.0	5.50	2620	461089
Hull 1	34.5	3.00	-4.80	6.00	9.00	3.19	15.0	5.00	1579	118883
Hull 2	29.5	7.80	6.00	9.50	5.00	8.43	15.8	12.7	1045	85664
Hull 3	125.4	16.29	9.50	23.04	4.50	9.26	15.8	12.7	4347	260722
Hull 4	113.4	29.01	23.04	34.88	4.00	9.58	15.8	12.7	3904	123315
Hull 5	363.9	53.38	34.88	71.88	4.00	9.83	15.8	12.7	12527	73080
Hull 6	145.5	79.28	71.88	86.68	4.00	9.83	15.8	12.7	5011	51775
Hull 7	210.0	98.51	86.68	11	4.00	8.35	15.8	12.7	7231	303408
Hull 8	40.3	11	111	11	4.00	7.78	15.8	12.7	1387	114332
Hull 9	20.3	11	117	11	4.50	9.14	15.8	12.7	703	65557
Hull 10	30.9	12	119	12	5.00	8.60	15.0	12.7	1027	110092
Hull 11	4.4	12	122	12	6.00	7.27	14.0	12.7	147	16637
Hull 12	30.6	12	123	13	6.00	3.46	12.0	10.0	745	129665
Wheelhou	146.9	8.10	3.00	11.60	16.0	17.08	13.5	10.5	24734	421873
Forecastle	200.0	11	112	13	13.0	9.85	12.0	5.00	19016	670748
Rest	11	60.38	-4.80	12	2.00	8.90	15.8	5.00	31421	1669543
Total	29	58.80								

Deadweig		
Deadweig	698	tons
LCG	65.49	m

Compone	Weight	LCG [m]	Start [m]	End [m]	VC	Weight/	comp	comp	I_{xx} [kgm^2]	I_{xx} [kgm^2]
Ballast 1	168.4	121	116	126	0.55	16.84	8.00	1.10	2919	613401
Ballast 2	135.4	115	110	120	0.55	13.54	8.00	1.10	2347	393320
Ballast 3	84.5	103	98.97	108	0.58	8.45	4.00	1.10	1109	153301
Ballast 4	84.8	104	99.00	109	0.58	8.48	4.00	1.10	1113	154061
Ballast 5	161.9	105	100	110	6.34	16.19	1.30	1.80	953	321974
Ballast 6	161.9	105	100	110	6.34	16.19	1.30	1.80	953	321974
Ballast 7	168.8	88.9	83.9	93.9		16.88				
Ballast 8	100.4	83.1	78.1	88.1		10.04				
Ballast 9	100.4	83.1	78.1	88.1		10.04				
Ballast 10	156.3	84.54	79.54	89.54		15.63				
Ballast 11	156.3	84.54	79.54	89.54		15.63				
Ballast 12	71.4	75.21	70.21	80.21		7.14				
Ballast 13	109.6	58.16	53.16	63.16		10.96				
Ballast 14	109.6	58.16	53.16	63.16		10.96				
Ballast 15	240.2	57.45	52.45	62.45		24.02				
Total	200	88.60								
Fuel 1	99.0	27.79	22.79	32.79	2.29	9.90	1.30	4.00	435	113272
Fuel 2	55.0	16.20	11.20	21.20	2.29	5.50	1.30	4.00	241	113281
Fuel 3	17.1	17.50	12.50	22.50	5.96	1.71	1.60	3.00	82164	33236
Fuel 4	16.6	17.38	12.38	22.38	5.57	1.66	1.60	3.00	56909	32440
Fuel 7	2.6	10.20	5.20	15.20	7.95	0.26	2.00	1.00	41650	68622
Fuel 8	15.0	7.54	2.54	12.54	7.77	1.50	2.00	1.50	221	43789
To	205.3	21.28								

Remain. 1	29.4	2.98	-2.02	7.98	6.27	2.94	1.30	4.00	194836	100897691
Remain. 2	33.3	2.84	-2.16	7.84	6.28	3.33	1.30	4.00	222196	114828279
Remain. 3	2.3	12.17	7.17	17.17	8.64	0.23	1.50	2.00	50716	5614261
Remain. 4	1.0	13.72	8.72	18.72	7.03	0.10	1.50	2.00	9702	2290494
Remain. 5	0.9	15.13	10.13	20.13	8.29	0.09	2.50	3.00	17707	1942293
Remain. 6	0.5	9.15	4.15	14.15	7.63	0.05	4.00	3.50	7766	1374571
Remain. 7	0.6	9.16	4.16	14.16	0.95	0.06	5.00	1.10	6892	1649307
Remain. 8	3.4	5.41	0.41	10.41	7.00	0.34	1.50	1.50	31875	10721857
Remain. 9	13.3	7.09	2.09	12.09	8.61	1.33	2.00	1.50	289580	39474755
Remain.	6.5	13	8	18		0.65				
Remain.	1.1	14.51	9.51	19.51		0.11				
Remain.	0.9	8.46	3.46	13.46		0.09				
Remain.	1.3	8.45	3.45	13.45		0.13				
Total	94.5	5.07								
Cargo 1	50.0	40.00	18.60	113.32	4.00	0.53	13.00	6.00	854167	61177998
Cargo 2	40.0	98.51	98.18	98.84	6.39	60.61	13.00	8.50	1032651	55384001
Cargo 3	40.0	25.58	25.25	25.91	6.39	60.61	13.00	8.50	1032651	52145909
Cargo 4	1504.0	85.61	73.36	98.18	5.10	60.60	13.00	15.00	51201173	973379425
Cargo 5	2707.0	48.52	25.91	71.14	6.50	59.85	13.00	18.00	128131333	954985318
Cargo 6	331.0	21.92	18.60	25.25	5.60	49.77	13.00	18.00	14445943	524156189
Total	4672.0	58.72								

Figure B. 1 Mass distribution of the ship

Appendix C

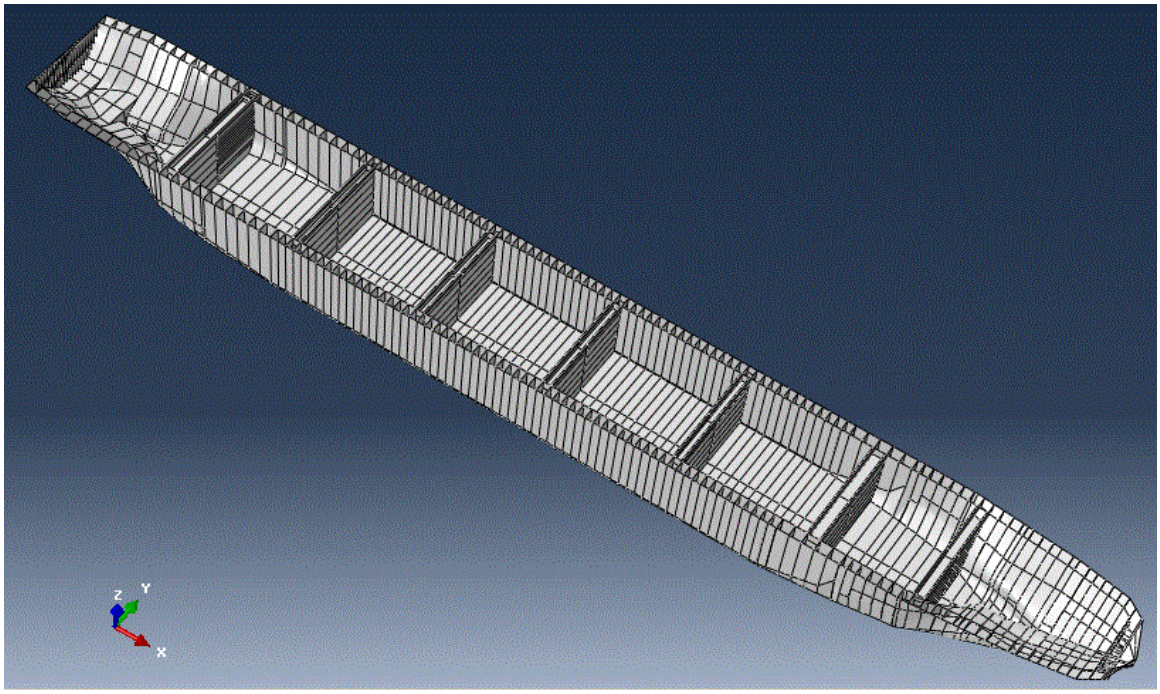

Figure C. 1 ABAQUS ship model with 7 bulkheads

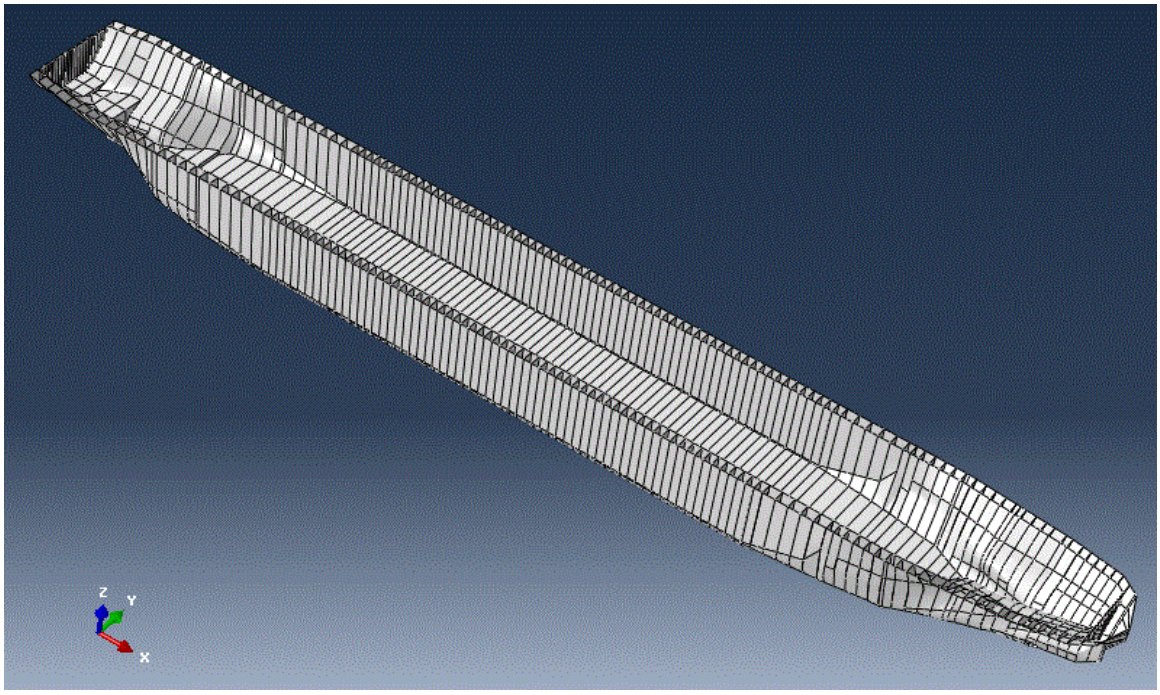

Figure C. 2 ABAQUS ship model with no bulkhead

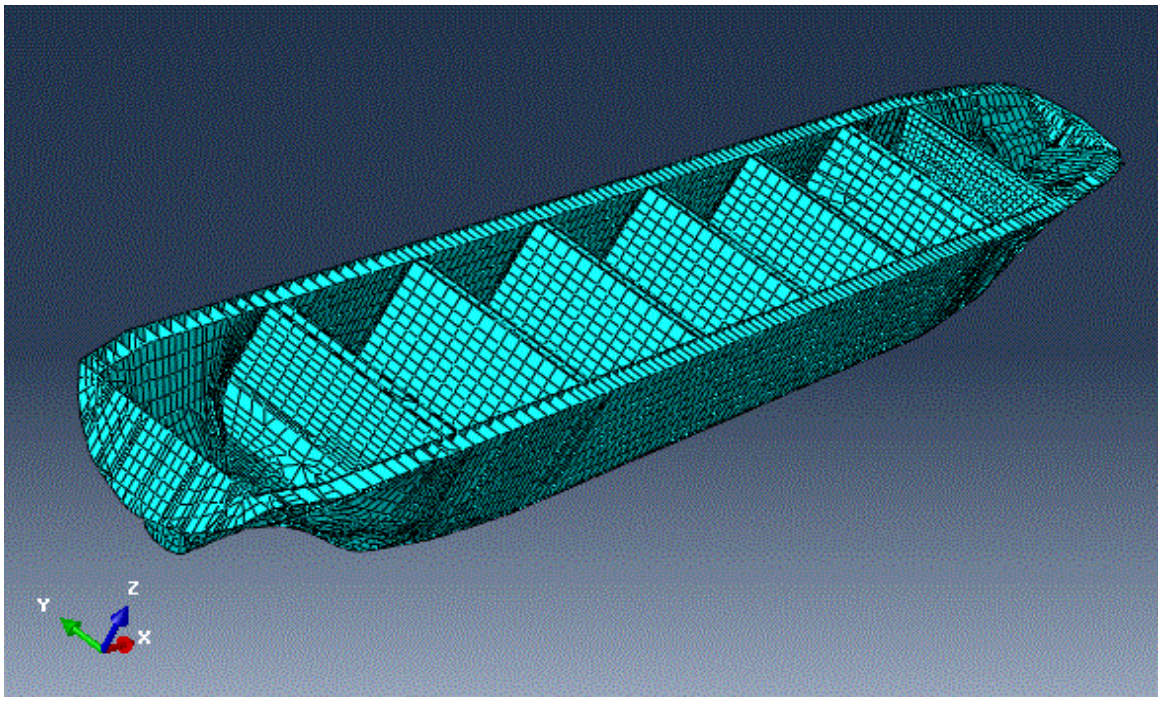

Figure C. 3 Mesh model of ship with 7 bulkheads

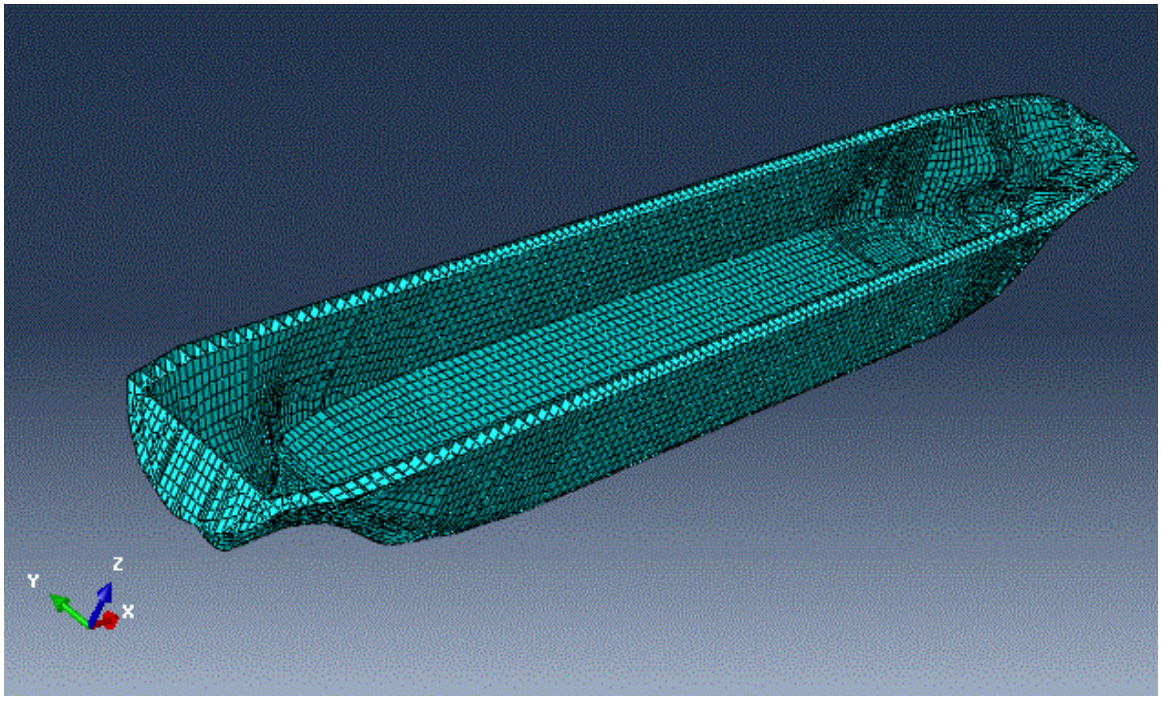

Figure C. 4 Mesh model of ship with no bulkhead